Small Solar Organic Rankine Cycle for Electricity Generation

by
Hans Jurgens Lombard

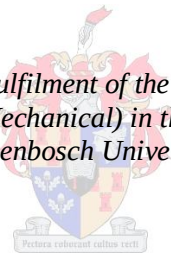

Thesis presented in partial fulfilment of the requirements for the degree of Master of Engineering (Mechanical) in the Faculty of Engineering at Stellenbosch University

Promotor: Mr Robert Dobson

December 2015

Declaration

By submitting this thesis electronically, I declare that the entirety of the work contained therein is my own, original work, that I am the sole author thereof (save to the extent explicitly otherwise stated), that reproduction and publication thereof by Stellenbosch University will not infringe any third party rights and that I have not previously in its entirety or in part submitted it for obtaining any qualification.

Date: 20 November 2015

Abstract

The global the demand for energy has risen dramatically in recent years and the cost of electricity has risen considerably. Local electricity sales prices followed the global trend, increasing by an average of 25% per annum from 2008 to 2012. This upward trend has opened the market for new technologies, such as renewable energy alternatives, better use of waste streams and low temperature power generation.

The Organic Rankine Cycle is an example of a low temperature power generation cycle that can utilize a renewably energy source. The Organic Rankine Cycle is in essence a Rankine Cycle that employs a different working fluid than water. The primary objective of this thesis is to build a functioning ORC. The cycle is to utilize a low temperature (< 120°C) and pressure heat source to generate up to 1 kW of electricity. Each component has to be sized and bought or designed and manufactured. The performance of each component is to be predicted using theoretical mathematical models. This model will be validated through comparison with the experimental results obtained. The condenser has to be driven by natural convection in order to minimize the energy consumption of the system. Finally the feasibility of such a system will be investigated.

The experimental Organic Rankine Cycle was run for several different scenarios and measurements were taken to characterize and evaluate the performance of this system. The performance of the system components was satisfactory in comparison with the design specifications with the exception of the boiler and scroll expander electric motor. The boiler capacity was experimentally determined to be 8 kW, much lower than the design capacity of 20 kW. The lowered boiler capacity inhibited the system performance by as much as 25%. The conversion efficiency of the scroll expander electric generator was low at 7%, but the scroll expander demonstrated an isentropic efficiency up to 47%.

A theoretical model was developed to predict the thermodynamic performance of the system components. The theoretical model predicted the performance of the system components within 10%, except for the pump performance which deviated due to the bypass valve adjustment

A study was conducted to determine the feasibility of an Organic Rankine Cycle system. The study takes into account the initial capital cost, discount rate, operations and maintenance costs and system life span. The study found that the ORC is currently a viable option for remote, off-grid electricity generation with an levelized cost of electricity of R 2,55 compared to the Eskom tariff of R 3,90. The additional cost of line rental increases the Eskom tariff considerably. For urban generation the levelized cost of electricity for renewable sources is still higher (R 2,55) than the Eskom tariff (R 1,00), but the increasing Eskom tariff and decreasing cost of renewable energy solutions should see renewable energy technologies become a financially feasible solution by the year 2020.

Opsomming

'n Drastiese toename in die wêreldwye aanvraag na energie die afgelope paar het die koste van elektrisiteit aansienlik laat toeneem. In Suid Afrika het die prys van elektrisiteit met 'n gemiddeld van 25% jaarliks, gedurende die tydperk van 2008 tot 2012, gestyg. Hierdie opwaartse neiging in die mark het dit makliker gemaak vir hernubare energie bronne, die beter benutting van energie strome en lae temperatuur kragopwekking om die markte betree.

'n Voorbeeld van 'n lae temperatuur kragopwekkingsiklus wat hernubare bronne kan benut, is die organiese Rankine siklus. 'n Rankine siklus wat 'n organiese vloeier gebruik in plaas van water, staan bekend as 'n organiese Rankine siklus. Die primêre doel van hierdie tesis is om 'n werkende organiese Rankine siklus te bou. Die siklus moet gebruik maak van 'n lae druk en lae temperatuur hitte bron van minder as 120C. Die siklus moet in staat wees om 1 kW op te wek. Komponente moet ontwerp en vervaardig word waar nodig of gekoopte komponente se grootte moet bepaal word. 'n Teoretiese model wat in staat is om die werksverrigting van elke komponent voorspel moet opgestel word. Die teoretiese model moet geverifieer word deur gebruik te maak word van die eksperimentele resultate. Die kondensor moet gedryf word deur natuurlike konveksie om die energie verbruik van die stelsel te verminder. Laastens word ondersoek ingestel om die finansiële lewensvatbaarheid van so 'n stelsel te bepaal.

Die eksperimentele organiese Rankine siklus was getoets onder verskillende omstandighede en metings is geneem om die eienskappe van die stelsel, asook die werksverrigting van die onderskeie komponente, te bepaal. Die werksverrigting van die onderskeie komponente was bevredigend in vergelyking met die ontwerp werksverrigting, met die uitsondering van die stoomketel en die scroll turbine generator. Die stoomketel kapasiteit was eksperimenteel bepaal as 8 kW, heelwat minder as die ontwerp kapasiteit van 20 kW. Die omskakelings effektiwiteit van die generator was slegs 7% terwyl die isentropiese effektiwiteit van die scroll turbine bereken was as 47%. Dit word aanbeveel dat die generator vervang word met 'n GS generator of 'n WS generator

met 'n aparte terminale vir die stator windings om die omskakelings effektiwiteit te verbeter.

'n Teoretiese model was ontwikkel om die termodinamiese werksverrigting van die stelsel komponente te voorspel. Die teoretiese model voorspel die werksverrigting van die komponente binne 10%, met die uitsondering van die stoomketel toevoerpomp, omdat die hersirkulasie klep verstel word.

'n Studie om die lewensvatbaarheid van 'n organiese Rankine siklus te bepaal, was ook gedoen. Die studie neem in ag die aanvanklike kapitaal inset koste, afslag koers, bedryfskoste en instandhoudings koste asook die lewensduur van die stelsel. Die studie het bevind dat die organiese Rankine siklus tans lewensvatbaar is in landelike gebiede met 'n koste van R 2,55/kWh teenoor die R3,90/kWh tarief van Eskom. Die addisionele koste van die lyn huur dra 'n aansienlike deel by tot die Eskom tarief. Die stedelike Eskom tarief van R1,00/kWh is steeds minder as die koste van 'n hernubare stelsel (R2,55/kWh), maar dit word verwag dat die stelsels teen 2020 lewensvatbaar sal wees.

Dedication

To Landi, without your motivation, love and support I would not have been able to complete this task.

Acknowledgements

I would like to thank my supervisor, Mr Dobson, for his guidance and support during the course of this project. Thank you for your tolerance, understanding and nagging to complete the task. Without your financial support I would not have been able to achieve this milestone.

I would like to thank my parents Harold and Lize-Marié Lombard, my sisters, Anna-Marie and Jolandi, and my extended family for their continued support, both financial and moral. For always showing interest in my studies, both at undergraduate and postgraduate levels. Thank you for allowing me to study mechanical engineering at Stellenbosch University and realise my dreams.

I would like to specially thank Landi Nesenberend for her patience, support and motivation throughout the entire project. Your help was both greatly needed and appreciated. To her father, Andries Nesenberend, who was always willing to help with advice and contacts. Thanks to Petrie van Wyk and my grandfather, Frans Coetzer, who helped with the editing and proof reading.

Lastly I would like to thank all those at the university that helped with the manufacturing of my project or contributed in any other way, your efforts were greatly appreciated.

Table of Contents

List of Figures

List of Tables

Nomenclature

A	Area
c	Specific heat
D	Diameter
E	Energy, Annual electricity generation
F	Thermal resistance of annular film
f	Friction factor
G	Mass flux, Solar radiation
g	Gravity
H	Head
h	Enthalpy, Heat transfer coefficient
K	Coefficient values
k	Thermal conductivity
L	Length
LCOE	Average lifetime levelized electricity generation
M	Molecular weight
ṁ	Mass flow rate
N	Lifespan of the system
Nμ	Nusselt number
P	Pressure
Pr	Prandtl number
Q	Heat transfer rate
q	Heat flux
R	Surface roughness
Ra	Raleigh number
Re	Reynold's number
r	Discount rate
S	Fin spacing
s	Entropy
T	Temperature
V	Volume flow rate

v	Velocity
w	Work
x	Vapour fraction
Z	Height

Greek

α	Void fraction
β	Inverse of film temperature
η	Thermal efficiency
ϴ	Angle of inclination
K	Condensation coefficient
μ	Dynamic Viscosity
ν	Kinematic viscosity
ρ	Density
χ	Martinelli parameter

Superscript

*	Reduced
‘	New value

Subscript

a	Ambient, Air
b	Boiling
carnot	Carnot cycle
cr	Critical
D	Diameter
elec	Electrical
F	Friction
f	Fluid
fg	Latent heat

forced	Forced Convection
g	Gravity
H	High
h	Hydraulic
i,j	Counters
in	In
L	Low
l	liquid
loss	Loss
M	Momentum
m	Mean
natural	Natural
opt	Optimal
out	Out
p	Plate
pump	Pump
S	Fin spacing
s	Surface
sat	Saturation
th	Thermal
turbine	Turbine
v	Vapour
w	Wall
1-6	Component number
a	Actual exit condition
s	Isentropic exit condition

List of Abbreviations

CSP	Concentrating Solar Power
DHI	Diffuse Horizontal Irradiation
DNI	Direct Normal Irradiation
FH	Feed Heater
GHI	Global Horizontal Irradiation
GWP	Global Warming Potential
IRP	Integrated Resource Plan for electricity
LCOE	Levelized Cost of Electricity
ODP	Ozone Depletion Potential
ORC	Organic Rankine Cycle
PHE	Plate Heat Exchanger
PV	Photovoltaic

1. Introduction

Multiple methods of electricity generation exist ranging from gas and coal to renewable alternatives like solar and wind. The most common energy source in South Africa is coal which accounts for about 90% of electricity generated (Eskom Holdings SOC Limited, 2012). While coal is inexpensive it has two major drawbacks. Firstly the supply of coal is finite, which means that ultimately this fuel supply will have to be abandoned. Furthermore, global warming and environmental agencies apply increasingly more pressure to limit the expulsion of CO_2 into the atmosphere which requires more sophisticated and more expensive technologies (Eskom Holdings SOC Limited, 2012).

Renewable energy sources have enjoyed much attention since the allocation of generation capacity in IRP 2010-2030. This document makes provision for 3750 MW of electricity with 1850 MW of onshore wind generation, 1450 MW of photovoltaic generation and 200 MW of concentrated solar thermal as the main contributors.

1.1 Motivation

Globally the demand for energy has risen dramatically in recent years and with continued pressure to reduce the dependency on fossil fuels for electricity generation the cost of electricity has risen considerably. Local electricity sales prices followed the global trend, increasing by as much as 30% in 2009 (Eskom Holdings SOC Limited, 2012). Figure 1 shows the increase in electricity sales price from 2001 to 2012 (Eskom Holdings SOC Limited, 2012). The upward trend of Figure 1 has opened the market for new technologies such as renewable energy alternatives, better use of waste streams and low temperature power generation. Popular renewable energy technologies are photovoltaic cells, Stirling engines, wind turbines and ORC's.

The ORC is an example of a low temperature power generation cycle the can utilize a renewably energy source. The ORC is in essence a Rankine Cycle that employs a different working fluid than water. The Rankine Cycle is the most common power generation cycle in the South African industry. This cycle uses high temperature heat to vaporize liquid,

usually water, which drives a turbine connected to a generator. This cycle is discussed in more detail in Chapter 2.

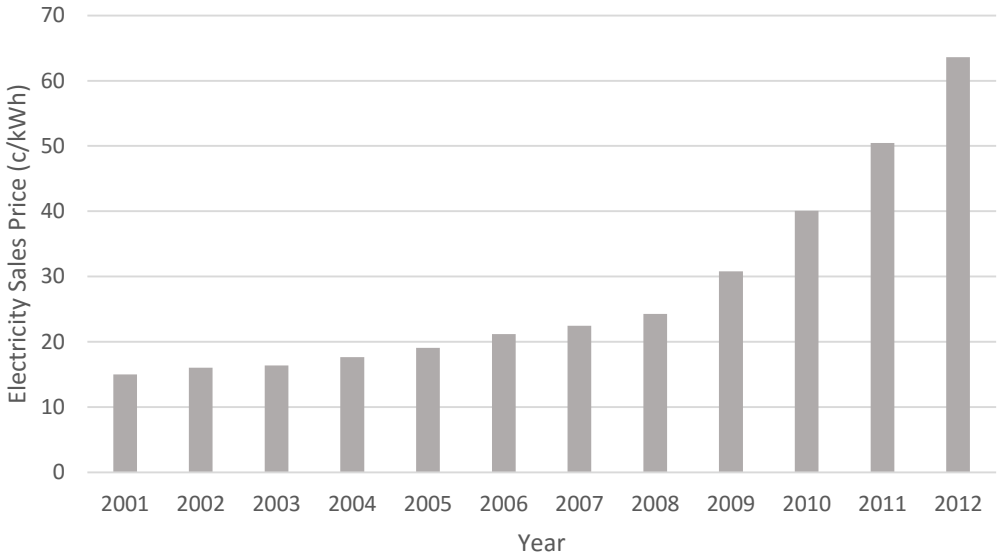

Figure 1: Eskom electricity sales price history from 2001 to 2012

The advantage of these alternatives being the ability to produce electricity independently or in conjunction with Eskom. The opportunity to generate electricity in conjunction with Eskom offers the user the advantage of clean, renewable energy while maintaining the stability of Eskom's network. During times of high output the user can supply electricity to the Eskom grid and in times of high demand the user can supplement generation with electricity from the grid. This allows the user to install a smaller capacity system with lower initial capital cost.

Remote generation has a duel advantage, both for the user and Eskom. By supporting remote, independent generating Eskom eliminates losses due to lengthy transmission lines as well as the upkeep of these lines, while the end user can use the monthly line rental fee to initially buy the electricity generation equipment. Even though the Levelized Cost of Electricity (LCOE) of most renewable sources cannot compare with Eskom electricity tariffs these calculations exclude the monthly line rental, which may significantly increase the cost of electricity depending of the amount of kWh used per

month. For these reasons renewable energy solutions appear to be a suitable solution to the current energy crisis in South Africa.

1.2 Objectives

An ORC has been shown to effectively generate electricity from low temperature heat sources (< 400°C). The system itself is relatively simple and can be used with various heat sources, without having to invest in major modifications. Currently there is no commercial package available for domestic or commercial use in South Africa. This creates a financial opportunity for the use and manufacturing of these systems. It was therefore considered to be prudent to investigate the manufacturability, performance and feasibility of such a system.

The primary objective of this thesis is thus to build a functioning ORC. The cycle is to utilize a low temperature (< 120°C) and pressure heat source, for safety reasons, to generate up to 1 kW of electricity. Each component has to be sized and bought or designed and manufactured. The performance of each component is to be predicted using theoretical mathematical models. This model will be validated through comparison with the experimental results obtained. The condenser has to be driven by natural convection in order to minimize the energy consumption of the system. Finally the economic and commercial feasibility of such a system will be investigated, conclusions drawn and recommendations made.

1.3 Thesis Layout

The layout of this thesis is summarized per chapter as follows:

2. Literature Survey

This chapter presents a short overview of the work carried out and published by other parties relevant to the research conducted. These topics, as per the contents page, include power cycles, organic fluids, expanders, heat exchangers, solar energy and alternative heat sources.

3. Theory

The relevant theory used to size, design and model the major components in the system is presented here. The theory is taken from textbooks and relevant works published in journal articles.

4. Experimental Test System

A flow diagram of the system is presented and the design requirements for each major component are given in this chapter. Different solutions are compared and the selected components are stated.

5. Experimental Work

The experimental work done is discussed in this chapter. This includes the procedures followed, the set points used, experimental checks and error diagnostics.

6. Feasibility Study

The feasibility of an Organic Rankine Cycle for remote, off-grid generation is discussed in this chapter. The current cost of electricity is compared to the capital investment required to generate electricity by various means.

7. Results

In this chapter both the experimental and the theoretical results are presented. The heat transfer in the heat exchangers are calculated, both from experimental data and the theory presented in Chapter 3. The Condenser heat transfer is also calculated from theory and experimentally determined. Furthermore, the electrical output and isentropic efficiency of the scroll compressor are determined from the experimental results and calculated from theory.

A discussion about the system as a whole is presented along with comments on the various components. The calculated and measured values for the different system components are compared and discussed. The validity of the theory used to predict the performance of the components is discussed.

8. Conclusions and Recommendations

Conclusions pertaining to the system, the components used and the performance of each component are presented. Recommendations are made regarding the changes in hardware. Conclusions are drawn about the validity of the presented theory and recommendations are made to improve results.

2. Literature Survey

The literature survey is a summary of works and publications that are relevant to this project. A basic overview of power cycles is given followed by organic fluids and their ideal properties. Expanders are also discussed followed by heat exchangers, solar energy and alternative heat sources.

2.1 Power Cycles

There are a number of different ways to generate power, but many share the same fundamental thermodynamic characteristics. This section will discuss the different types of thermodynamic cycles that can be used to describe power generation processes.

2.1.1 Introduction

Engines are devices that produce a net power output and thus the thermodynamics cycles of these engines are known as power cycles (Çengel & Boles, 2007) . When a power cycle is completely reversible it is known as an ideal or Carnot cycle. It can be shown that the Carnot cycle is the most efficient of all thermodynamic cycles due to this reversible nature. Thermodynamic cycles can be separated based on the phase of the working fluid into two main categories namely: gas cycles and vapour cycles (Çengel & Boles, 2007) . In gas cycles the working fluid remains a gas throughout the entire cycle, whereas the working fluid in vapour cycles is liquid in one part of the cycle and vapour in the other.

2.1.2 The Carnot Cycle

The Carnot cycle is the most efficient power generation cycle that can be operated between a source at temperature T_H and a sink at temperature T_L. (Çengel & Boles, 2007). The *T-s* diagram of a Carnot cycle can be seen in Figure 2. From stage 1 to stage 2 thermal energy is added to the system, while isentropic expansion occurs between stage 2 and 3.

In order to move from stage 3 to stage 4 thermal energy must be removed. Finally isentropic compression completes the cycle and returns to stage 1 (Çengel & Boles, 2007).

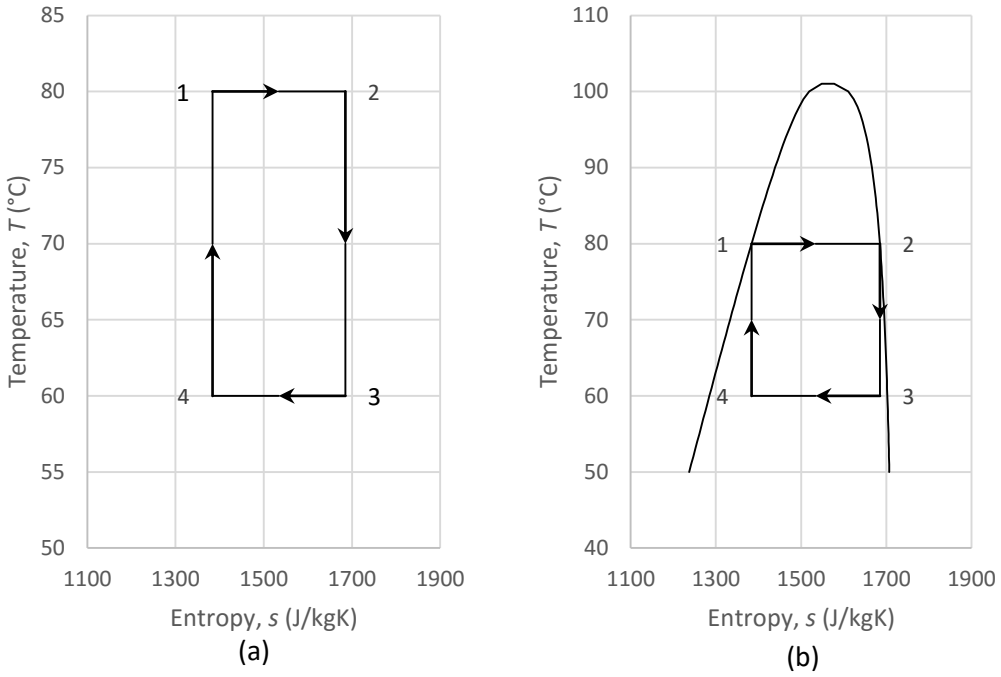

Figure 2: (a) The *T-s* diagram of a gas Carnot cycle. (b) The *T-s* diagram of a vapour Carnot cycle

The thermal efficiency of the Carnot cycle (Carnot efficiency) is expressed as:

$$\eta_{Carnot} = 1 - \frac{T_L}{T_H} \qquad (1)$$

The Carnot efficiency is most often used as a comparison for the thermal efficiency of actual power cycles. The thermal efficiency of a cycle can be increased by raising the source temperature or by lowering the sink temperature (Çengel & Boles, 2007).

2.1.3 Gas Power Cycles

Reciprocating engines, gas turbines and Stirling engines are examples of gas power cycles. Reciprocating engines, both diesel and petrol, are commonly used in small generator sets for electricity generation. The power generation capacity of such small units is usually limited to a few kW. Small generator sets are relatively inexpensive and commonly available. Gas turbines are employed on a much larger scale, mainly in the MW range, in

the power generation industry. This is mostly due to the high capital cost of these turbines. Both of these cycles are internal combustion engines and rely on a fossil or liquid fuel to provide the thermal energy needed by the boiler. On the other hand a Stirling engine, essentially being an external combustion engine, can utilize a wider range of thermal energy sources.

Stirling engines are useful devices as they can operate from any heat source, such as fire or solar radiation. The heat source is applied externally, which makes it easy for the user to switch between heat sources. The biggest disadvantage with these engines is that they respond slowly to changes in input. This means that the work output from the Stirling engine is limited in range and responsiveness, thus limiting its application.

2.1.4 Vapour Power Cycles

An example of a vapour cycle is the Rankine cycle. A graphic representation of this cycle is given in Figure 3. The basic Rankine cycle consists of five components namely: a pump, boiler, turbine, condenser and working fluid. Liquid enters the pump at stage 1 and undergoes isentropic compression to stage 2 (Çengel & Boles, 2007). From here the liquid enters the boiler and thermal energy is added to reach stage 3. During this addition of thermal energy the liquid is transformed to superheated vapour. The superheated vapour enters the turbine and undergoes an isentropic expansion to reach stage 4. Here the vapour enters the condenser and thermal energy is extracted in order to return to stage 1 (Çengel & Boles, 2007).

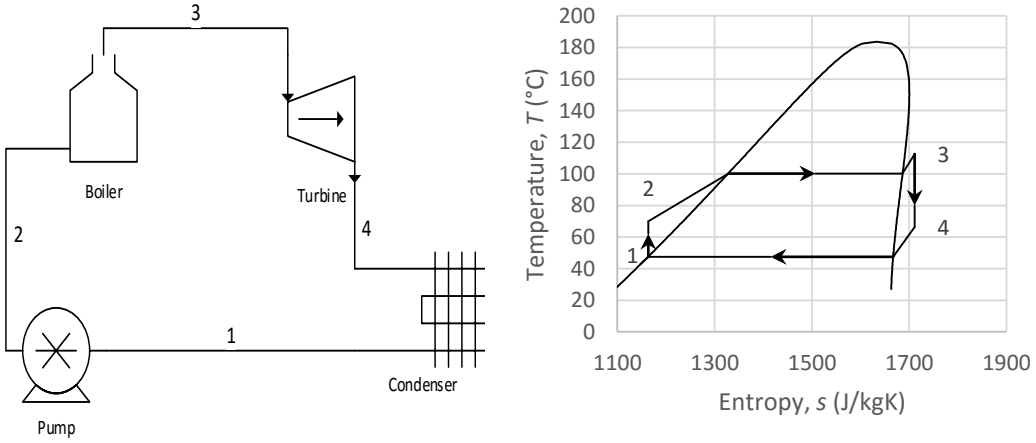

Figure 3: A schematic of a simple ideal Rankine cycle and the corresponding *T-s* diagram

Most Rankine cycles use water as a working fluid, but other fluids can also be used. If an organic fluid, such as a hydrocarbon or fluorocarbon, is used the cycle is known as an ORC. Organic fluids have lower boiling points than water at the same pressure. This allows the system to reach higher pressures at lower temperatures. The lower temperatures in turn implies a lower temperature heat source, which makes this cycle attractive for power generation from waste heat and solar radiation.

2.2 Organic Fluids

There are three different types of fluids that can be used in an ORC, namely wet fluids, dry fluids and isentropic fluids. Wet fluids experience a decrease in vapour quality during isentropic expansion. For a wet fluid the gradient of the line to the right of the critical temperature is negative as shown in Figure 4(a). Isentropic fluids maintain a constant vapour quality, while dry fluids experience an increase in vapour quality during the expansion process. For a dry fluid the gradient of the line to the right of the critical temperature is positive as shown in Figure 4(b). Figure 4 illustrates the difference between a wet and a dry fluid.

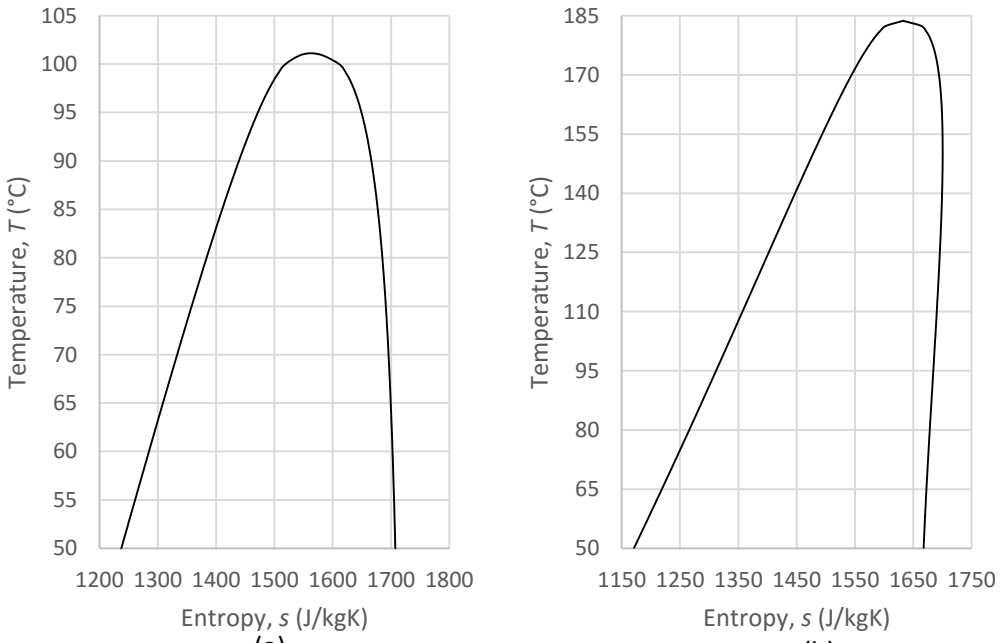

Figure 4: *T-s* diagram for a (a) wet and (b) a dry fluid

Research has shown that using dry fluids instead of wet fluids yield higher efficiencies (Marion, et al., 2012). The properties of a good working fluid are high densities, low cost, moderate pressures in heat exchangers, low ozone depletion potential (ODP) and low global warming potential (GWP) (Marion, et al., 2012).

2.3 Expanders

A wide range of expanders exist for power generation. Expanders convert vapour at a high temperature and pressure into mechanical work. A brief overview of 5 different types of expanders are presented.

2.3.1 Turbines

The most common type of expander is the turbine, although turbines are a proven technology with isentropic efficiencies reaching up to 85% these machines operate at very high speeds and are not commercially available in small scale (Yamamoto, 2001). Turbines do not work well with wet fluids and performance characteristics worsen drastically if they are not operated near the design conditions (Yagoub, et al., 2006).

2.3.2 Reciprocating Piston

Reciprocating pistons have been around since 1765 when the first steam engine was built and has since matured as a technology (The Editors of Encyclopædia Britannica, 2014). One of the major drawbacks of this type of expander is high friction losses (Baek, et al., 2005). They also require significant balancing and timing to function properly. Reports of isentropic efficiencies as high as 62% have been published, but these have yet to be employed in ORCs (Zhang, et al., 2007).

2.3.3 Rotary Vane

Like the reciprocating piston rotary vane devices also have high friction losses. Furthermore, their performance suffers due to leakage through the vanes and rotor end faces (Mohd.Tahir, et al., 2010). Rotary vane devices are simple, robust and can handle high pressures. Isentropic efficiencies of up to 48% in ORCs have been reported but usage of these devices have been limited thus far (Yang, et al., 2009).

2.3.4 Rolling Piston

Much the same as the rotary vane the rolling piston is a simple, robust design that can handle high pressures (Wang, et al., 2010). Some variations exist that reduce the amount of friction and leakage (Subiantoro & Ooi, 2010). The highest isentropic efficiency reported for rolling piston expanders is 45.2% (Haiqing, et al., 2006).

2.3.5 Scroll

The scroll expander has been tested extensively in literature with isentropic efficiencies as high as 83% reported (Schuster, et al., 2009). Although the scroll expander has a complex geometry, scroll compressors are widely used and inexpensive to buy and modify (Mathias, et al., 2009). Scroll expanders have also shown good performance when conditions deviate from design conditions (Kim, et al., 2007).

2.4 Heat Exchangers

Shell and tube heat exchangers require simple numerical equations for design, performance calculation and are easy to manufacture (Çengel & Ghajar, 2008). Achieving the required heat transfer area, however, can be challenging if size is limited (Çengel & Ghajar, 2008). The plate heat exchanger offers a very small and compact unit with high heat transfer coefficients and large surface areas (Mechinox Heat Exchangers, 2011). Sizing and simulation of a plate heat exchanger is however much more complex and performance curves are usually determined experimentally (Mechinox Heat Exchangers, 2011). Plate heat exchangers are very cost effective when compared to the shell and tube heat exchangers. The use of plate heat exchangers as evaporators and condensers in ORCs is widely documented and was thus implemented in this project (Longo & Gasparella, 2007).

2.5 Solar Energy

Solar radiation is the primary source of energy on Earth. Solar radiation, a form of radiant energy, can be converted into thermal and electrical energy. The 2 main technologies that are currently used to capture the energy from solar radiation are photovoltaic (PV) cells and solar collectors (Swanepoel, 2007). PV converts solar radiation into electricity while solar collectors are used to transform solar radiation into thermal energy. The thermal

energy produced has numerous applications ranging from utility scale electricity production to domestic water heating (Swanepoel, 2007).

2.5.1 Solar Radiation

The sun, like all objects, emits electromagnetic radiation due to the collision of particles. The intensity and frequency of vibrating particles in matter is based on the temperature of that matter. Near the surface of an object energy can be ejected in the form of electromagnetic waves (Mills, 1999). These waves have an intensity and a frequency distribution that is a function of the surface temperature of that object. This spectral distribution can be divided into three parts based on the wave length (Swanepoel, 2007):

- 250-400 nm – Ultraviolet, this range is not visible to the human eye and only makes up a small portion of solar radiation.
- 400-700 nm – Visible, as the name suggests this is the frequency range that humans can see.
- 700-4000 nm – Infrared, this range makes up a considerable part of the solar radiation measured on earth.

Integration of this spectrum yields the total energy flux emitted by the Sun. Outside the atmosphere the solar constant has a reference value of 1367 W/m^2 while absorption reduces this value to 1000 W/m^2 at sea level on a sunny day (Swanepoel, 2007).

2.5.2 Solar resource analysis

In order to understand solar resource maps and what they represent a basic understanding of the different types of irradiation is essential. There are four different types of irradiation (Swanson, 2009):

- Direct Normal Irradiation (DNI) – Radiation from the sun measured on a plane normal to the angle of the sun while in direct sunlight.
- Diffuse Horizontal Irradiation (DHI) – Radiation from the sun measured on a horizontal plane while not in direct sunlight.

- Global Horizontal Irradiation (GHI) – Radiation from the sun measured on a horizontal plane while in direct sunlight, thus containing part of the DNI and all of the DHI.

- Latitude Tilt Irradiation (LTI) – Radiation from the sun measured on a plane that is tilted such that the tilt angle is equal to the latitude.

Different solar collectors utilize different components of irradiation and thus the type of measurement that has to be taken on a proposed site is dependent on the type of the proposed collector. PV for example will use GHI or LTI while concentrating solar power (CSP) technologies will use DNI (Gielen, 2012). Figure 5 below shows the annual DNI for South Africa.

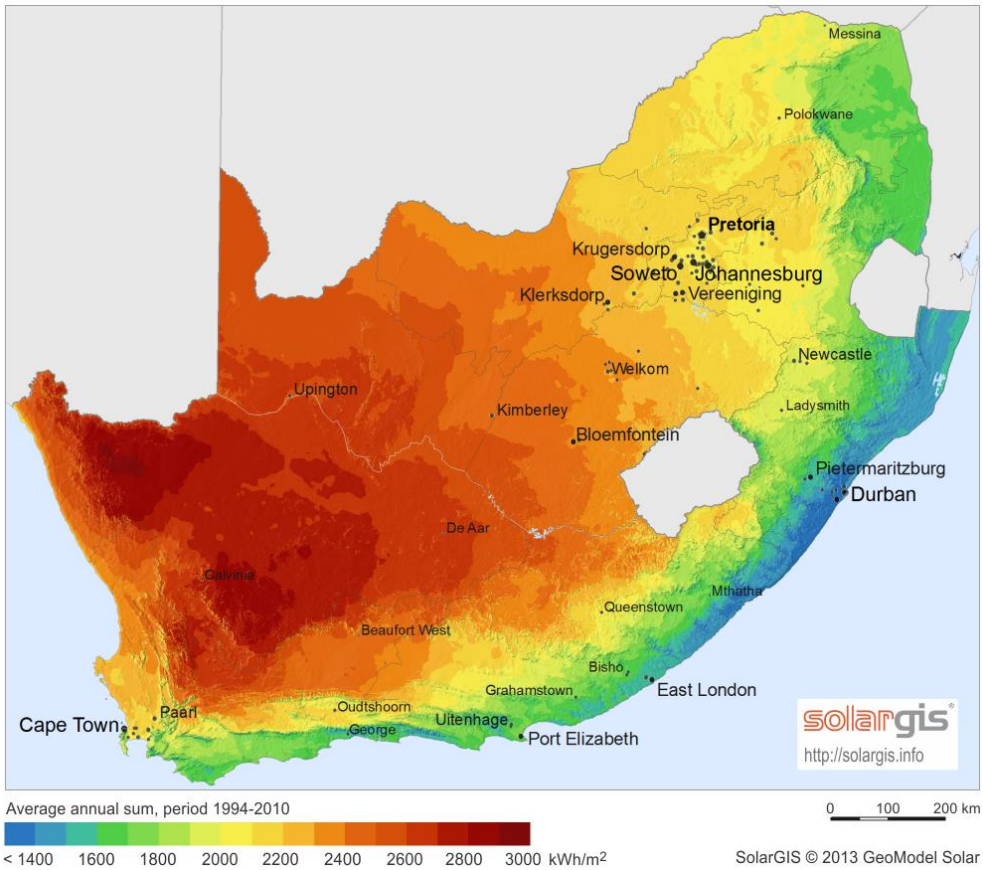

Figure 5: Annual Solar Irradiation for South Africa (GeoModel Solar, 2013)

As seen above South Africa has an abundance of solar resource and is ideal for the application of solar power generation, which makes this research valuable and relevant to the country.

2.5.3 Photovoltaic Cells

The PV industry is experiencing rapid technology advances and increased market share. Over the last two decades, PV production has grown by a factor of 200, reaching 5 GW in 2008, while the total capacity installed by the end of 2011 is in the order of 70 GW (Gielen, 2012). This is minor in comparison with the world's 4000 GW of installed electric generation capacity. However, industry leaders anticipate similar growth over the coming years, with PV generation a main supplier of electricity in the future (Swanson, 2009)

There are a wide variety of PV cells currently available on the market, with efficiencies ranging from 6% to 20%. High efficiency PV cells are significantly more expensive than slightly less efficient ones and therefore a balance between cost and efficiency must be achieved to ensure client satisfaction (Swanepoel, 2007). As the technology matures and manufacturing methods improve cost will decrease along with a slight increase in efficiency.

The major limitation of PV cells however is not the cost or the efficiency. The problem lies in the intermittence of the supply of electricity. In order to mitigate the problem batteries can be installed at a significant additional cost and these in turn have a limited operating lifetime (Swanepoel, 2007).

2.6 Alternative Heat Sources

Alternative heat sources like biogas, geothermal, waste heat or fossil fuels exist, each with their advantages and disadvantages.

2.6.1 Biogas

Biogas is released when organic material is biologically broken down in an environment deprived of oxygen. This energy source is renewable, can be produced on small scale and has low input costs, since waste material is usually used to create biogas. Biogas can also

be used as an automotive fuel or heat source (Economy Watch, 2010). The production of biogas is dependent on the temperature of the environment and supply can therefore be intermittent. It is therefore ideal as a supplementary heat source to solar radiation. The disadvantage of biogas is the hazards that accompanies the storage of flammable gasses.

2.6.2 Geothermal

To harness geothermal energy a hole is drilled deep into the earth. A working fluid is then circulated through this hole where it is heated by the earth's core. The installation cost of such a system is extremely high (Conserve Energy Future, 2014). Geothermal energy is a relatively new technology and is therefore not viable for small scale utilization unless in the form of hot water springs, and these are quite scarce. It does however offer an energy source that can be utilized night and day (Conserve Energy Future, 2014).

2.6.3 Waste Heat

Waste heat from production processes can also be used to drive an ORC. The advantage of such a system is that the energy has already been paid for. Normally only minor adjustments and capital expenditure is required to utilize the waste heat. Another benefit of the ORC is the time during which electricity is produced. The ORC will be operational whenever the process is running, which is the same time as the energy from the ORC is needed most. Waste heat is however a limited resource in terms of location, quantity and quality.

3. Theory

In this chapter the theoretical performance mode of a small ORC that operates using solar radiation as a heat source to generate electricity is presented. The elements that make up the cycle will be analysed and theoretical models presented. This is done by applying conservation of mass, momentum and energy along with thermodynamic relationships to each of the components and/or control volumes constituting the system shown in Figure 6.

3.1 Organic Rankine Cycles

The theory for an ORC is similar to that of a standard Rankine cycle, except for the properties of the working fluid and therefore the procedure presented by Çengel & Boles was followed. The working fluid used in an ORC usually have much lower boiling points than water. This allows the system to operate at lower temperatures and pressures than traditional Rankine cycles. In this section three concepts will be discussed. Firstly an energy analysis of a basic ORC, followed by deviations of the actual vapour power cycle from the ideal ORC and thirdly ways of improving the efficiency of an ideal ORC will be discussed.

All the components of the ORC are considered as steady-flow devices and may thus be analysed as steady-flow processes. The changes in potential and kinetic energy of the working fluid are usually relatively small in comparison to the heat transferred and the work done, therefore these changes in kinetic and potential energy can be neglected (Çengel & Boles, 2007). The steady-flow energy equation per unit mass of working fluid applicable to a control volume then reduces to:

$$(q_{in} - q_{out}) + (w_{in} - w_{out}) = (h_{out} - h_{in}) \quad (2)$$

Referring to the components in Figure 6 the energy equation for each component can be derived as:

Pump (q=0)

$$w_{in} = (h_2 - h_1) \quad (3)$$

Feed Heater (FH) (q=0) $$(h_3 - h_2) = (h_6 - h_7) \quad (4)$$

Boiler (w=0) $$q_{in} = (h_4 - h_3) \quad (5)$$

Super Heater (w=0) $$q_{in} = (h_5 - h_4) \quad (6)$$

Turbine (q=0) $$w_{out} = (h_5 - h_6) \quad (7)$$

Condenser (w=0) $$q_{out} = (h_7 - h_1) \quad (8)$$

The thermal efficiency of the entire cycle is then determined as the net work divided by the thermal energy input:

$$\eta_{th} = \frac{w_{out} - w_{in}}{q_{in}} \quad (9)$$

A schematic of a simple ORC system is shown in Figure 6.

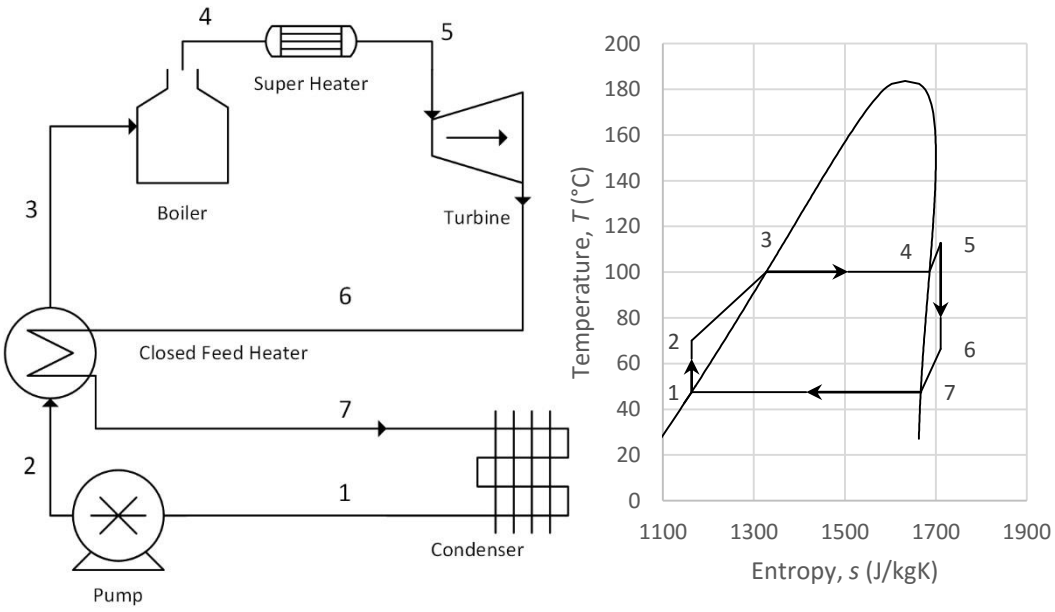

Figure 6: Simplified organic Rankine cycle schematic and T-s diagram

Figure 7 shows how the actual vapour power cycle differs from the ideal Rankine cycle. These deviations are caused by irreversibilities in the various system components. The most common causes of these irreversibilities are fluid friction and the loss of thermal energy to the environment (Çengel & Boles, 2007).

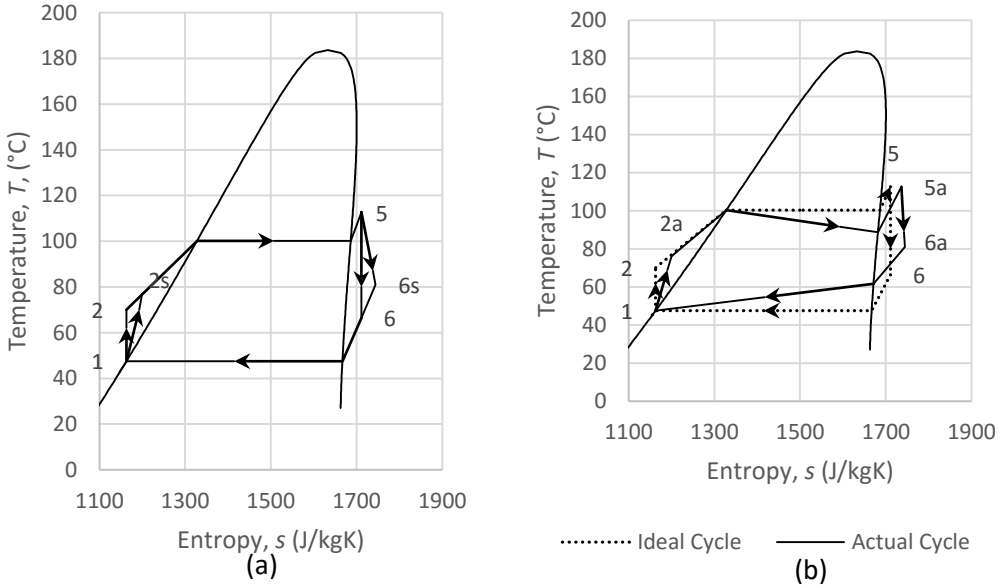

Figure 7: (a) The effect of pump and turbine irreversibilities on the ideal Rankine cycle (b) Deviation of actual vapour power cycle from the ideal Rankine cycle

The pressure drops in the boiler, condenser and the piping between components due to fluid friction. The total pressure drop in the system due to fluid friction must then be overcome by the pump. This requires a larger work input to the pump and decreases the thermal efficiency of the cycle (Çengel & Boles, 2007). The other main cause of irreversibilities is the thermal energy lost from the working fluid to the environment through the various components. Thus in order to maintain the same level of energy output more thermal energy has to be supplied by the boiler, again this lowers the thermal efficiency of the cycle (Çengel & Boles, 2007).

The irreversibilities occurring within the pump and the turbine cause deviations from the ideal Rankine cycle and adversely influences the cycle efficiency. Irreversibilities that occur in the pump cause the pump to use more power in order to achieve the required operating conditions, thus the cycle efficiency decreases with an increase in irreversibility

(Çengel & Boles, 2007). Similarly the turbine produces a smaller work output as a result of irreversibilities, again decreasing the cycle efficiency. Under ideal conditions these devices can be considered to be isentropic. The isentropic efficiency is used to account for the deviation of the actual performance of pumps and turbines from the isentropic performance and is calculated as follows (Çengel & Boles, 2007) for the pump and turbine respectively:

$$\eta_{pump} = \frac{h_{2s} - h_1}{h_{2a} - h_1} \quad (10)$$

$$\eta_{turbine} = \frac{h_5 - h_{6a}}{h_5 - h_{6s}} \quad (11)$$

Stages 2a and 6a represent the actual exit conditions of the pump and turbine, while stages 2s and 6s represent the isentropic exit conditions as shown in Figure 7.

There are 3 basic ways that can be employed to increase the thermal efficiency of the Rankine cycle:

- The maximum temperature of the working fluid can be increased.

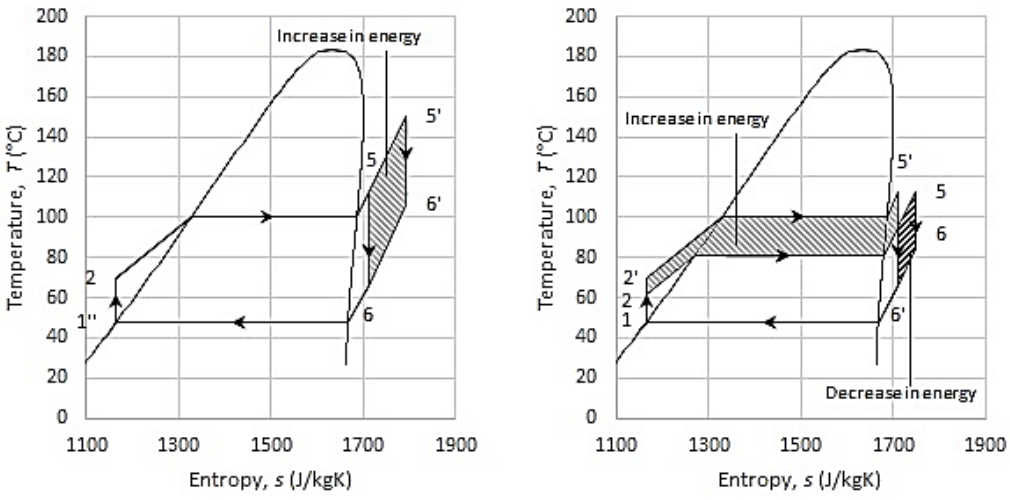

Figure 8: The effect of increasing (a) the maximum temperature and (b) the boiler pressure of the ideal Rankine cycle

- As shown in Figure 8 increasing the boiler pressure increases the boiling temperature, which in turn increases the thermal efficiency (Çengel & Boles, 2007).
- The condenser pressure can be lowered as shown in Figure 9 (Çengel & Boles, 2007). By decreasing the condenser pressure from P_6 to P'_6 the condenser temperature is also decreased which increases the thermal efficiency of the cycle (Çengel & Boles, 2007). The condenser temperature is limited by the method of cooling. Wet cooling offers the lowest temperature, theoretically equal to the wet bulb temperature, followed by dry cooling which has a theoretical limit equal to the ambient temperature. Both wet and dry condensers can be operated as natural convection or forced convection.

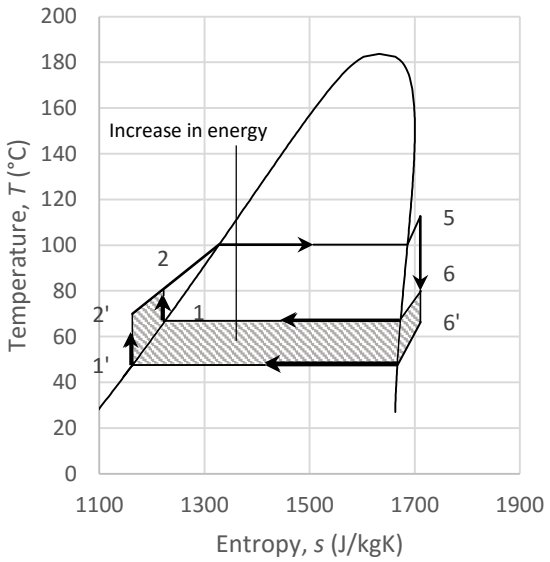

Figure 9: The effect of lowering the condenser pressure on the ideal Rankine cycle

3.2 Pump

The performance of a pump is analysed by using two fundamental parameters. Firstly the mass flow rate through the pump, or more commonly known as the volume flow rate for incompressible flow. The second parameter used is the net head. The net head is equal to the change in head between the inlet and outlet of the pump, also known as the

Bernoulli head (Çengel & Cimbala, 2006). The net head is expressed by the following equation:

$$H = \left(\frac{P}{\rho g} + \frac{v^2}{2g} + z\right)_{out} - \left(\frac{P}{\rho g} + \frac{v^2}{2g} + z\right)_{in} \quad (12)$$

For the special case where the inlet and outlet diameters of the pump are the same, there is no change in elevation and the liquid being pumped is incompressible the equation reduces to (Çengel & Cimbala, 2006):

$$H = \frac{P_{out} - P_{in}}{\rho g} \quad (13)$$

A typical pump performance curve will start at the shutoff head. The shutoff head is normally defined as the point at which the mass flow rate is zero (Çengel & Cimbala, 2006). The flow rate then increases as the net head decreases until the maximum flow rate is reached, as shown in Figure 10. A pump can only operate along the performance curve for steady conditions, but the performance curve can be altered by varying the rotational speed of the pump (Çengel & Cimbala, 2006). The efficiency of the pump is zero at the shutoff head, increases to the maximum as the flow rate increases and then decreases as the flow rate is increased further.

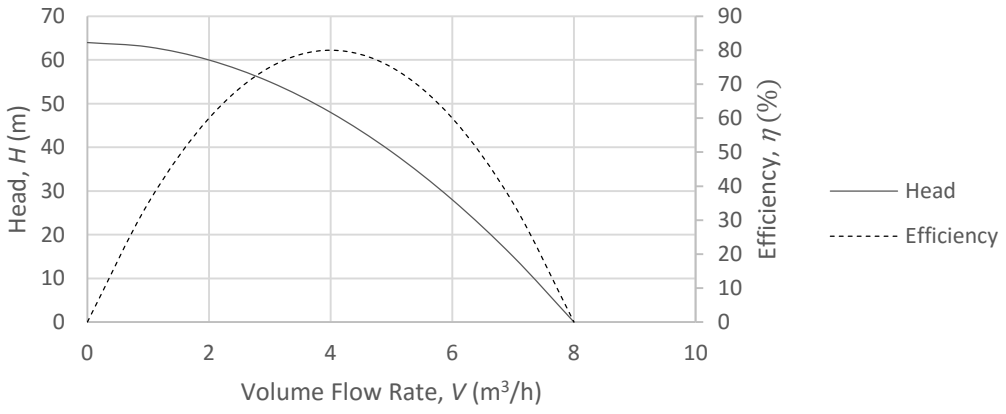

Figure 10: Typical pump performance curve

The performance curve of the pump is used to determine the operating point of the system. The operations point is the point where the net head required by the system is equal to the net head provided by the pump. The net head required by the system is equal to the sum of the major and minor pressure losses (Çengel & Cimbala, 2006). The losses through each component are considered to be major losses, while the losses due to valves, piping and measurement devices are considered to be minor losses. The system pressure loss can be expressed mathematically as (Çengel & Cimbala, 2006):

$$H_{loss} = \sum_i H_i + \sum_j K_{loss,j} \frac{v_j^2}{2g} \quad (14)$$

Where H_i is the pressure drop through system component *i* and K_j is the loss coefficient of the minor component, *j*.

3.3 Plate Heat Exchanger

Due to the compact size, high heat transfer capacity and low cost of plate heat exchangers the range of applications have become very wide. For the same reason plate heat exchangers have been chosen for this project. Due to the construction features of plate heat exchangers turbulent flow can be obtained at very low flow rates. Therefore all flow through the plate heat exchangers are considered to be turbulent. Turbulent flow improves heat transfer coefficients due to the mixing properties of the flow. Improved heat transfer coefficients require a smaller area to deliver the same total heat transfer capacity, thus reducing the cost and size of the heat exchanger.

3.3.1 Two-phase flow fluid properties

Assuming homogenous, well mixed flow implies that the velocity of the vapour is equal to the velocity of the liquid. In order to calculate the density the void fraction must be determined first (Mills & Ganesan, 2009):

$$\alpha = \frac{A_v}{A_v + A_l} = \frac{A_v}{A} \qquad (15)$$

Thus the density can be calculated by use of the following equation (Mills, 1999):

$$\rho = \alpha\rho_v + (1-\alpha)\rho_l \qquad (16)$$

The specific heat (Mills, 1999):

$$c = \alpha c_v + (1-\alpha)c_l \qquad (17)$$

The thermal conductivity (Mills, 1999):

$$k = \alpha k_v + (1-\alpha)k_l \qquad (18)$$

And the viscosity (Mills, 1999):

$$\frac{1}{\mu} = \frac{x}{\mu_v} + \frac{(1-x)}{\mu_l} \quad (19)$$

3.3.2 Turbulent flow convective heat transfer coefficient

The boiler is heated by oil flowing through the plate heat exchanger. Due to the large dependency of the viscosity on the oil temperature the following equation is recommended (Warnakulasuriya & Worek, 2008):

$$Nu = 0{,}292\, Re^{0{,}705} Pr^{0{,}35} \left(\frac{\mu_f}{\mu_w}\right)^{0{,}14} \quad (20)$$

If the viscosity of the fluid is not highly dependent on the fluid temperature the equation becomes (Khan, et al., 2010):

$$Nu = 0{,}1437\, Re^{0{,}7810} Pr^{0{,}35} \left(\frac{\mu_f}{\mu_w}\right)^{0{,}14} \quad (21)$$

The Nusselt number is then used to calculate the heat transfer coefficient (Çengel & Ghajar, 2008):

$$h = \frac{Nu\, k}{D_h} \quad (22)$$

3.3.3 Turbulent flow pressure drop

The friction factor for flow through a plate heat exchanger can be calculated by (Çengel & Cimbala, 2006):

$$f = 23{,}8\, Re^{-0{,}205} \quad (23)$$

The total head loss through the plate heat exchanger is then calculated by (Çengel & Cimbala, 2006):

$$H = f \frac{L}{D_h} \frac{v^2}{2g} \quad (24)$$

3.3.4 Boiling heat transfer coefficient

The equation presented by Cooper (Cooper, 1984) shows good correlation for refrigerant vaporization in plate heat exchangers (Longo & Gasparella, 2007). The equation uses reduced fluid properties as follows:

$$h_b = 55\, P^{*\left(0{,}12-0{,}2\log_{10} R_p\right)}(-10\log_{10} P^*)^{-0{,}55} q^{0{,}67} M^{-0{,}5} \qquad (25)$$

Where M is the molecular weight of the fluid, P^* is the reduced pressure:

$$P^* = \frac{P}{P_{cr}} \qquad (26)$$

And R_p (µm) is the surface roughness of the plate heat exchanger as defined in German standard DIN 4762/1 (Longo & Gasparella, 2007).

3.3.5 Two-phase flow pressure drop

The pressure gradient is calculated as follows (Mills & Ganesan, 2009):

$$\frac{dP}{dz} = \left(\frac{dP}{dz}\right)_F + \left(\frac{dP}{dz}\right)_g + \left(\frac{dP}{dz}\right)_M \qquad (27)$$

The pressure gradient consist of three parts namely the wall friction (*F*), gravity (g) and the momentum changes (M). The wall friction is based on the friction factor which is calculated with the following equation for turbulent flow (Mills, 1999):

$$f = [0{,}79\ \ln Re_D - 1{,}64]^{-2} \qquad (28)$$

And for laminar flow (Mills, 1999):

$$f = \frac{64}{Re_D} \qquad (29)$$

The pressure gradient due to the wall friction then becomes (Mills, 1999):

$$\left(\frac{dP}{dz}\right)_F = -\frac{f}{D}\frac{G^2}{2\rho} \quad (30)$$

The energy balance dictates that the change in quality must be (Mills, 1999):

$$\frac{dx}{dz} = -\frac{\dot{Q}}{L}\frac{1}{\dot{m}\, h_{lv}} \quad (31)$$

Thus the change in density is (Mills, 1999):

$$\frac{d\rho}{dz} = (\rho_v - \rho_l)\frac{dx}{dz} \quad (32)$$

The pressure gradient attributed to momentum changes can now be calculated (Mills, 1999):

$$\left(\frac{dP}{dz}\right)_M = \left(\frac{G}{\rho}\right)^2 \frac{d\rho}{dz} \quad (33)$$

All that remains is the change in pressure due to gravity (Mills, 1999):

$$\left(\frac{dP}{dz}\right)_g = -\rho g \sin\theta \quad (34)$$

3.4 Scroll Expanders

The hermetically sealed scroll expander was originally a scroll compressor, but has been converted to operate as an expander as per section 4.4 and Appendix D. Considering a control volume around the scroll expander, an energy balance can be written as follows (Çengel & Cimbala, 2006):

$$E_{in} = E_{out} + W_{out} \quad (35)$$

$$\left(\frac{P}{\rho} + \frac{1}{2}v^2 + gz\right)_{in} = \left(\frac{P}{\rho} + \frac{1}{2}v^2 + gz\right)_{out} + W_{out} \quad (36)$$

The change in energy due to height is taken to be negligible and thus the expression simplifies to (Çengel & Cimbala, 2006):

$$\left(\frac{P}{\rho} + \frac{1}{2}v^2\right)_{in} = \left(\frac{P}{\rho} + \frac{1}{2}v^2\right)_{out} + W_{out} \quad (37)$$

The energy produced by the expander can thus be expressed as (Çengel & Cimbala, 2006):

$$W_{out} = \left(\frac{P}{\rho} + \frac{1}{2}v^2\right)_{in} - \left(\frac{P}{\rho} + \frac{1}{2}v^2\right)_{out} \quad (38)$$

Taking into account the conversion efficiency of the expander the electrical power output can be written as (Çengel & Boles, 2007):

$$W_{elec} = \eta W_{out} \quad (39)$$

$$W_{elec} = \eta\left[\left(\frac{P}{\rho} + \frac{1}{2}v^2\right)_{in} - \left(\frac{P}{\rho} + \frac{1}{2}v^2\right)_{out}\right] \quad (40)$$

3.5 Condensers

For the condenser coil aluminium fins are pressed onto copper tubes. Due to the high conductivity of these two materials and the low heat flux the surface temperature is assumed to be constant. The fin dimensions and spacing is defined as in Figure 11 below.

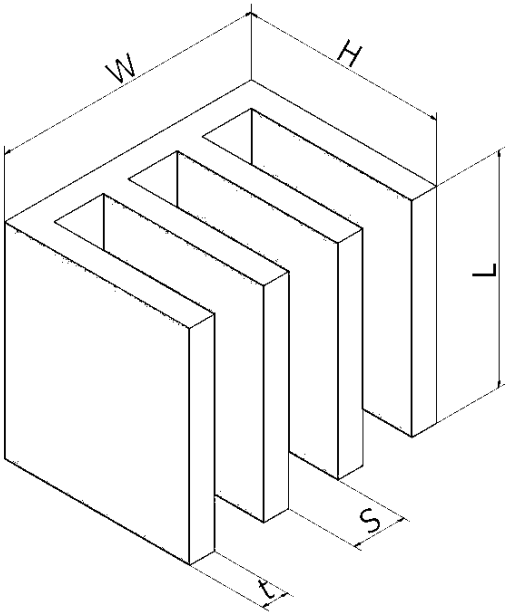

Figure 11: Dimension definition of a finned surface

3.5.1 Natural convection heat transfer coefficient

If the spacing between the vertical plates is taken to be the characteristic length the Raleigh number is calculated by (Çengel & Ghajar, 2008):

$$Ra_S = \frac{g\beta(T_s - T_\infty)S^3}{\nu^2} Pr \qquad (41)$$

For vertical isothermal plates the recommended relation for the Nusselt number is (Çengel & Ghajar, 2008):

$$Nu = \left[\frac{576}{(Ra_S S/L)^2} + \frac{2{,}873}{(Ra_S S/L)^{0.5}}\right]^{-0{,}5} \qquad (42)$$

The optimum fin spacing for a constant temperature surface is (Çengel & Ghajar, 2008):

$$S_{opt} = 2{,}714\left(\frac{S^3 L}{Ra_S}\right)^{0{,}25} \quad (43)$$

By substitution of the three equations above it can be shown that (Çengel & Ghajar, 2008):

$$Nu = 1{,}307 \quad (44)$$

3.5.2 Forced Convection heat transfer coefficient

For the laminar flow between the fins the Nusselt number is taken as 7,54 and can be calculated for turbulent flow using the following equation (Çengel & Ghajar, 2008):

$$Nu = 0{,}023\, Re^{0{,}8}\, Pr^{0{,}4} \quad (45)$$

Where the Reynolds number is evaluated using the fin spacing.

3.5.3 Assisting Flow heat transfer coefficient

The natural convection Nusselt number is combined with the forced convection Nusselt number in the following equation in order to calculate the overall Nusselt number (Mills, 1999):

$$Nu = \left(Nu_{natural}^3 + Nu_{forced}^3\right)^{1/3} \quad (46)$$

With the Nusselt number and the fin spacing known the heat transfer coefficient can be calculated from (Çengel & Ghajar, 2008):

$$h = \frac{Nu\, k}{S_{opt}} \quad (47)$$

3.5.4 Condensation heat transfer coefficient

Refrigeration condensers mostly operate under annular flow conditions. The following correlation scheme has been recommended (Mills, 1999). First the Reynolds number is calculated for each phase respectively:

$$Re_l = \frac{G(1-x)D}{\mu_l} \quad (48)$$

$$Re_v = \frac{G\ x\ D}{\mu_v} \quad (49)$$

Followed by the Nusselt number for Re_v > 35000 (Mills, 1999):

$$Nu = 0{,}15\ \frac{Pr_l {Re_l}^{0,9}}{F}\left(\frac{1}{\chi} + \frac{2{,}85}{\chi^{0{,}476}}\right) \quad (50)$$

Where χ is the Martinelli parameter (Mills, 1999):

$$\chi = \left(\frac{\mu_l}{\mu_v}\right)^{0,1}\left(\frac{1-x}{x}\right)^{0,9}\left(\frac{\rho_v}{\rho_l}\right)^{0,5} \quad (51)$$

and *F* represents the thermal resistance of the annular film (Mills, 1999):

$1125 < Re_l$ $\quad F = 5\ Pr_l + 5\ \ln(1 + 5\ Pr_l) + 2{,}5\ \ln\left(0{,}0031\ {Re_l}^{0,812}\right)$ (52)

$50 < Re_l < 1125$ $\quad F = 5\ Pr_l + 5\ \ln(1 + 5\ Pr_l) + 2{,}5\ \ln\left(0{,}0031\ {Re_l}^{0,812}\right)$ (53)

$Re_l < 50$ $\quad F = 5\ Pr_l + 5\ \ln(1 + 5\ Pr_l) + 2{,}5\ \ln\left(0{,}0031\ {Re_l}^{0,812}\right)$ (54)

The Nusselt number for Re_v<35000 (Mills, 1999):

$$Nu = 0{,}728\ K\left[\frac{g\ \rho_l\ (\rho_l - \rho_v)\ D^3\ h_{lv}}{\mu_l k_l (T_{sat} - T_w)}\right]^{0,25} \quad (55)$$

Where (Mills, 1999):

$$K = \left[1 - \left(\frac{1-x}{x}\right)\left(\frac{\rho_v}{\rho_l}\right)^{2/3}\right]^{-0,75} \quad (56)$$

3.5.5 Pressure gradient

Assuming homogenous flow through the condenser the pressure gradient in a straight horizontal tube can be simplified to (Mills, 1999):

$$\frac{dP}{dz} = \left(\frac{dP}{dz}\right)_F + \left(\frac{dP}{dz}\right)_M \quad (57)$$

3.6 Solar collectors

A solar collector contains the optical part along with the energy conversion path, from solar radiation to thermal, in a solar thermal energy system. Solar collectors are used to add thermal energy to a liquid medium flowing through the collector in order to use or store the thermal energy elsewhere. Figure 12 below shows a basic solar collector with its components and energy flow paths (Gauché, 2012).

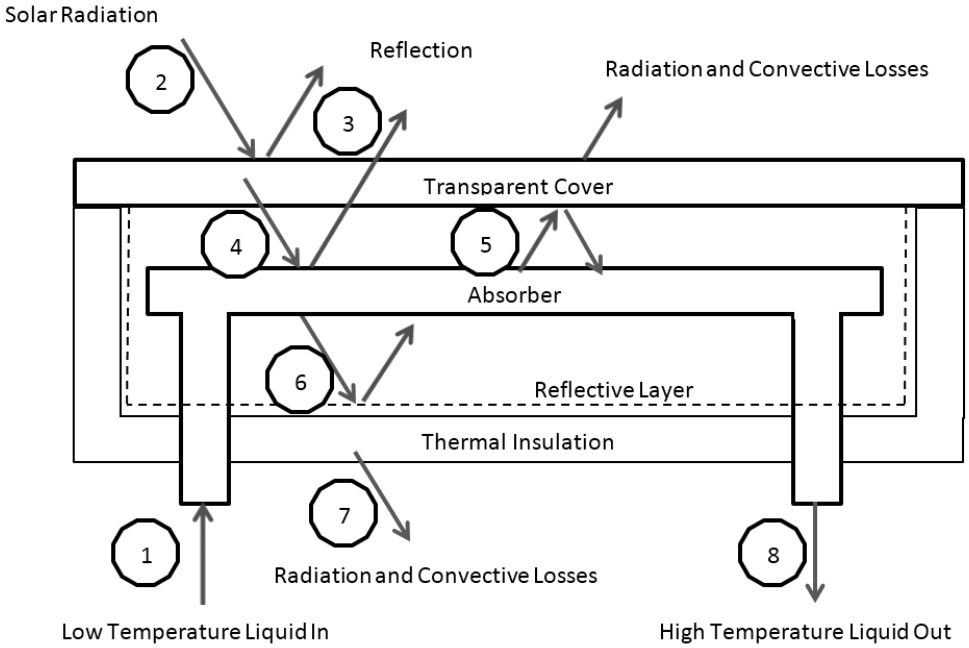

Figure 12: Energy flows in a basic solar collector (Gauché, 2012)

The basic solar collector in Figure 12 operates in the following way:

1. Liquid enters the solar collector at a low temperature.
2. Solar radiation hits the collector face.
3. Due to the nature of the cover a small portion of the radiation is reflected. At this point the spectral distribution is still the same and the cover appears transparent.
4. The rest of the radiation is allowed to pass through the cover and hits the absorber and the electromagnetic radiation is converted into thermal energy, heating the absorber.
5. Due to the elevated temperature of the absorber it now starts to loose heat in the form of thermal radiation and convection. Due to the relatively low temperature of the absorber the radiation frequencies are substantially lower and at these lower frequencies the cover appears opaque and acts as a radiation shield.
6. The cover now absorbs the radiation which in turn causes the cover temperature to rise. Energy is then lost from the solar collector via radiation and convection losses at the cover.
7. A reflective layer is used to line the interior of the collector to limit losses through the back and sides of the collector.
8. To further reduce the losses insulation is added to the back and sides of the collector but convective and radiation losses still occur at the outer surfaces.
9. The liquid now exits the solar collector at a raised temperature due to the addition of thermal energy from the absorber.

There are various types of solar collectors available such as uncovered absorbers, glazed flat plate solar collectors, flat plate collectors with selectively coated and evacuated tube solar collectors. Figure 13 below shows the performance of typical samples of each type of collector (Gauché, 2012).

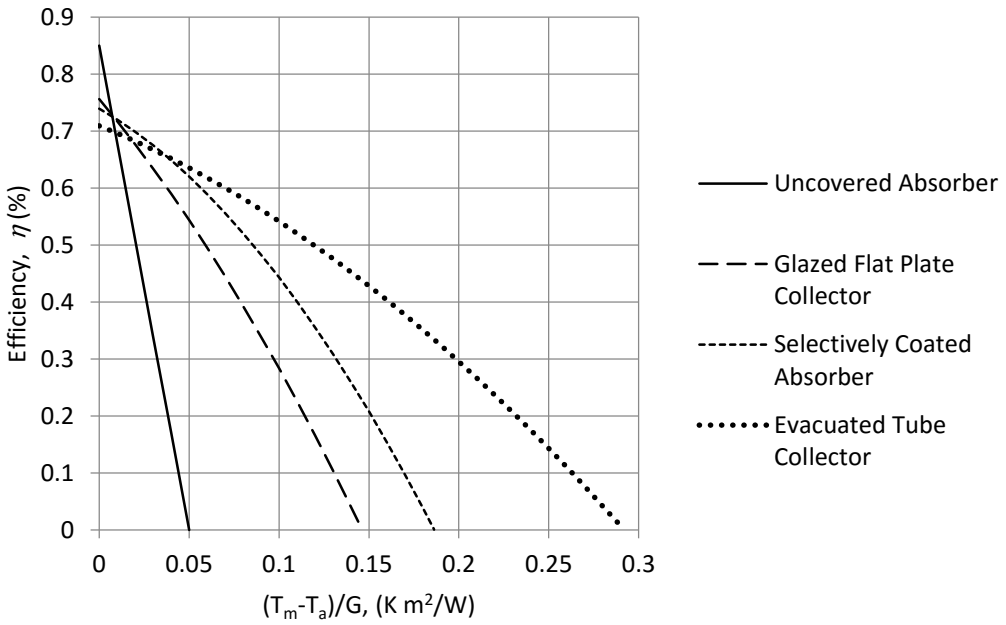

Figure 13: Typical performance curves for various types of solar collectors (Gauché, 2012)

The efficiency curve is normalized for the solar radiation, G, and the difference between the average collector temperature and the ambient temperature. From Figure 13 it can be seen that an uncovered absorber offers the highest maximum efficiency, but the maximum outlet temperature is the lowest. In contrast an evacuated tube collector has the lowest maximum efficiency and the highest outlet temperature. The flat plate collector with the selective coating offers high outlet temperatures and average efficiency, but it offers the largest aperture and thus the best output per m^2 of installation. Due to this high output the flat plate collector with the selective coating will be used in simulations.

3.7 Levelized Cost of Electricity

The LCOE combines the capital cost and operation cost of an electricity generation unit and normalizes these cost over the system lifetime. The LCOE is calculated using the formula below (NREL, 2013):

$$LCOE = \frac{1}{E}\left[\frac{rI}{1-\frac{1}{(1+r)^N}} + O\right] \quad (58)$$

4. Experimental Test System

The schematic given in Figure 14 shows the various components that are required to build the experimental system. The design requirement of each system component is discussed in this section. Figure 14 also shows all the needed instrumentation, thermocouples for temperature, pressure transducers and flow meters, for the purpose of the experiment.

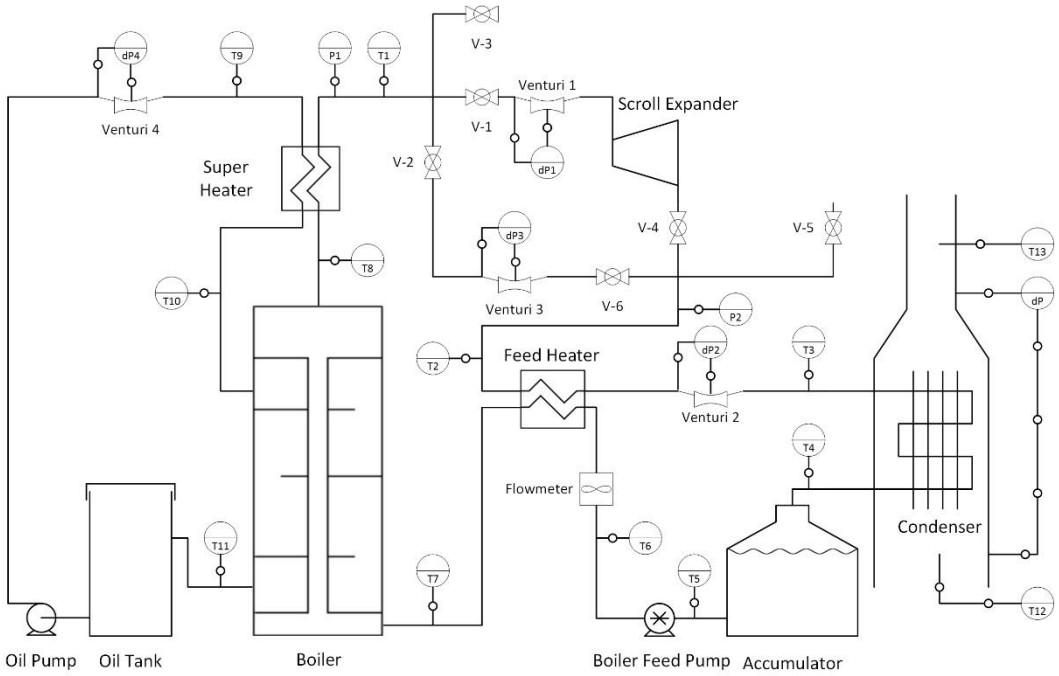

Figure 14: Experimental system schematic

Liquid is pumped from the accumulator to the FH by the boiler feed pump. The volume flow rate is measured at the outlet of the pump. The liquid stream is heated by the vapour stream exiting the turbine in the FH. Liquid then enters the boiler where thermal energy is transferred from the oil to the working fluid. The outlet stream of the boiler then passes through the super heater where additional thermal energy is transferred from the oil to the working fluid to ensure that liquid does not enter the expander.

The vapour stream then passes through the scroll expander where energy is extracted from the fluid and converted to mechanical energy. The mechanical energy is then converted to electrical energy by the electric generator attached to the scroll expander. A bypass valve was installed to divert flow away from the scroll expander if needed. This

can also be used to control the rotational speed of the scroll expander. A venturi flow meter was installed in each line to monitor the flow rate through each path.

The combined flow then passes through the FH to pre heat the liquid flowing to the boiler. A third venturi flow meter is installed at the FH outlet to confirm the measurement from the bypass line and the scroll expander line. The vapour then enters the natural convection condenser where the energy is transferred from the working fluid to the air flowing over the fins of the condenser. Liquid leaves the condenser and flows to the accumulator.

The as design specified operating points are given below in Table 1. For design purposes the isentropic efficiency of the pump was take to be 60% and the isentropic efficiency of the scroll expander was taken to be 50%. The required electrical output was chosen as 1 kW. Using the inlet and outlet enthalpy of the scroll expander in Table 1 below the mass flow rate could be calculated as 0,0833 kg/s. For a sample calculation see Appendix I

Table 1: Design operation conditions for ORC

Point Number	Temperature (K)	Temperature (°C)	Pressure (Bar)	Entropy (J/kgK)	Enthalpy (kJ/kg)	Description
1	315,71	42,71	2	1,1463	243,12	*Pump Inlet, Condenser Outlet*
2s	315,5	42,5	8	1,1463	243,22	*Isentropic Pump Outlet*
2	315,5	42,5	8	1,1452	243,29	*Pump Outlet, FH Cold Inlet*
3	342	69	8	1,2274	270,18	*FH Cold Outlet, Boiler Inlet*
3,*l*	373,36	100,36	8	1,3278	306,01	*Saturated Liquid*
4	373,36	100,36	8	1,6863	439,88	*Boiler Outlet, Super heater Inlet*
5	383	110	8	1,7075	448,11	*Super heater Outlet, Turbine Inlet*
6s	338	65	2	1,7075	422,86	*Isentropic Turbine Outlet*
6	354,5	81,5	2	1,7411	435,49	*Turbine Outlet, FH Hot Inlet*
7	321,2	48,2	2	1,667	408,59	*FH Hot Outlet, Condenser Inlet*
8	315,71	42,71	2	1,1463	243,12	*Condenser Outlet, Pump Inlet*

The design operating points are presented in the form of a *T-s* diagram in Figure 15.

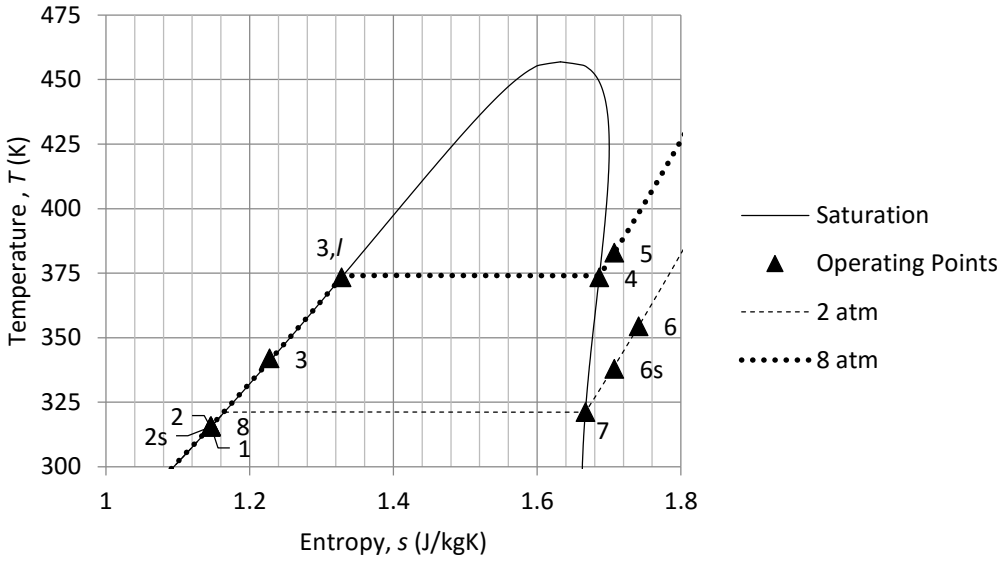

Figure 15: *T-s* diagram indication the design operation conditions

With both the design operating conditions and mass flow rate the nominal capacity of each component could be calculated. The nominal design capacity of each component is given in Table 2 along with the required capacity.

Table 2: The nominal design capacity and required capacity of the ORC components

Component	Nominal Design Capacity	Required Capacity
FH (kW)	2,2	3
Boiler (kW)	14,1	20
Condenser (kW)	13,8	20
Super Heater (kW)	0,7	3
Turbine (kW)	1,05	3
Oil Tank (kW)	14,8	15
Boiler Feed Pump (kW)	0,014	0,02

4.1 Working Fluid

In utility scale electricity plant water is used as the working fluid. When water is used as working fluid the minimum condenser temperature for a positive pressure is 100°C, but the aim of this project is to generate electricity from a low temperature heat source (80°C

to 120°C). Thus a different working fluid is required with a boiling point much lower than that of water (100°C at 1 atm). Such fluids are normally used in the refrigeration and air-conditioning industries and are thus called refrigerants. Refrigerant boiling points vary from about -80°C for R23 to almost 27°C for R123 at 1 atm (NIST, 2013). The lower boiling point allows the system to maintain positive pressures, while operating at lower temperatures.

4.1.1 Requirements

Safety is important in this project, as in any project, and thus a decision was made to limit the maximum pressure of the system. Since the pneumatic pressure in factories is usually limited to 8 bar the maximum pressure of the system was chosen as 10 bar. This means that the pressure of the working fluid at 120°C must be less than 10 bar. At the same time the low pressure side must maintain a positive pressure so that the system cannot be contaminated if leaks occur because the flow would be from the system to the environment. A positive pressure is also more favourable for leak detection and sealing of the experimental system. The working fluid must not be harmful to the environment and/or personnel in case of leaks. This eliminates all flammable and toxic working fluids from contention.

4.1.2 Comparison and Selection

The properties of suitable working fluids are high densities, low cost, moderate pressures in heat exchangers, low ODP and GWP (Marion, Voicu, & Tiffonnet, 2012, p. 104). Various refrigerants are shown in Table 3 (NIST, 2013).

Table 3: Refrigerant properties (NIST, 2013)

Refrigerant	Property					
	Density @ 20°C (kg/m^3)	Boiling Point (°C)	Pressure @ 120°C (Bar)	ODP	GWP	Type
R 123	1477	26.7	7.9	0	0.02	Dry
R134a	1225	-26.3	40	0	1300	Wet
R 11	1488	23.8	8.3	1	4000	Isentropic

R11 was eliminated due to the large environmental impact and R134a requires the operation pressure to exceed the maximum allowable pressure. This leaves R123 which satisfies all the requirements. It has a high density, moderate pressures in the heat exchangers, low ODP and GWP. R123 unfortunately is only available in bulk in South Africa, thus an excessive amount had to be purchased greatly increasing the cost of the project. The *T-s* Diagram with constant pressure lines for R123 is given in Appendix A, Figure 25.

4.2 Boiler Feed Pump

The working fluid is pumped from the accumulator through the feed heater to the boiler by the boiler feed pump. The pump has to overcome the pressure loss of the entire system and control the flow rate throughout the system. The pump converts electric power into mechanical power that is transferred to the fluid. The electricity consumption of the pump directly influences the overall system efficiency. The higher the electricity consumption of the pump, the lower the system efficiency will be.

4.2.1 Requirements

For the boiler feed pump the requirements were a head in the order of 6 bar and a small flow rate of about 200 L/h. The pump has to be compatible with the refrigerant chosen as working fluid and no leakage is allowed.

4.2.2 Comparison and Selection

After the appropriate research was completed it was concluded that the pump requirements could only be met by a positive displacement pump. This narrowed the choice to two pumps. Both were magnetically coupled to prevent leaks and both were rotary vane pumps. Pump specifications are given in Table 4.

Table 4: Boiler feed pump specifications (Fluid-o-Tech, 2011) (NU.ER.T Srl, 2012)

Property	Pump Model	
	Fluid-o-Tech TMOT104A	NU.ER.T. MAG-PR2 SXE
Max Flow Rate (L/h)	250	250
Max Head (Bar)	13	17
Electric Motor (W)	90	180
Material	Brass	Stainless Steel
Lead Time (Weeks)	6-7	4
Cost (R)	R 15 561,00	R 5 900,00

Both of the pumps meet all the requirements, but the NU.ER.T. pump consumes twice the amount of electricity. The difference in price however is too significant to be ignored along with the shorter delivery time. This motivated the pump from NU.ER.T. to be imported from Italy. For the exact pump curve refer to Appendix B, Figure 26.

4.3 Heat Exchanger

The system contains three heat exchangers. A feed heater, a boiler and a super heater. Initial cost per unit heat transfer (R/kW) along with size considerations have led to more research into plate heat exchangers (PHE) and their performance characteristics. The research showed that PHEs are commonly used for such applications.

4.3.1 Requirements

The FH is required to recover as much heat as possible from the expander vapour outlet stream and heat the liquid entering the boiler. Taking into account the design operation temperatures the maximum heat that can be recovered is 2,2 kW. The design and required capacity is given in Table 2 as 2,2 kW and 3 kW respectively.

The boiler must be capable of vaporizing the liquid entering. The design capacity is given in Table 2 as 14 kW and the required minimum capacity as 20 kW, allowing enough spare capacity, 6 kW, if the FH or super heater fail.

From Table 2 the super heater nominal capacity is 0,7 kW and the required capacity is 3 kW. The PHEs must be able to handle the maximum pressure of 10 bar with a safety factor of at least 1,5 at the maximum temperature of 120°C.

4.3.2 Comparison and Selection

For each PHE two different manufacturers were considered. Due to the similarity between the feed heater and the super heater the same size PHE was chosen for both. Alfa Laval is an extremely high quality product and offered the most cost effective solution that satisfied the requirements. The specifications for the two different PHEs are given in Table 5 below. The AC-70X-20M was chosen for the feed heater and super heater while the CB30-50H was chosen to serve as a boiler. The technical specifications of the AC-70x-20M and the CB30-50H are given in Figure 27 and Figure 28 respectively.

Table 5: Plate heat exchanger specifications (Mechinox Heat Exchangers, 2011)

Property	Model	
	Alfa Laval AC-70X-20M	Alfa Laval CB30-50H
Max Pressure (bar)	32	32
Allowable Pressure Safety Factor	3,2	3,2
Capacity (kW)	2,1	22
Maximum Temperature (°C)	150	225
Cost (R)	R 5 633,88	R 8 184,06

4.4 Scroll Expander

Vapour travels from the super heater to the scroll expander where the mechanical energy of the fluid is transferred to the scroll expander. The scroll expander is connected to an electric generator to which the mechanical energy is transferred and converted into electricity.

4.4.1 Requirements

Research showed that an inexpensive alternative to a turbine is to convert a scroll compressor into a scroll expander. The electric generator and scroll assembly should be able to generate about 1 kW of electricity. It must also be possible to modify the scroll compressor so that it can operate in reverse. This entails removing the no return valve inside the compressor assembly.

4.4.2 Comparison and Selection

The ZR40k3e-TFD Copeland scroll compressor was selected to serve as a scroll expander. The non-return valve was removed and the compressor was modified to allow maintenance checks to be performed (Reid, 2010). The scroll expander housing includes

an electric motor capable of producing 3 kW of electricity at the manufacturer design flow rate of 157 l/min.

4.4.3 Scroll Compressor Conversion

In order to allow the scroll compressor to operate in reverse some modifications had to be made. The compressor was cut open to allow access to the scroll for maintenance and wear checks during operation. Two flanges were welded to either side to facilitate the opening and closing of the unit. Furthermore the non-return valve located at the compressor outlet (turbine inlet) had to be removed to allow fluid to flow in the opposite direction.

The first attempt suffered from severe leakage at the scroll inlet and downward pressure on the scroll increased the friction considerably. During air tests it was found that the system flow rate would not allow the generator to spin at the required revolutions per minute. The scroll compressor was thus scrapped and replaced with a smaller model, ZR28, allowing design problems with the first attempt to be corrected. The final design for the replacement scroll expander can be seen in and Figure 30 to Figure 33 in Appendix D.

4.5 Condenser

The vapour that exits the feed heater is fed to the condenser where it is cooled until it returns to liquid from. The liquid then exits the condenser and flows to the accumulator tank where it is stored until the process repeats itself. Air cooled condensers reject the heat to the surrounding air and therefore the condenser performance is a function of the ambient temperature. Due to the proposed application of this system it was assumed that most of the system operation would be during the evening when the ambient temperature has already began to decrease. This meant that the size of the condenser could be decreased significantly cutting expenses.

4.5.1 Requirements

No size constraints were placed on this component, the emphasis was shifted to the amount of electricity consumed. The condenser had to use natural convection and allow

for the fitment of a fan at a later stage if necessary. The condenser must be able to deliver 20 kW of cooling to the system.

4.5.2 Design Specifications

In order to maximise the natural convection and minimize the pressure drop, the fin spacing of the condenser was chosen to be 6 fins per inch, the lowest offered by the manufacturer. The condenser coil was designed to have 12 passes and 4 rows with a sheet metal plenum that could be calibrated to allow for the measurement of the air flow across the coil. The fin depth was chosen to be 110 mm while the width was limited to 760 mm and the length calculated as 1500 mm. The plenum dimensions can be seen in Appendix E, Figure 34.

4.6 Electric Heaters

For the purpose of the experimental system electric heaters were chosen to heat the oil in the oil tank and serve as a heat source. Electricity offers a heat source that is both easy to control and very reliable. This allows the user to control the temperature of the oil independently from the vagrancies of the weather. The electric heaters would be replaced with a solar thermal heat source for the final system.

4.6.1 Requirements

Due to the nature of the oil the maximum heat flux must not exceed 2,4 W/m^2. The total heating capacity is required to be 15 kW. It was noted that more elements offer better control of the temperature and energy input to the system, but the cost is increased. Additionally the elements should be able to reach 120°C.

4.6.2 Comparison and Selection

As the amount of elements increase the capacity of each element decreases. Due to the maximum heat flux an increase in heating capacity will result in an increase in element size. Larger elements will result in a larger oil tank which increases cost. An optimal solution was found to be 10 heating elements with a capacity of 1,5 kW each. The heaters were custom made to offer uniform heating and spacing in the oil tank.

4.7 Oil Circulation Pump

The oil circulation pump circulates hot oil through the super heater and boiler to simulate a heat source.

4.7.1 Requirements

The first requirement for the oil circulation pump is that it should be able to circulate oil at temperatures up to 120 °C. The second requirement is that the flow rate and head should be sufficient for the system. The flow rate specified was around 1 l/s, this limits the change in temperature to less than 10 °C. The high flow rate and small change in input temperature ensures a high rate of heat transfer and reduces the cost and size of the plate heat exchangers.

4.7.2 Comparison and Selection

Research showed that while circulating pumps are easy to find the oil that has to be pumped complicates the selection process. Due to the nature of the oil special seals have to be fitted to reach the temperature requirement. Three different options were compared and the details are listed below in Table 6.

Table 6: Oil pump specifications (Grundfos, 2012) (NU.ER.T Srl, 2012) (Viking Universal Seal Pumps, 2007)

Property	Pump Model		
	Wilo IPH-W 32/125-0, 18/4	**Grundfos CR3-3**	**Viking HL 124**
Pump Type	Single stage centrifugal	3 stage centrifugal	Gear
Maximum Temperature (°C)	210	120	232
Max Flow Rate (L/s)	2,4	1,25	1,56
Max Head (Bar)	0,5	1,4	14
Electric Motor (W)	180	370	2 200
Lead Time (Weeks)	6-8	1	1
Cost (R)	R 18 069,00	R 6 502,56	R 15 180,24

The Grundfos pump met all the requirements, but has the lowest maximum operating temperature. Having a higher maximum operation temperature would make the system

more flexible and increase the electrical output. The increase in price, however, does not justify the higher operating temperature. Therefore the Grundfos pump was purchased. For more detail regarding the pump and its operating curve refer to Figure 35 and Figure 36 in Appendix F.

5. Experimental Work

In this chapter the procedures followed during the experimental work are discussed to ensure the accuracy and repeatability of the results. Before the operator is allowed to start the ORC he/she should familiarise themselves with the safety risks and concerns as stipulated in Appendix H. If the operation procedure is not followed this machine could cause serious injuries to the operator, as also discussed in Appendix H.

5.1 Experimental Procedures

To ensure the accuracy of the experimental results all thermocouples were calibrated as discussed in Appendix G. The calibrations data is presented in Table 9 and Table 10 in Appendix G while the constants for each thermocouple are given in Appendix G, Table 11. The procedures are divided into 3 phases namely the start-up, power generation and shut-off phase. For the duration of the start-up phase the oil is heated to the desired temperature for power generation. The power generation phase is entered when the oil temperature has stabilized while the shut-off phase is entered once the experiment has been concluded.

5.1.1 Start-up Phase

The start-up phase procedure is as follows:

1. Ensure that all the heating elements are plugged in along with the control box and the sensors.
2. Connect the sensors to a computer to enable monitoring of the system during the start-up phase.
3. Check that the control box has power, increase the thermostat temperature from the minimum until you can hear the relays in the control box engage. The temperature should be close to the ambient temperature. Repeat with the second thermostat.
4. Switch on the oil pump. Ensure that the pump is functioning properly by visually confirming that oil enters the outlet pipe of the oil tank. Also check that the oil flow sensor is registering flow. If either of these checks fail, open the valve located at the highest point in the galvanised pipe section to allow air to escape, but care must be taken to avoid oil spillage. If this fails to resolve the problem or if the

system has not been used recently it may be necessary to prime the pump. There is a port located on the front of the pump for this purpose. Loosen the plug in the port until the sound of air escaping is audible. Note that the plug should not be removed completely since there is only a small amount of air trapped in the pump and the time needed to react to oil starting to flow from the port will result in excessive spilling.

5. Let the pump run for a few minutes to ensure that all the air has been expelled from the system. Air bubbles flowing into the oil tank will be clearly audible.
6. Switch on the heating element switches. The lights of the switches should still be off at this point. Adjust the left thermostat to 30°C and the right thermostat to the desired testing temperature +5°C. Once the thermostats are adjusted the red switches of the heating elements should be illuminated. This is a visual indication that the heating elements are now on.
7. Wait until the thermostat switches the heating elements off. Continue this pattern until the set temperature is reached upon which the set temperature should be increased by 10°C – 20°C until the desired operating temperature is attained. Do not turn the pump off while the heating elements are still on. If the pump should stop during this operation immediately turn off all the heating elements to avoid overheating the oil.
8. Once the oil temperature has stabilised at the desired operating temperature the boiler feed pump can be switched on. Ensure that all the valves in the refrigeration loop are open prior to the pump start.

5.1.2 Power Generation Phase

The power generation phase should be operated as follows:

1. Once the boiler feed pump has been turned on the working fluid will start to heat up. Once the system temperatures have stabilized the bypass valve should be closed halfway.
2. Jump start the scroll expander by supplying 230 VAC and immediately switch the scroll expander off again. Check to ensure that the scroll is still spinning. If the scroll stops when the power is switched off, close the bypass valve a little and repeat the jump start sequence.

3. With the scroll spinning close the bypass valve completely. Allow the system to stabilize once more.
4. Load can now be applied to the generator. Apply load and wait for the system to stabilize before taking measurements. If the generator is overloaded the capacitor will drain, causing the magnetic field to collapse. This will cause the scroll to speed up excessively which will cause extra wear or even component failure. In the event that this occurs the generator load should be disconnected immediately. The scroll should then be jump started again to get the magnetic field back.

5.1.3 Shut-Off Phase

When the testing is complete turn the heating elements off, but keep the pumps running. Leave the system running until the oil temperature falls below 60°C. Do not leave the system unattended while the oil is above 60°C.

5.2 Operation Checks

The following operational checks should be performed:

1. During operation the inlet pressure and temperature should be monitored constantly.
2. The inlet stream to the scroll should be checked to ensure that there no liquid present.
3. The boiler feed pump flow rate can be adjusted by setting the bypass valve on the pump.

5.3 Error Diagnostics

If the boiler feed pump leaks the O-ring on both sides of the rotary vane should be replaced. The refrigerant hardens the seals over time.

5.4 Accuracy and Error Analysis

For accuracy the thermocouples have been calibrated prior to installation as documented in Appendix G. Four flow meters have been installed so that the readings can be compared and used to obtain a more accurate reading. Energy analysis can be done for each component to verify the measured flow rate. Digital pressure transducers and analogue

pressure gauges have been fitted to increase accuracy. An analogue thermometer has also been placed on the oil line flowing from the reservoir to the super heater.

6. Feasibility Study

This section investigates the feasibility of the proposed system in terms of cost, system life span and the amount of electricity generated. Alternatives are also given and compared to the ORC system. The investigation was conducted for 2 locations, namely a remote location and an urban location. Both locations have electricity available from Eskom.

6.1 Initial Capital Cost and Running Cost

Assuming that the average temperature of the collector is 70°C and the solar radiation is 1000 W/m^2 the collector efficiency can be determined by using the collector curve such as the one in Figure 13 (Swanepoel, 2007). At the conditions given the collector efficiency is calculated as ±40%. To be able to generate 1 kW of electricity the system requires 13 kW of thermal energy as stated in Chapter 4. For 13 kW of thermal energy the collector aperture should be 32,5 m^2. The collector cost is ±R 1 800/m^2 (Imperial Crown Trading, 2009) and thus the collectors for the system would cost about R60 000. In addition to the collector cost the ORC system would cost about R 70 000, which brings the total system cost to R 130 000. The capacity factor for the ORC system is estimated as 20%, the same as the manufacturer provided for the PV alternative (Swanson, 2009), bearing in mind that the capacity factor is site specific. The running cost of an ORC is taken to be negligible with the only cost coming from refilling the R123 from time to time.

6.2 System Life Time

The system life is based on the component with the shortest operating life. For systems that utilize solar thermal radiation the first component to fail are normally the components exposed to the radiation. For the chosen solar collector the operating life span is given as 25 years (Imperial Crown Trading, 2009).

6.3 Alternatives

Similar assumptions were made in the analysis of the alternative solutions. For a petrol generator the overall efficiency was given by the supplier (Genpower, 2012) and the petrol price was taken to be R 13 per litre (AA, 2014). The diesel generator was calculated with a diesel price of R 12,50 (AA, 2014). For the generator the cost of electricity

generation was heavily reliant on the cost of fuel with the initial capital investment almost negligible.

For the renewable alternatives the opposite was found. The initial capital cost was the major contributing factor. For PV it was given that the initial capital cost was R 105 000 and operating life of the batteries is 10 years (Imperial Crown Trading, 2009). The capacity factor for this system was given by the supplier as 20% (Imperial Crown Trading, 2009). For wind the capacity factor was estimated at 30% and the initial system would cost about R 80 000 while the system life would be 10 years as it utilizes the same type of batteries as the PV system (Imperial Crown Trading, 2009).

The most expensive system was found to be a gas power ORC. This system has a high initial cost and uses a large amount of fuel in order to generate electricity. Since this system has no components exposed to the sun the system life is expected to be equal to that of the scroll expander and pump which is estimated at 30 years (Emerson Electric Co., 2014). The price of gas was taken to be R24/kg (Departement of Energy, 2014) and the thermal energy taken to be 13,8 kWh/kg (Afrox, 2013). The system cost was taken to be R 70 000, the same as the ORC system using solar radiation excluding the cost of the solar collectors.

Eskom tariffs for rural locations were taken from the monthly invoice. The residential tariffs were taken as R 1,40 from the Eskom tariff booklet (Eskom Holdings SOC Limited, 2012).

6.4 Comparison

In order to compare the different solutions the LCOE will be used. This incorporates the capital cost, fuel cost, the system life span and the amount of electricity generated. The systems were all scaled for the same amount of electricity usage per month. The LCOE is influenced greatly by the assumptions made and therefore comparison with other published works should be made carefully. All the assumptions and values are given in Table 7.

Table 7: Calculation and assumption of the LCOE for various technologies

	Gas ORC	Solar ORC	PV	Onshore Wind	Petrol Generator	Diesel Generator	Eskom Rural	Eskom Urban
System Life Span (Years)	30	25	10	10	5	10		
Discount Rate (%)	5%	5%	5%	5%	5%	5%		
Capital Cost (R/kW)	R 70 000	R 130 000	R 104 617	R 80 000	R 5 000	R 10 000		
Capacity Factor (%)	100%	20%	20%	25%	100%	100%		
Operation Cost (R/kW-year)	R 115 632				R 51 815,4	R 21 900		
Conversion efficiency (L/kWh)	1,1				0,91	0,4		
Fuel Cost (R/L)	R 24,00				R 13,00	R 12,50		
Electricity Price (R/kWh							R 3,90	R 1,00
Cost Escalation Rate (%)							10%	10%
Energy generated (kWh/year)	4380	4380	4380	4380	4380	4380		
WACC (%)	7%	7%	7%	7%	7%	7%		
LCOE (R)	R 27,69	R 2,55	R 3,40	R 2,60	R 12,11	R 5,33	R 3,90	R 1,00

Figure 16 shows the LCOE for each solution and the Eskom tariff for a rural and an urban location. The gas powered ORC is by far the most expensive solution than a petrol generator followed by a diesel generator.

The interest of this project, however, lies with the feasibility of an ORC. It is clear from Figure 16 that renewable technologies are more expensive to use than the Eskom grid in urban locations, but for rural locations PV, wind and solar ORCs are already viable options.

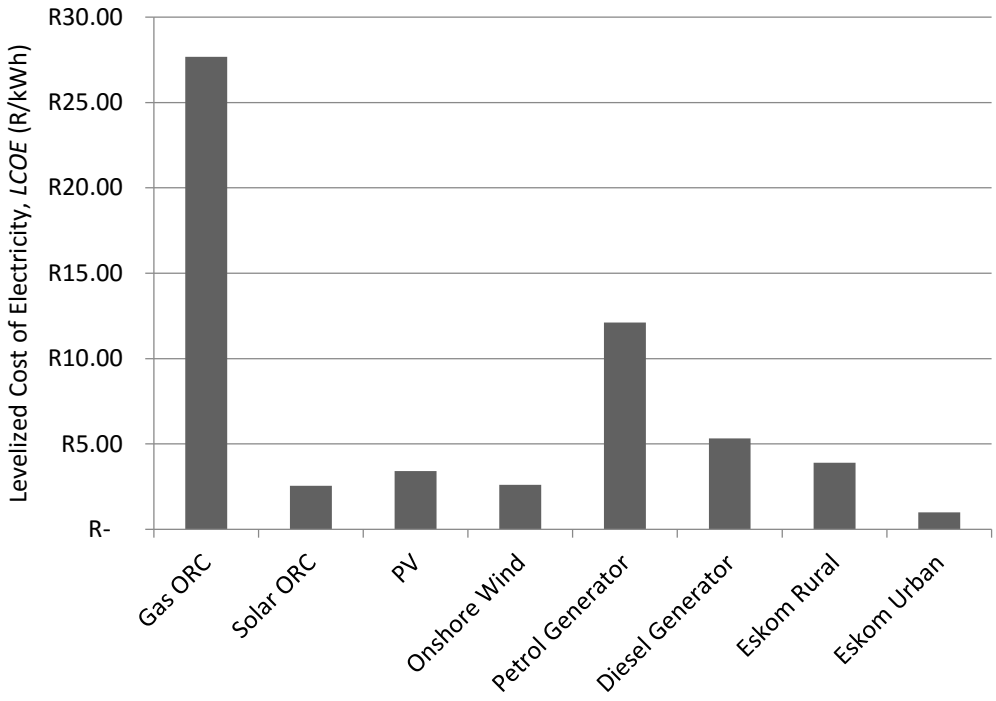

Figure 16: LCOE comparison for various technologies

6.5 Summary

The feasibility study indicated that currently the cost of electricity from Eskom in urban areas is still less expensive than the alternatives. In remote locations the cost of electricity from Eskom is higher than the LCOE of PV, wind and solar ORCs.

7. Results

The results calculated from theory are presented in this section along with the experimental results. Followed by a comparison of the theoretical results and the experimental results.

7.1 Calculated Results

For the given conditions at the 120°C set point the performance of the different components were calculated using the theory described in Chapter 3. Sample calculation are given in Appendix I.

7.1.1 Boiler Feed Pump Theoretical Performance

The theoretical flow rate that the pump can provide at a pressure difference of 4 bar is 220 L/h, or 0,091 kg/s. It should be noted that this flow rate is the maximum flow rate that the pump can deliver. If the bypass valve is opened the flow rate can be reduced to less than the predicted 0,091 kg/s.

7.1.2 Boiler Theoretical Performance

From the calculations it is evident that the overall heat transfer coefficient of the boiler is dominated by the convective heat transfer coefficient of the oil. Typical values for the convective heat transfer coefficient of the oil was calculated to be around 700 W/m^2K. This along with the log mean temperature difference brings the calculated capacity of the boiler to 8,6 kW, well below the 20 kW claimed by the manufacturer. One of the possible explanations for this discrepancy is the behaviour of two-phase flow in narrow channels.

7.1.3 Super Heater Theoretical Performance

Since the boiler capacity has been shown to be greatly reduced the super heater now serves as a secondary boiler. Therefore the same trend in heat transfer coefficients can be seen with the convective heat transfer of the oil dominating the overall heat transfer coefficient. For the super heater the typical heat transfer coefficient calculated for the oil was around 1600 W/m^2. This along with the log mean temperature difference brings the calculated capacity of the super heater to 4,3 kW.

7.1.4 Scroll Expander Theoretical Performance

The total energy available to the scroll expander is calculated as 1,8 kW, but heat loss through thermal radiation and convection reduces the energy to 1,05 kW. Insulation can be placed to reduce the amount of heat loss. The isentropic efficiency is expected to be about 50% which translates to 500 W of mechanical work. A turbine that has been designed specifically for the application can achieve a higher efficiency, up to 85% (Yagoub, et al., 2006). The expected performance is reasonable if the expander cost is taken into account.

7.1.5 Feed Heater Theoretical Performance

The FH has liquid R123 travelling from the boiler feed pump to the boiler. The liquid is heated by the vapour travelling from the scroll expander to the condenser. The overall heat transfer coefficient was calculated to be around 225 W/m^2K with the liquid and vapour heat transfer coefficients calculated as 510 W/m^2K and 400 W/m^2K respectively while the capacity was calculated as 2,75 kW for the operating conditions.

7.1.6 Condenser Theoretical Performance

The condenser heat transfer coefficient is dominated by the natural convection heat transfer coefficient on the air side. The heat transfer coefficient was calculated to be 6 W/m^2K on the air side and 400 W/m^2K on the working fluid side where condensation is taking place. Taking into account the different heat transfer areas the overall heat transfer was calculated as 10,95 kW.

7.2 Experimental Work

The experimental system was tested at three heat source temperatures: 80°C, 100°C and 120°C. The best results were obtained during the tests at 120°C and thus the system performance is discussed in detail for this set point with only observations stated for the 80°C and 100°C set points.

80°C: Even at this low temperature the system is able to generate mechanical energy through the scroll expander. The conversion from mechanical work to electrical energy is very low at these low scroll expander speeds, generating only 0,52 W.

100°C: The increase in temperature allows for an increase in pressure and flow at the inlet of the scroll expander. The combination of these factors increases the amount of mechanical energy extracted by the scroll expander, which in turn increases the efficiency of the system as a whole. The increase in flow causes an increase in rotational speed of the scroll expander which increases the conversion efficiency from mechanical energy to electrical energy slightly, generating 4 W.

120°C: For the current experimental system this is the maximum operating temperature, as per the manufacturer of the oil circulating pump. Again the increase in temperature and pressure allows more flow through the scroll expander, increasing the mechanical energy available for extraction. The increased flow rate corresponds to a higher rotational speed and therefore an increase in conversion efficiency and electrical output is measured at 40 W.

The operating temperatures and pressures are given in Table 8 with the cycle shown on a *T-s* diagram in Figure 17. The scroll expander inlet pressure reached about 5,2 bar absolute and a temperature of almost 113°C.

Table 8: System operation points at 120°C

Point Number	Temperature, *T* (K)	Enthalpy, *h* (kJ/kg)	Entropy, *s* (kJ/kg*K)	Pressure, *P* (Bar Absolute)	Description
1	297.216	222.990	1.080	1.895	*Pump Inlet, Condenser Outlet*
2	299.474	226.140	1.090	5.961	*Pump Outlet, FH Cold Inlet*
2s	297.500	223.080	1.080	5.961	*Isentropic Pump Outlet*
3	339.743	268.510	1.223	5.957	*FH Cold Outlet, Boiler Inlet*
4	357.172	393.020	1.743	5.372	*Boiler Outlet, Super Heater Inlet*
5	385.947	454.290	1.746	5.186	*Super Heater Outlet, Turbine Inlet*
6	368.300	446.468	1.770	2.302	*Turbine Outlet, FH Hot Inlet*
6s	356.000	437.055	1.746	2.302	*Isentropic Turbine Outlet*
7	315.219	388.410	1.599	1.992	*FH Hot Outlet, Condenser Inlet*
8	297.216	222.990	1.080	1.895	*Condenser Outlet, Pump Inlet*

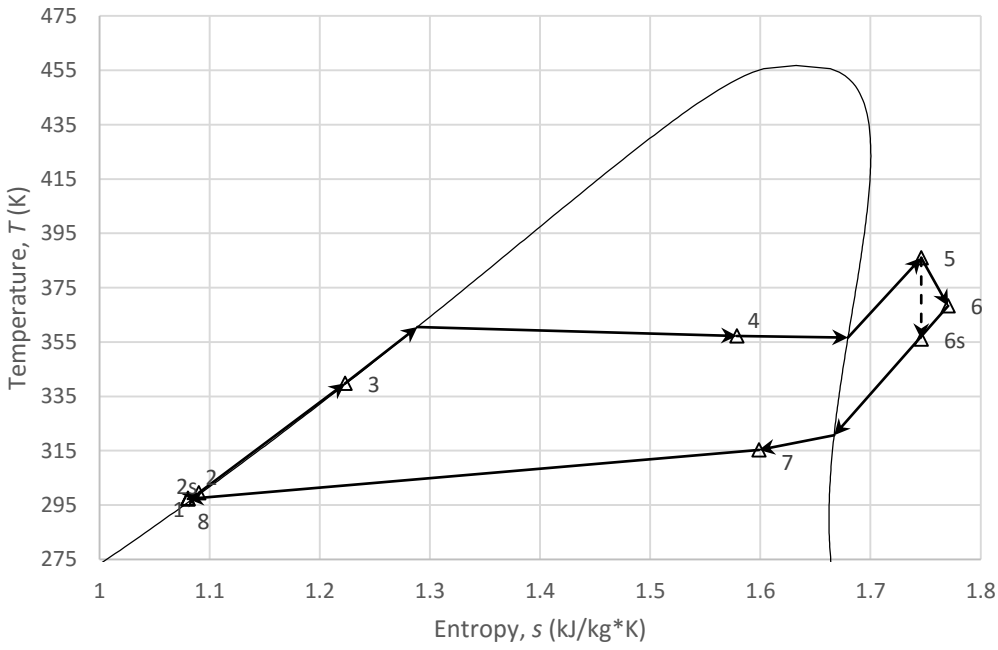

Figure 17: System *T-s* diagram for operation at 120°C

The *T-s* diagram indicates the performance of the system in its entirety while the performance of individual components is assessed further on. Though the *T-s* diagram is similar to the design specification the position of point 4 is expected to be located on the downward slope of the saturation curve. Therefore it is evident that the boiler performance is not satisfactory and requires further investigation. The expectation is that point 7 should fall on the saturation curve. The shift indicates that the FH performance is exceeding initial expectations and a more in depth analysis is required.

The performance of the super heater and the condenser seem to be satisfactory from the *T-s* diagram while the isentropic efficiency of the pump seems very low and requires further investigation. The *T-s* diagram does not offer much insight into the performance of the scroll expander.

7.2.1 Boiler Feed Pump Performance

The typical inlet temperature of the boiler feed pump was 24°C and the outlet temperature was about 26,3°C. The change in pressure over the pump was measured to be 4,1 bar at a measured flow rate of 0,067 kg/s. The power consumption of the pump was measured as 240 W. The isentropic efficiency was calculated to be 3%.

7.2.2 Boiler Performance

The boiler managed to transfer almost 8,2 kW of thermal energy from the oil to the refrigerant. With the oil inlet at 112°C and the outlet temperature at 111°C the mass flow rate was 1,08 kg/s while the liquid R123 entered at a temperature of 66,6°C and a mass flow rate of 0,067 kg/s. The 8,2 kW was enough to vaporize 75% of the fluid at a saturation temperature of 84°C.

7.2.3 Super Heater Performance

The super heater transferred 4,1 kW of thermal energy from the oil to the refrigerant. At the super heater exit all the liquid had been vaporized and the temperature recorded was 112,8°C. The oil entered at 113,8°C and a mass flow of 1,08 kg/s while at the super heater exit the temperature had decreased to 112°C.

7.2.4 Scroll Expander Performance

The refrigerant entered the scroll expander at a temperature of 112,8°C and a mass flow rate of 0,067 kg/s. At the scroll expander housing exit the temperature measured was 75,8°C. Taking into account the heat loss of 875 W through the housing the energy absorbed by the scroll expander was 566 W which correlates to a scroll exit temperature of 95,2°C. The isentropic efficiency was 47% while the overall efficiency for converting fluid power into electricity was a mere 7%.

The no-load voltage reached up to 120 V for this set point. The scroll expander was placed under load by switching on a 40 W bulb and a 100 W bulb. As the load increased the current drawn increased to 0,38 A, but the voltage decreased to 104 V. This brings the electric power to 39,5 W.

7.2.5 Feed Heater Performance

The FH recovered 2,8 kW from the refrigerant after it had passed through the expander and heated the liquid refrigerant between the pump and the boiler. The vapour temperature was 75,8°C at the FH inlet and 42°C at the outlet to the condenser while the liquid entered at 26,3°C and exited at 66,6°C. It was noted that the vapour started to condense in the FH.

7.2.6 Condenser Performance

The condenser extracted 11 kW of thermal energy from the R123 and transferred the energy to the air flowing over the fins. The R123 entered the condenser at a vapour quality of 0,86 and a temperature of 42°C. At the condenser outlet the vapour quality was 0 and the temperature had decreased to 24°C. The air entered the sheet metal plenum at 17°C and a relative humidity of 27%. At the outlet of the plenum the air temperature was measured to be 36,9°C and the relative humidity was 8%. The velocity profile at the outlet was measured and is shown in Figure 18.

The velocity was the lowest in the corners and highest in the centre. The velocity profile is as expected since the velocity at the wall is always zero. The shape of the velocity profile matches that found in literature reasonably well (Çengel & Cimbala, 2006). The outlet velocity, outlet temperature, inlet temperature and inlet relative humidity was used to calculate the air mass flow rate as 0,57 kg/s.

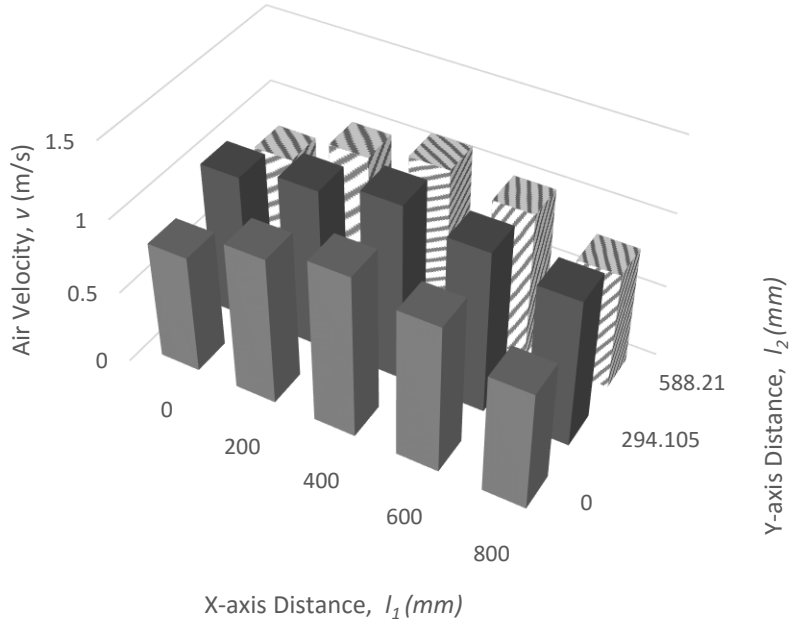

Figure 18: Condenser air outlet velocity profile at 120°C set point

7.3 System Performance

Considering the performance of the experimental system as a whole the following problem areas have been identified.

1. The boiler capacity is considerably less than what is required. The experimental results showing a capacity of 8,6 kW in comparison with the required capacity of 14,1 kW.
2. The conversion of mechanical energy to electricity by the scroll expander is very poor. The experimental efficiency calculated at 7%.
3. The volume flow rate through the scroll expander should be increased. The experimental flow rate was 20% less than the design flow rate. Increasing the volume flow rate would improve the performance of the electric generator attached to the scroll expander. A higher volume flow rate would increase the

rotational speed of the generator which would produce a higher output voltage. A higher output voltage would generate a stronger magnetic field. The stronger magnetic field would cause the motor to produce an even higher output voltage.

4. The amount of pressure measurement points should be increased. The pressure is currently only measured at 2 places in the system. The theoretical pressure drop through components have to be summed to enable the comparison with the experimentally measured pressure drop value. This makes the evaluation of the theoretical models very difficult. Increasing the number of pressure measurements would allow the comparison of the theoretical and experimental pressure drop through each single component.
5. The temperature control of the heating elements is very coarse and therefore slow to react to changes in temperature. A more sophisticated control system is needed. This would ensure a more constant heat source temperature and therefore more consistent experimental measurements.

7.4 Comparison and Discussion

Figure 19 shows the experimental and theoretical volume flow rate at the boiler feed pump outlet. The theoretical volume flow rate is considerably higher than the experimental volume flow rate. The deviation reaches about 31%. The cause of this deviation is the bypass valve located in the pump casing. The bypass valve was adjusted to reduce the flow rate through the boiler. The more fluid is allowed to flow through the bypass valve the larger the deviation from the theoretical volume flow rate will be.

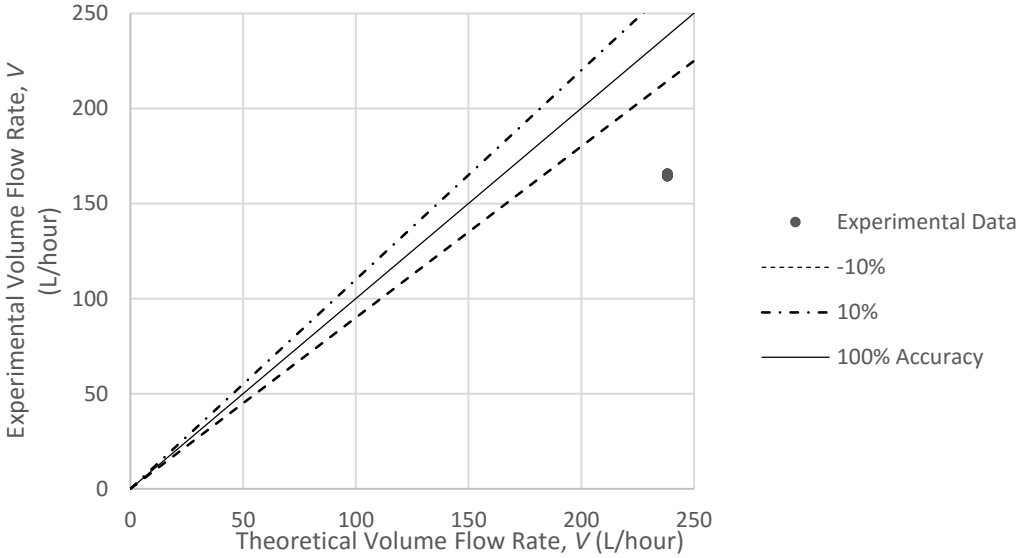

Figure 19: Comparison on the theoretical and experimental volume flow rate at the boiler feed pump outlet

Using the experimental temperatures and mass flow rate the theoretical model predicting the heat transfer rate to the working fluid in the boiler compares well to the experimental heat transfer rate. The theoretical model heat transfer rate for the boiler deviates from the experimental heat transfer rate with an average deviation of 3% and a maximum deviation of 5%. The boiler model consistently over predicted the heat transfer, therefore a small adjustment could be made to the constants given in Equation (20) and (21) to reduce the average and maximum deviation. The comparison is shown in Figure 20.

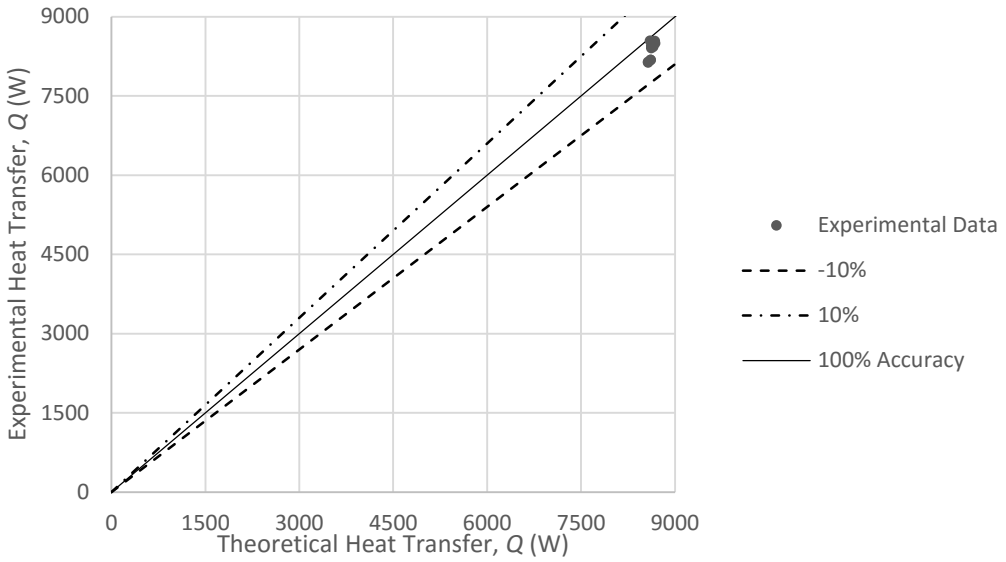

Figure 20: Comparison of experimental and theoretical heat transfer rates of the boiler

For the super heater the theoretical and experimental heat transfer deviated by a maximum of about 7%. In most cases the theoretical heat transfer was higher than the experimental heat transfer rate. The super heater theoretical model heat transfer rate showed an average deviation of 3% and a maximum deviation of 8% from the experimental heat transfer rate as shown in Figure 21. The model performance is satisfactory for the application, but shows a tendency to over predict the heat transfer rate. Adjusting the constants in equation (20) and (21) would result in a better fit to the experimental data, reducing both the average and the maximum deviation.

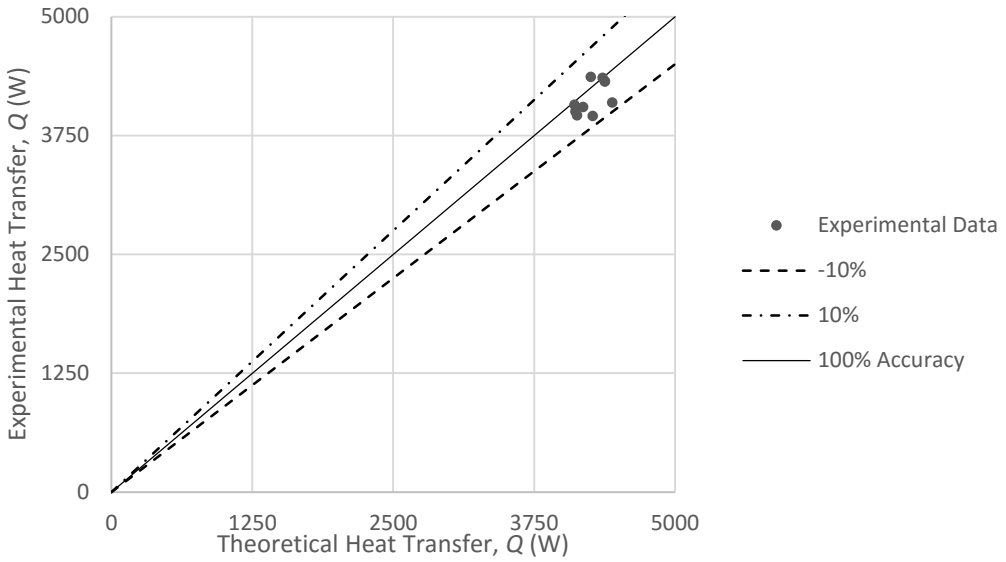

Figure 21: Comparison of experimental and theoretical heat transfer in the super heater

Figure 22 shows the theoretical and experimental energy lost by the ORC across the scroll expander. The scroll expander model showed an average deviation of 7% and a maximum deviation of 10%. The model only predicts the energy available to the scroll expander and could be expanded to include isentropic efficiency, rotational speed and mechanical output power.

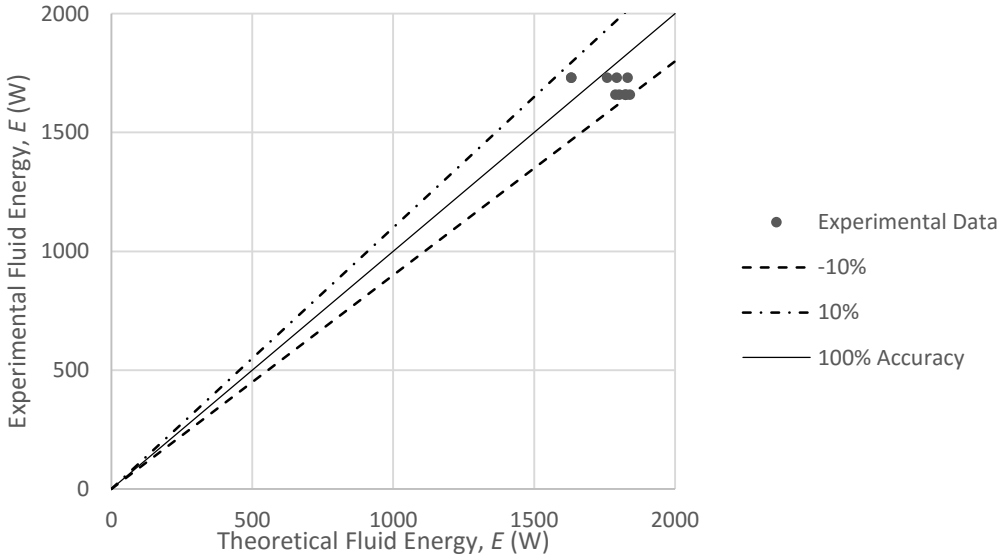

Figure 22: Comparison of the theoretical and experimental fluid energy at the scroll expander

The FH theoretical heat transfer rate closely matches the experimental heat transfer rate. The FH consistently under predicts the heat transfer rate by an average of 3% and a maximum of 4%. The accuracy could be improved by updating the model slightly, adjusting the constants in Equation (20) and (21) would fit the data better, reducing both the average and the maximum deviation.

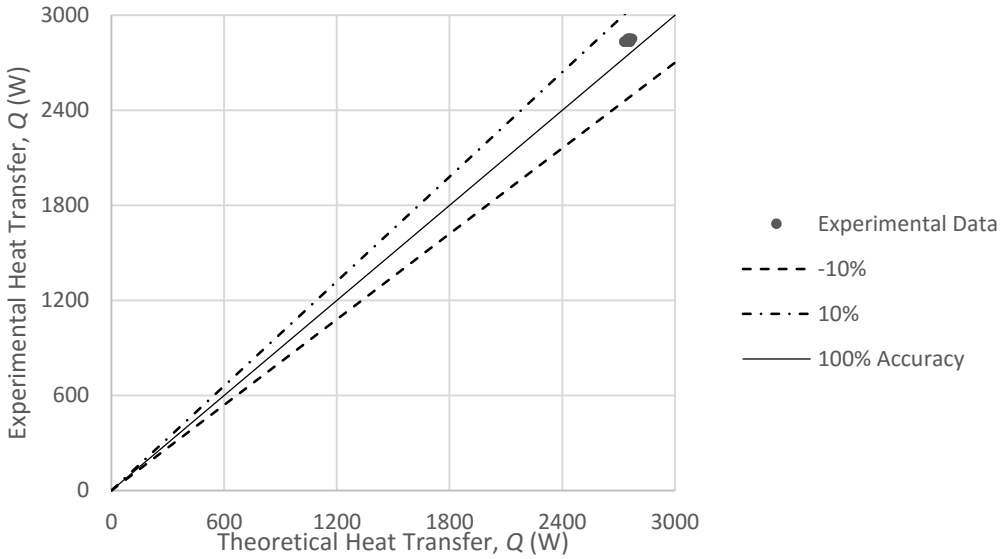

Figure 23: Comparison of the theoretical and experimental heat transfer of the FH

Figure 24 shows the theoretical and experimental heat transfer rate from the working fluid to the air flowing over the condenser fins. The theoretical heat transfer rate is consistently lower than the experimental heat transfer rate with an average deviation of 3% and a maximum deviation of 6%. The accuracy of the theoretical model could be improved by adjusting the constants in Equation (50) and (55). This would reduce both the average and the maximum deviation.

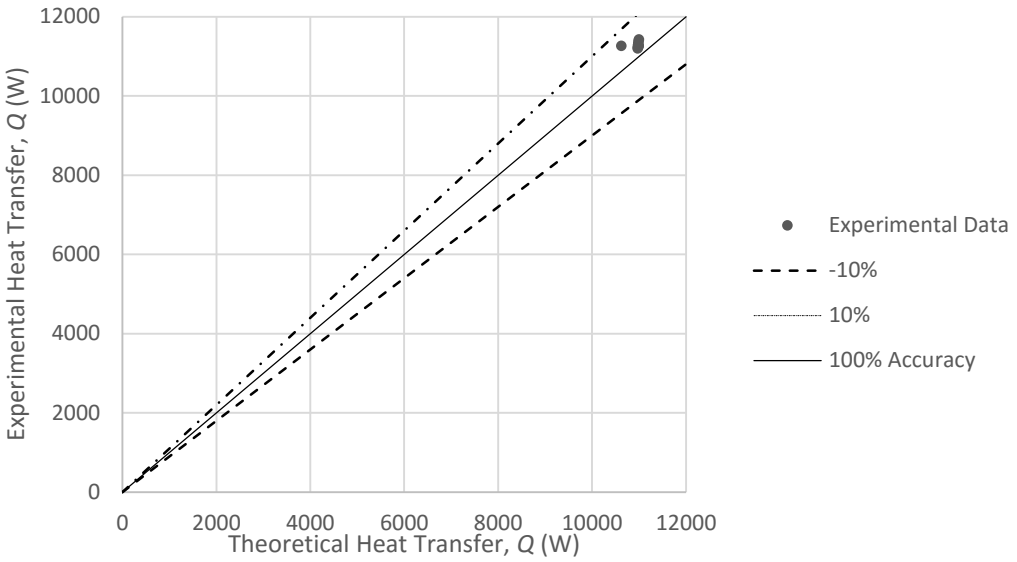

Figure 24: Comparison of the theoretical and the experimental condenser heat transfer

7.5 Feasibility

From the feasibility study conducted in this project it is determined that the LOCE of a solar ORC is less than the Eskom tariff making it a viable option for remote, off-grid electricity generation. Other renewable technologies such as wind and PV would also be possible solutions. In urban locations the LCOE of renewable technologies cannot yet compete with Eskom tariffs. With the current price increases in electricity and the decreasing cost of renewable technologies it would seem that around the year 2020 renewable technology systems would become viable solutions, even in urban locations. Renewables at utility scale should become cost effective solutions even sooner, but the large initial capital cost and the intermittency of electricity generation will delay construction. Concentrating solar power (CSP) with storage has however shown great promise with the only deterrent being the high capital cost.

8. Conclusions and Recommendations

Conclusions pertaining to the research conducted are given in this chapter along with recommendations. In particular the current system construction and performance, proposed upgrades to the current system and future work to be carried out on the system will be considered.

8.1 Feasibility Study

The feasibility study found that the ORC is currently a viable option for remote, off-grid electricity generation. The additional cost of line rental increases the Eskom tariff considerably. For urban generation the LCOE for renewable sources is still higher than the Eskom tariff. The increasing Eskom tariff and decreasing cost of renewable energy solutions should see renewable energy technologies become a financially feasible solution by the year 2020.

8.2 Model Upgrade

Overall the theoretical models performed satisfactory. It is recommended that the theoretical model of the pump should be updated to include the bypass valve to ensure better results. The scroll expander model should be improved to predict isentropic efficiency, rotational speed and mechanical work output.

Minor adjustments could be made to the boiler, super heater and FH theoretical models to improve results. Adjusting the constants is Equation (20), (21), (50) and (55) would provide a better fit for the experimental data. It is however recommended to test the theoretical model over a wider range of heat source temperatures and mass flow rates before such changes are made.

8.3 Component Performance

The pumps performed well, but the o-rings hardened over time causing the pump to start leaking. It is therefore recommended that the o-rings on the pump be replaced with some made of a more suitable material like Viton. This would stop the hardening and leaking problem that currently exists. Reference to the material safety data sheet should be made when selecting the material. It is also the recommendation of the designer that the

plumbing around the pump be changed in such a way that the pump can be used to charge the system with refrigerant from an external source.

The boiler performance was considerably less than the manufacturer claimed (Mechinox Heat Exchangers, 2011) due to the two-phase flow in the narrow passages between the plates. There are multiple ways to increase the capacity, three of which are given here:

1. Raising the oil temperature would increase the boiler capacity, but this would require a different pump and thermostats. It should be noted that the design temperature of the boiler is 150°C and the temperature should not be raised higher than this point.
2. If the oil is changed to water the heat transfer characteristics improve considerably and therefore increases the boiler capacity. However, for water to reach 120°C the oil tank would have to be exchanged for a sealed unit that can handle the saturation pressure of water at 120°C.
3. The simplest solution would be to replace the oil with a heat transfer fluid, for ex. Dowtherm. This requires no modifications to the system while offering an increase in boiler capacity.

The super heater performance was satisfactory. It should be noted that any changes made to increase the boiler heat transfer capacity would also increase the super heater capacity. Since the scroll expander can handle some liquid the super heater is not a critical component in the experimental system. Therefore, the super heater capacity would be more than sufficient.

The electricity output of the scroll expander is unacceptable. The cause of this poor output is the circular dependence of the magnetic field and the output voltage on one another. The higher the output voltage, the stronger the magnetic field and a stronger magnetic flied means a higher output voltage. A simple way to improve the output would be to replace the run capacitor with a much larger one. This would allow a larger current to be drawn with a smaller voltage drop, improving the power output.

A better solution would be to remanufacture the scroll expander housing and covert the hermetic scroll expander to a semi-hermetic scroll expander. A magnetic coupling is recommended since it ensures no leaks. The new configuration would allow for the measurement of mechanical work directly on the housing of the electric generator. The electric generator should be swapped for a DC generator or an induction generator with access to the stator winding terminals. If the stator winding terminals can be accessed the stator windings can be excited by a different power source, offering control of the magnetic field and therefore control of the output voltage.

The FH is not a critical system component, it serves to improve the overall performance of the system. The FH capacity is slightly higher than expected, reducing the required boiler and condenser capacity even more. If the refrigerant volume flow rate is increased the FH capacity would also increase and thus this components performance would still be satisfactory.

The natural convection condenser performed well according to the design extracting the required heat. If the volume flow rate of the refrigerant is increased however the outlet temperature of the condenser might rise. A rise in outlet temperature would result in a decrease in system efficiency. However the efficiency could easily be improved by installing a fan in the condenser plenum. This would increase the cooling capacity and lower the outlet temperature and pressure of the condenser, increasing the amount of energy available to the scroll expander and thus increasing the system efficiency as stated in section 3.1. The fan would require electrical input from the generator which would decrease the system output. A detailed investigation into the effect of a fan is required before any recommendations can be made.

8.4 Achievement of Objectives

The primary objective of this thesis, to build a functioning ORC, has been achieved. A working version of this system has been built and successfully tested. The system operates from a low temperature (< 120°C) and pressure heat source, which was the second objective set for this project. Each component was sized and bought or designed and

manufactured. The performance of each component was predicted using theoretical mathematical models. This model has been validated through comparison with the experimental results obtained. Finally the economic and commercial feasibility of such a system has been investigated, conclusions drawn and recommendations made as presented in section 8.

References

AA, 2014. *Fuel Pricing.* [Online] Available at: http://www.aa.co.za/on-the-road/calculator-tools/fuel-pricing.html [Accessed 17 July 2014].

Afrox, 2013. *Industrial Gas.* [Online] Available at: www.awsgroup.co.za /data/L.P.G.pdf [Accessed 12 Jun 2014].

Baek, J., Groll, E. & Lawless, P., 2005. Piston-cylinder work producing expansion device in a transcritical carbon dioxide cycle. Part I: experimental investigation. *International Journal of Refrigeration,* 28(2), pp. 141-151.

Çengel, Y. A. & Boles, M. A., 2007. *Thermodynamics: An Engineering Approach.* 6th ed. New York: The McGraw-Hill Companies, Inc.

Çengel, Y. A. & Cimbala, J. M., 2006. *Fluid Mechanics Fundamentals and Applications.* 1st ed. New York: McGraw-Hill.

Çengel, Y. A. & Ghajar, A. J., 2008. *Heat and Mass Transfer: Fundamentals and Applications.* 4th ed. Singapore: The McGraw-Hill Companies, Inc..

Conserve Energy Future, 2014. *Conserve Energy Future.* [Online] Available at: http://www.conserve-energy-future.com/Disadvantages_GeothermalEnergy.php [Accessed 23 January 2014].

Cooper, M., 1984. Heat flows rates in saturated pool boiling - a wide range examination using reduced properties. *Advanced in Heat Transfer,* pp. 157-239.

Departement of Energy, 2014. *Petroleum Sources.* [Online] Available at: http://www.energy.gov.za/files/esources/petroleum/November2014/LPG-Regulations.pdf [Accessed 10 November 2014].

Economy Watch, 2010. *Economy Watch.* [Online] Available at: http://www.economywatch.com/renewable-energy/advantages-of-biogas.html [Accessed 29 April 2013].

Emerson Electric Co., 2014. *Reliability.* [Online] Available at: http://www.emersonclimate.com/asia/en-AP/Products/Compressors/Scroll_Compressors/Pages/Reliability.aspx [Accessed 30 June 2014].

References

Eskom Holdings SOC Limited, 2012. *Electricity Technologies.* [Online] Available at: http://www.eskom.co.za/AboutElectricity/ElectricityTechnologies/Pages/Electricity_Technologies.aspx [Accessed 25 9 2014].

Eskom Holdings SOC Limited, 2012. *Tarriff History.* [Online] Available at: http://www.eskom.co.za/CustomerCare/TariffsAndCharges/Pages/Tariff_History.aspx [Accessed 19 6 2013].

Fluid-o-Tech, 2011. *Fluid-o-Tech.* [Online] Available at: http://www.fluidotech.it/Pages/mag-drive-rotary-vane-pump-tm30-200-series.aspx [Accessed 4 May 2012].

Gauché, P., 2012. *Solar thermal energy systems pre-reader for 2012.* 1st ed. Stellenbosch: Stellenbosch University.

Genpower, 2012. *Generators.* [Online] Available at: http://www.genpower.co.za/generators/ [Accessed 28 July 2014].

GeoModel Solar, 2013. *Free Solar Radiation Maps.* [Online] Available at: http://solargis.info/doc/free-solar-radiation-maps-DNI [Accessed 25 September 2014].

Gielen, D., 2012. *Solar Photovoltaics,* Abu Dhabi: International Renewable Energy Agency.

Grundfos, 2012. *Lenntech.* [Online] Available at: http://www.lenntech.com/uploads/grundfos/96537574/Grundfos_CR-3-3-A-FGJ-A-E-HQQE.pdf [Accessed 11 March 2012].

Haiqing, G., Yitai, M. & Minxia, L., 2006. Some design features of CO swing piston expander. *Applied Thermal Engineering,* 26(2), pp. 237-243.

Imperial Crown Trading, 2009. *Solar Heating Collectors.* [Online] Available at: http://www.sustainable.co.za/solar-water-heating/solar-heating-collectors.html [Accessed 9 June 2014].

Khan, T., Khan, M., Chyu, M.-C. & Ayub, Z., 2010. Experimental investigation of single phase convective heat transfer coefficient in a corrugated plate heat exchanger for multiple plate configurations. *Applied Thermal Engineering,* Issue 30, pp. 1058-1065.

Kim, H. J., Ahn, J. M., Park, I. & Rha, P. C., 2007. Scroll expander for power generation from a low-grade steam source. *Proceedings of the Institution of Mechanical Engineers, Part A: Journal of Power and Energy,* 221(5), pp. 705-711.

References

Longo, G. & Gasparella, A., 2007. Heat transfer and pressure drop during HFC refrigerant vaporisation inside a brazed plate heat exchanger. *International Journal of Heat and Mass Transfer,* Issue 50, pp. 5194-5203.

Marion, M., Voicu, I. & Tiffonnet, A.-L., 2012. Study and optimization of a solar subcritical organic Rankine cycle. *Renewable Energy,* 24 May, Issue 48, pp. 100-109.

Mathias, J. A. et al., 2009. Experimental Testing of Gerotor and Scroll Expanders Used in, and Energetic and Exergetic Modeling of, an Organic Rankine Cycle. *Journal of Energy Resources Technology,* 131(1), p. 012201.

Mechinox Heat Exchangers, 2011. *Heat Exchanger Products.* [Online] Available at: http://www.heat-exchangers.co.za/products/ [Accessed 20 June 2012].

Mills, A., 1999. *Heat Transfer.* 2nd ed. Los Angeles: Prentice Hall.

Mills, A. F. & Ganesan, V., 2009. *Heat Transfer.* 2nd ed. New Delhi: Dorling Kindersley (India) Pvt. Ltd..

Mohd.Tahir, M., Yamada, N. & Hoshino, T., 2010. Efficiency of Compact Oraginc Rankine Cycle System with Rotary-Vane-Type Expander for Low-Temperature Waste Heat Recovery. *International Journal of Environmental Science And Engineering,* 2(1), pp. 11-16.

NIST, 2013. *National Institute of Standards and Technology Chemistry Webbook.* [Online] Available at: http://webbook.nist.gov/chemistry/ [Accessed 16 February 2014].

NREL, 2013. *NREL - Energy Anaylis.* [Online] Available at: http://www.nrel.gov/analysis/tech_lcoe.html [Accessed 25 October 2013].

NU.ER.T Srl, 2012. *NU.ER.T Rotary Vane Pumps.* [Online] Available at: http://www.nuert.com/rotary-vane-pumps/standard-pumps.php [Accessed 4 May 2012].

Reid, A., 2010. *Low temperature power generation using HFE-7000 in a Rankine cycle.* 1st ed. San Diego: San Diego State University.

Schuster, A., Karellas, S., Kakaras, E. & Spliethoff, H., 2009. Energetic and economic investigation of Organic Rankine Cycle applications. *Applied Thermal Engineering,* 29(8), pp. 1809-1817.

Subiantoro, A. & Ooi, K., 2010. Design analysis of the Revolving Vane expander in a transcritical carbon dioxide refrigeration system. *International Journal of Refrigeration,* 33(4), pp. 675-685.

References

Swanepoel, R., 2007. *Renewable Energy Systems.* Stellenbosch: Centre for Renewable and Sustainable Energy Studies.

Swanson, R. M., 2009. Photovoltaics Power Up. *Science,* 15 May, 324(5929), pp. 891-892.

The Editors of Encyclopædia Britannica, 2014. *Steam Engine (Machine).* [Online] Available at: http://www.britannica.com/EBchecked/topic/564472/steam-engine [Accessed 21 10 2014].

Viking Universal Seal Pumps, 2007. *Axflow.* [Online] Available at: http://www.axflow.com/local/norge/produkt%20datablader/viking/viking%20universal%20serie%20%20sec_630_en.pdf [Accessed 14 March 2012].

Wang, X. et al., 2010. Performance evaluation of a low-temperature solar Rankine cycle system utilizing R245fa. *Solar Energy,* 84(3), pp. 353-364.

Warnakulasuriya, F. & Worek, W., 2008. Heat transfer and pressure drop properties of high viscous solutions in plate heat exchangers. *International Journal of Heat and Mass Transfer,* Issue 51, pp. 52-67.

Yagoub, W., Doherty, P. & Riffat, S., 2006. Solar energy-gas driven micro-CHP system for an office building. *Applied Thermal Engineering,* 26(14), pp. 1604-1610.

Yamamoto, T., 2001. Design and testing of the Organic Rankine Cycle. *Energy,* 26(3), pp. 239-251.

Yang, B. et al., 2009. Experimental investigation on the internal working process of a CO2 rotary vane expander. *Applied Thermal Engineering,* 29(11), pp. 2289-2296.

Zhang, B. et al., 2007. Development of a double acting free piston expander for power recovery in transcritical CO2 cycle. *Applied Thermal Engineering,* 27(8), pp. 1629-1636.

Appendix A – R123 Properties

This appendix contains some properties of refrigerant R123 that have been necessary to complete the project (NIST, 2013).

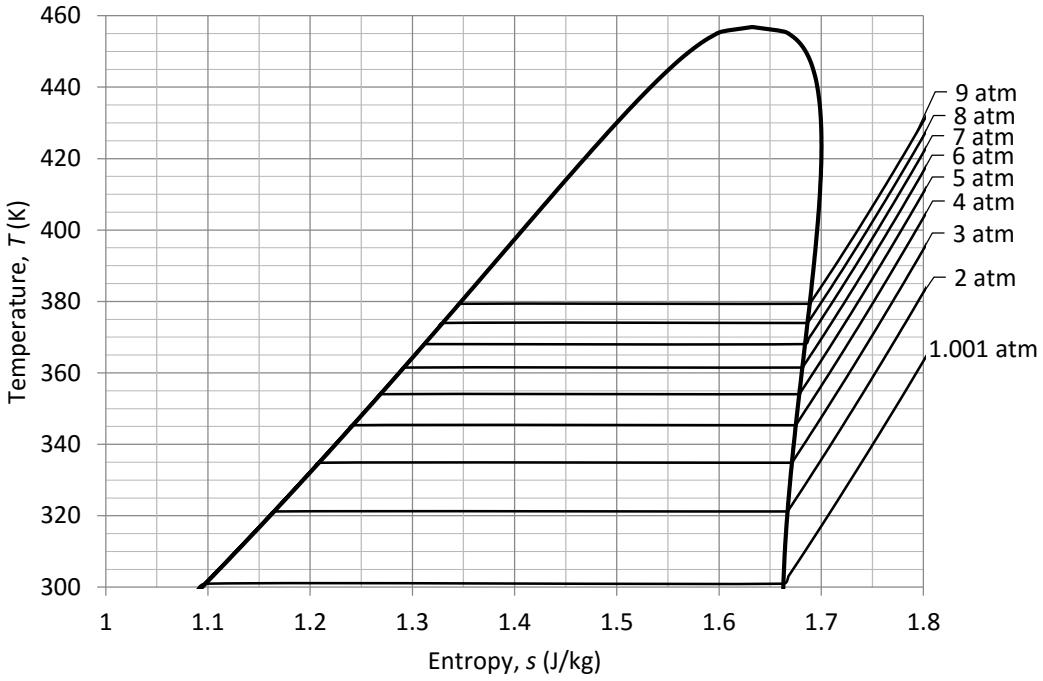

Figure 25: R123 *T-s* diagram

Appendix B – Boiler Feed Pump

The performance curve of the chosen rotary vane pump is shown in Figure 26.

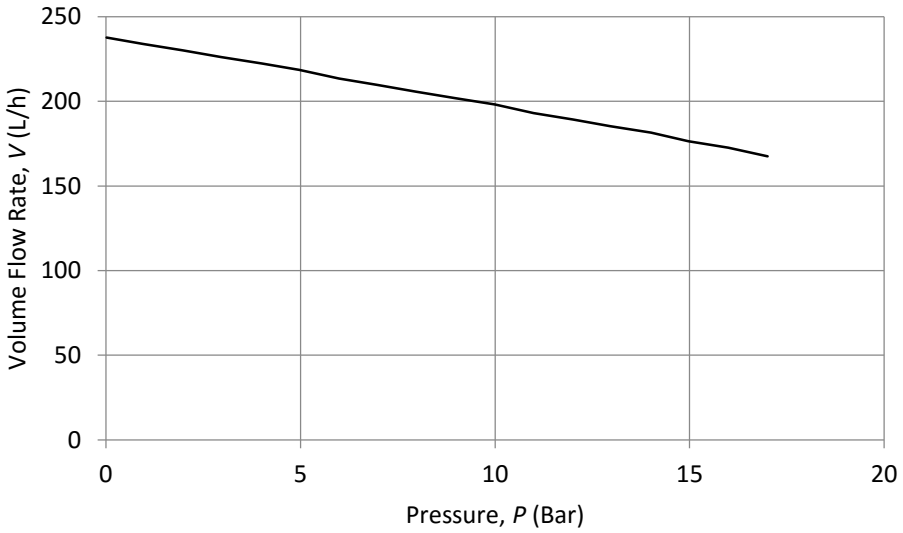

Figure 26: Boiler feed pump performance curve from supplier

Appendix C – Plate Heat Exchangers

The FH and super heater specifications as given by the supplier are presented in Figure 27.

Brazed Plate Heat Exchanger

Technical Specification

Model	: AC-70X-20M (32870 6578 7)		
Project	: (Untitled 0)	Units	:
ItemName	:	Date	: 18/10/2012

		Side1	Side2
Number of passes		1	1
Materialplate/ brazing		Alloy 316 / Cu	
ConnectionS1 (Hot-In)		Threaded (External)/ 1" ISO 228/1-G (B21) Alloy 304	
ConnectionS2 (Hot-Out)		Threaded (External)/ 1" ISO 228/1-G (B21) Alloy 304	
ConnectionS3 (Cold-In)		Soldering/ 16 mm (H39) Alloy 304	
ConnectionS4 (Cold-Out)		Soldering/ 1-1/8" (H21) Alloy 304	
Pressure vessel code		PED	
Design pressure at -196.0 Celsius	Bar	32.0	32.0
Design pressure at 150.0 Celsius	Bar	32.0	32.0
Design temperature	°C	-196.0/150.0	
Overall length x width x height	mm	81 x 111 x 526	
Net weight, empty / operating	kg	6.26 / 8.06	
Package length x width x height	mm	280 x 125 x 579	
Package weight	kg	0.5500	
Price RCPL incl Extras		0 EUR	
-Unit 32870 6578 7		550.00 EUR	

Performance is conditioned on the accuracy of customer's data and customer's ability to supply equipment

Figure 27: FH and Super Heater PHE technical specifications

The specifications of the PHE chosen as the boiler as given by the supplier are presented in Figure 28.

Brazed Plate Heat Exchanger

Technical Specification

Model : CB30-50H(32870 8378 7)
ItemName :
Units : 1
Date : 07/02/2013

		Hot Side Secondary side	Cold side Primary
Materialplate/ brazing		Alloy 316 / Cu	
ConnectionS1 (Hot-In)		Threaded (External)/ 1" ISO 228/1-G (B21) Alloy 304	
ConnectionS2 (Hot-Out)		Threaded (External)/ 1" ISO 228/1-G (B21) Alloy 304	
ConnectionS3 (Cold-In)		Soldering/ 1-1/8" (H21) Alloy 304	
ConnectionS4 (Cold-Out)		Soldering/ 1-1/8" (H21) Alloy 304	
Pressure vessel code		PED	
Design pressure at 90.0 Celsius	Bar	40.0	40.0
Design pressure at 225.0 Celsius	Bar	32.0	32.0
Design temperature	°C	-196.0/225.0	
Overall length x width x height	mm	153 x 113 x 313	
Net weight, empty / operating	kg	7.47 / 9.88	
Package length x width x height	mm	280 x 147 x 391	
Package weight	kg	0.4800	

Figure 28: Boiler PHE technical specifications

Appendix D – Scroll Expander

This appendix shows the assembly of the scroll expander along with the modifications made. A 3D CAD model of the proposed modification is shown in Figure 29.

Figure 29: Scroll expander inlet design

Figure 30 starts with the bare casing and electric motor. The components are then added one by one from Figure 31 to Figure 33 where the final assembly is shown.

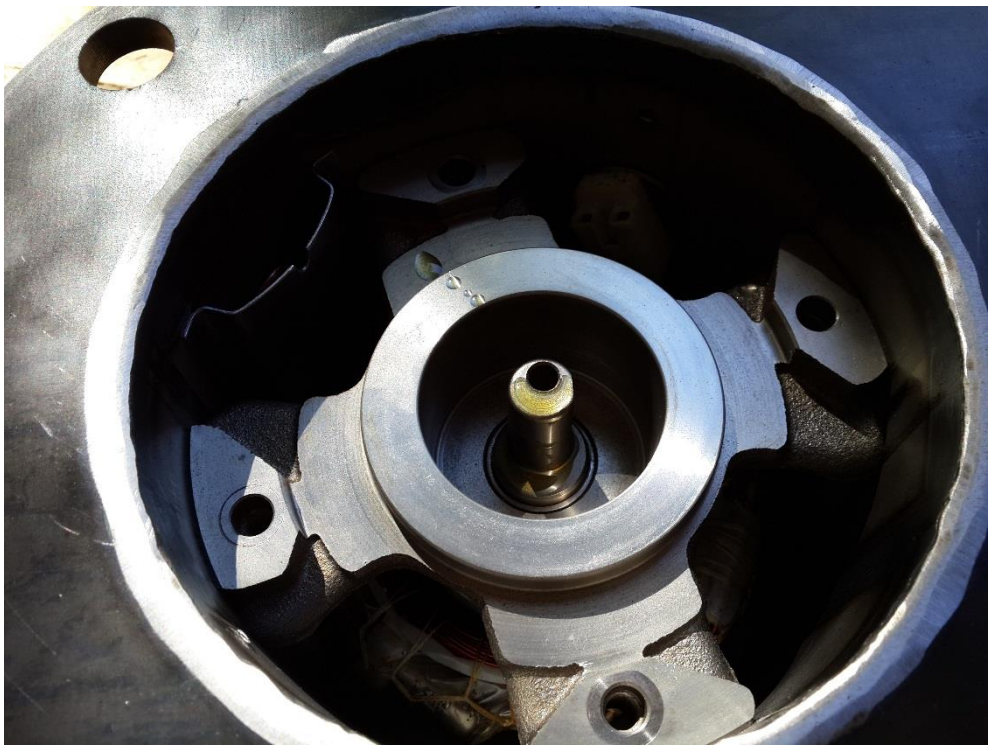

Figure 30: Scroll expander with eccentric shaft and lubrication hole

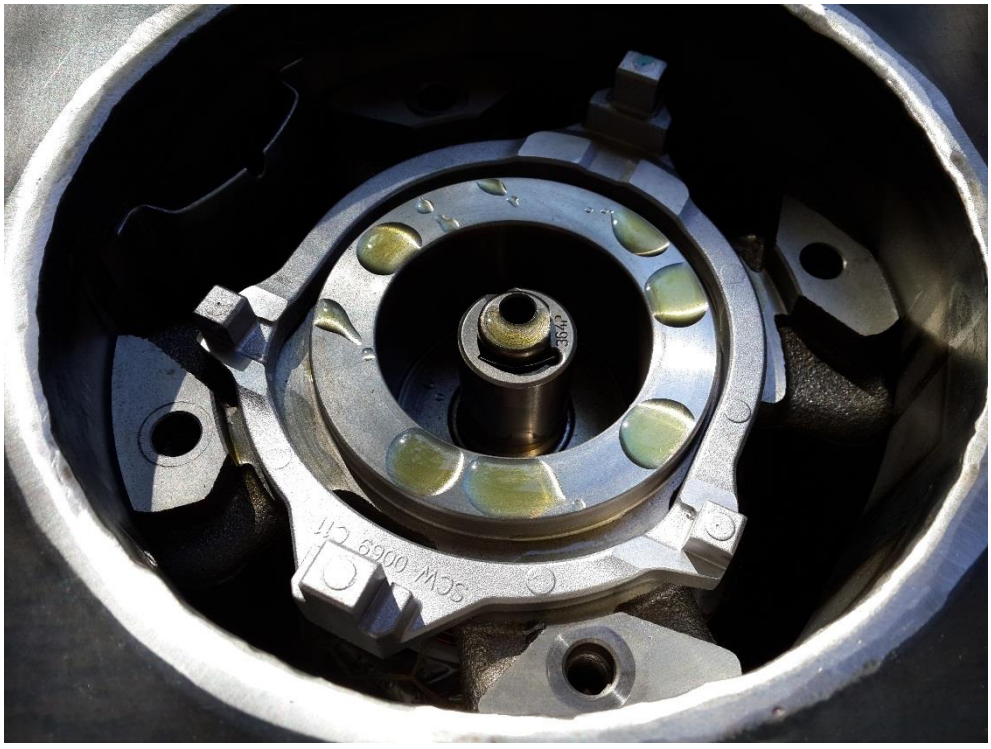

Figure 31: Scroll expander with "Oldham" retainer

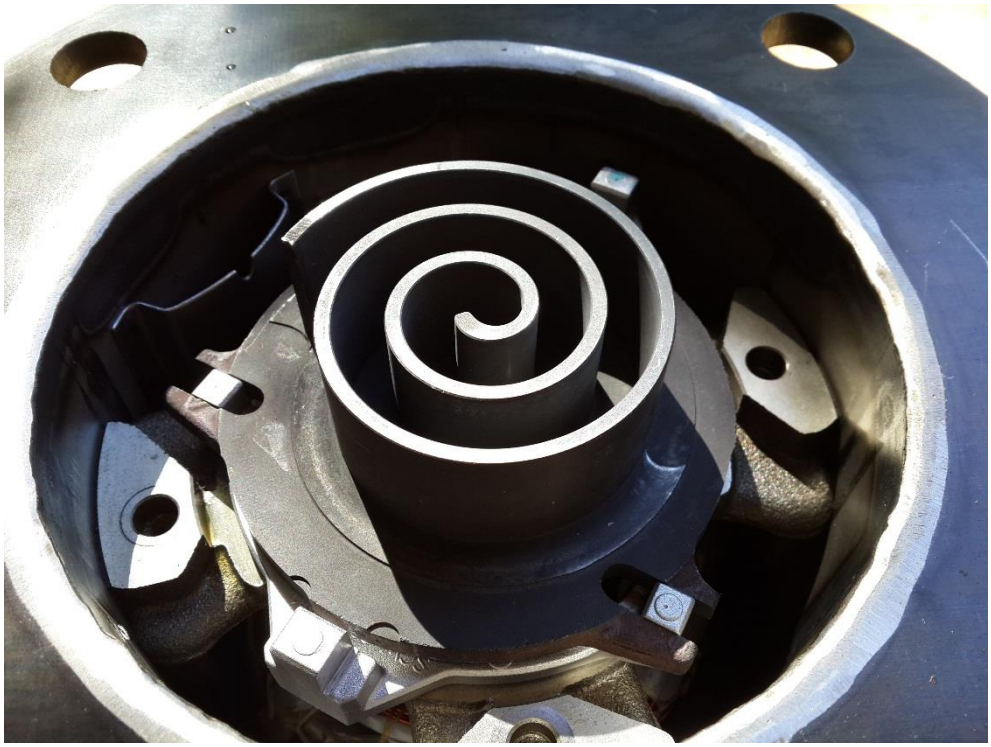

Figure 32: Scroll expander with bottom scroll in place

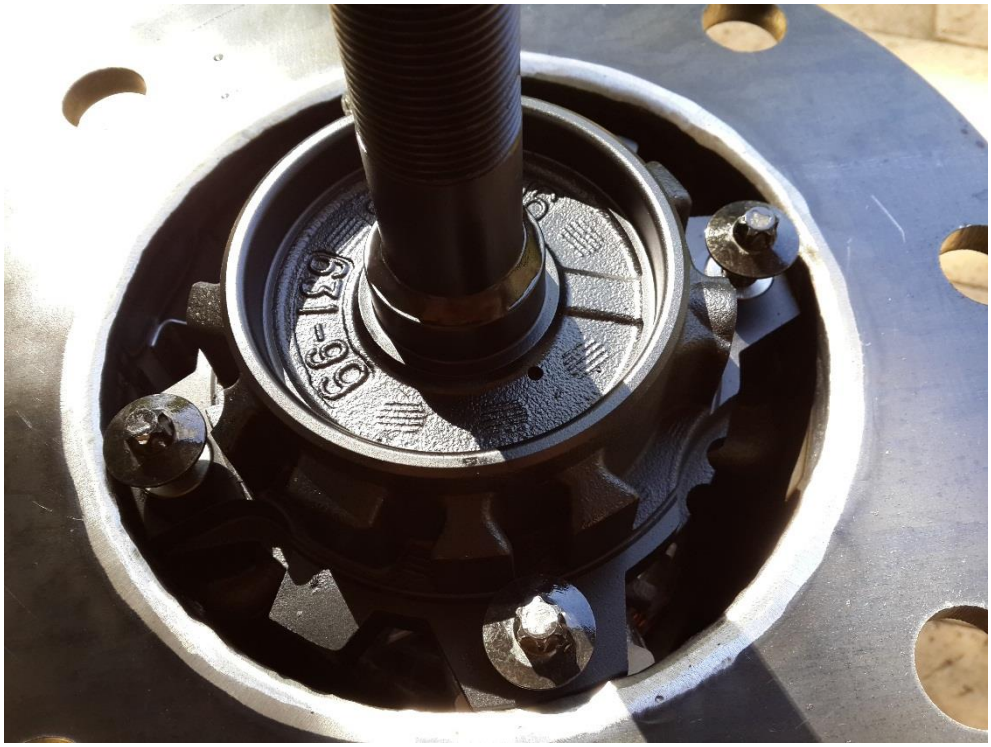

Figure 33: Scroll expander with pipe connection welded to scroll intake

Appendix E – Condenser

The manufacturing drawing created can be seen in Figure 34 along with the fin details and tube layout.

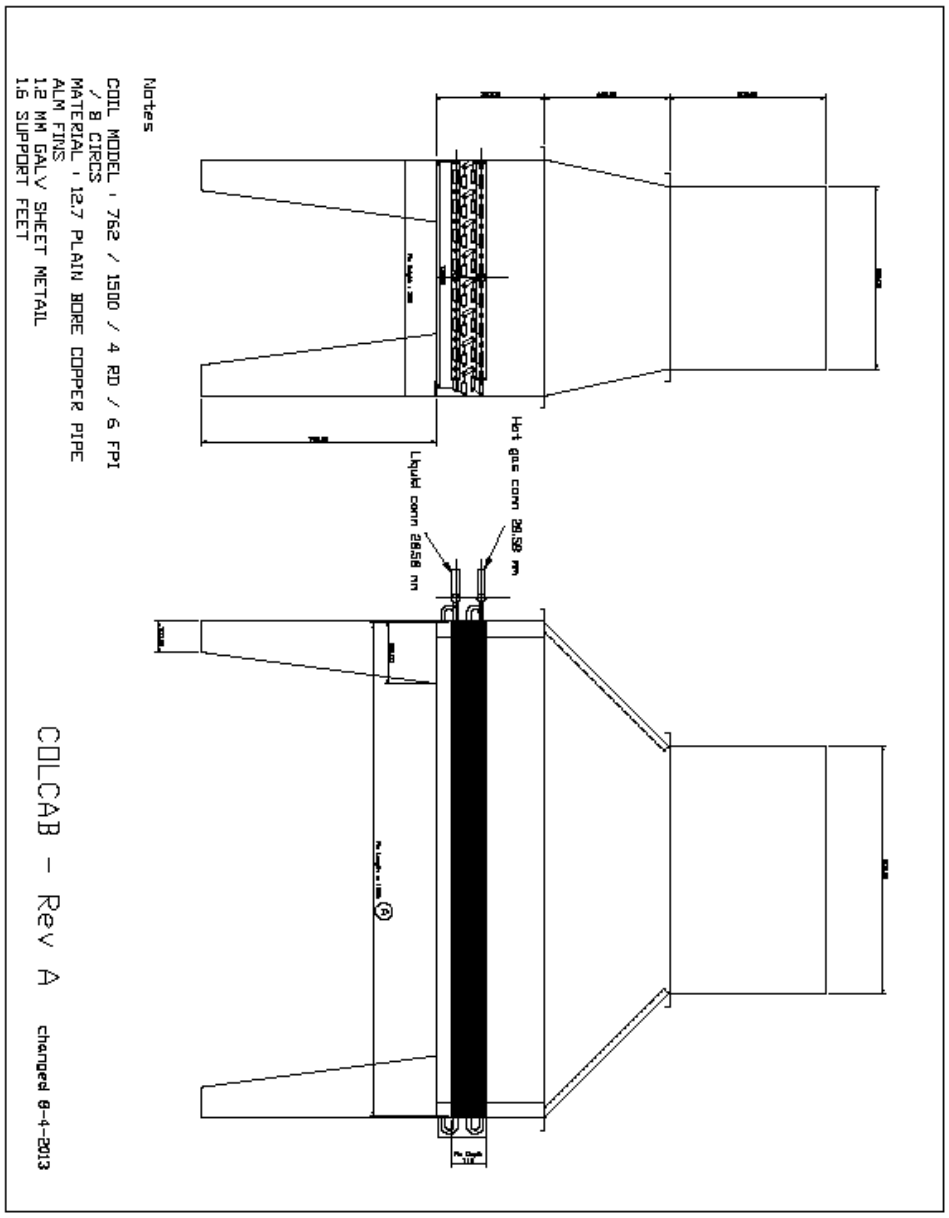

Figure 34: Condenser fabrication dimensions and details

Appendix F – Oil Circulation Pump

The manufacturer data sheet for the oil circulation pump is presented in Figure 35 and the pump dimensions are shown in Figure 36.

Description	Value
Product name:	CR 3-3 A-FGJ-A-E-HQQE
Product No:	96537574
EAN number:	5700397596357
Technical:	
Speed for pump data	2757 rpm
Rated flow:	3 m³/h
Rated head:	14 m
Impeller:	3
Shaft seal:	HQQE
Approvals on nameplate:	CE
Stages:	3
Pump version:	A
Model:	A
Materials:	
Pump housing:	Cast iron EN-JL1030 ASTM A48-30 B
Impeller	Stainless steel DIN W.-Nr. 1.4301 AISI 304
Material code:	A
Code for rubber:	E
Installation:	
Maximum ambient temperature:	40 °C
Max pressure at stated temp	25 bar / 120 °C 25 bar / -20 °C
Flange standard:	DIN
Connect code:	FGJ
Pipe connection:	DN 25 / DN 32
Pressure stage:	PN 16 / PN 25
Flange size for motor:	FT85
Liquid	
Liquid temperature range	-20 .. 120 °C
Density:	1000 kg/m³
Electrical data:	
Motor type:	71B
IE Efficiency class:	NA
Number of poles:	2
Rated power - P2:	0.37 kW
Power (P2) required by pump	0.37 kW 0.37 kW
Mains frequency:	50 Hz
Rated voltage:	1 x 220-230/240 V
Rated current:	2,95/2,70 A
Starting current	280 %
Cos phi - power factor:	0,99
Rated speed:	2770 rpm
Enclosure class (IEC 34-5):	55 (Protect. water jets/dust)
Insulation class (IEC 85):	F
Motor protec:	PTO
Motor No:	85215102
Others:	
Net weight:	23.7 kg
Gross weight:	26.1 kg
Shipping volume:	0.05 m3

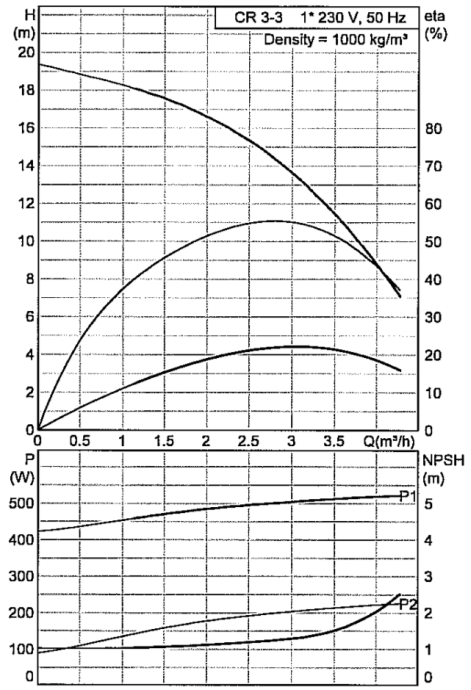

Figure 35: Oil pump specifications

Appendix F – Oil Circulation Pump

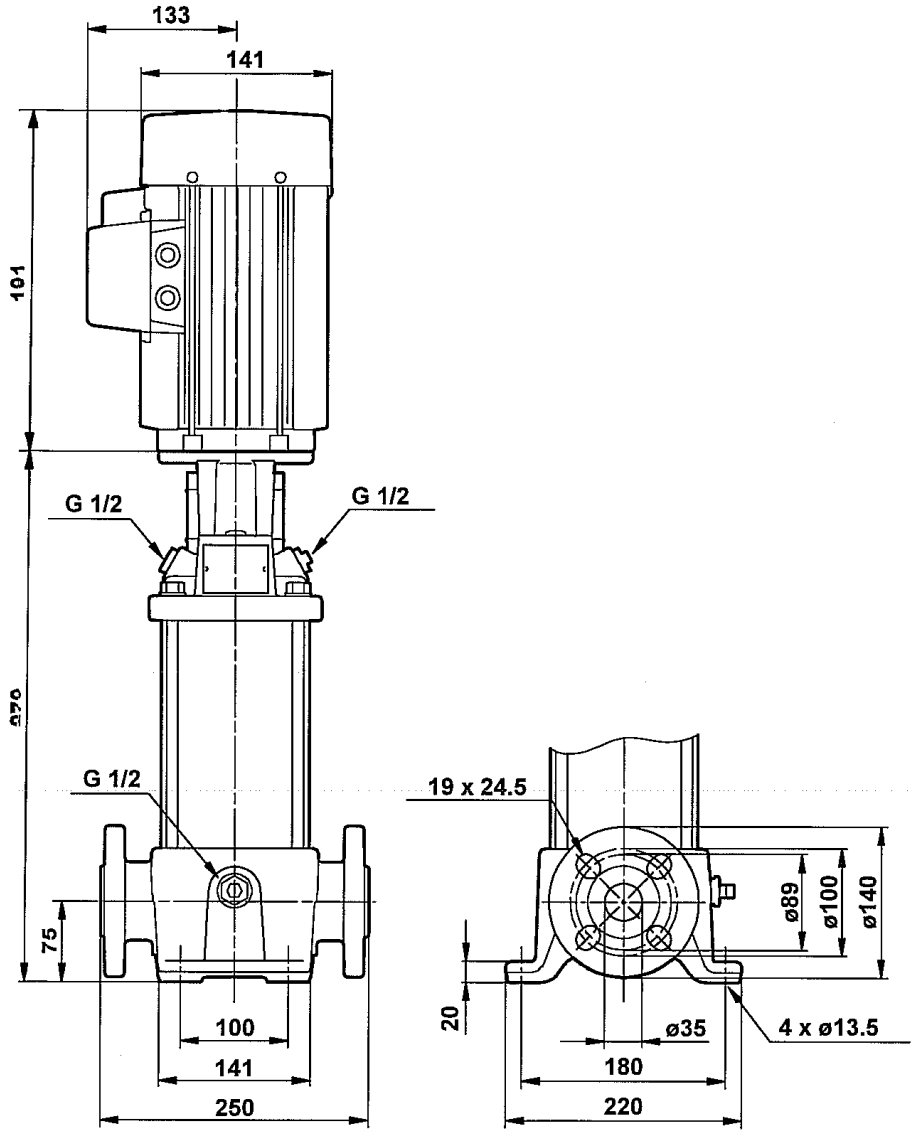

Figure 36: Oil pump dimensions

Appendix G – Thermocouple Calibration

All the thermocouples were calibrated before use for temperatures ranging from 10°C to 130°C. It was assumed that the output is linear for this temperature range. The set point temperature is measured using a calibrated temperature probe. The probe resistance is measured and used to calculate the measured temperature. The equation is a second order polynomial as give below:

$$T = 0.001116 * resistance^2 + 2.326552 * resistance - 243.767 \quad (59)$$

The temperature is thus calculated from the voltage output using the following equation form:

$$T = (slope) * Voltage + intercept \quad (60)$$

Where the slope and intercept are the experimental constants. The calibration is then verified by comparing the calculated value to a new random test temperature. The fit of the linear function is also calculated and represented by the R^2 value. Figure 37 shows the fit of a linear trend line through the data of T108 as well as the random test point.

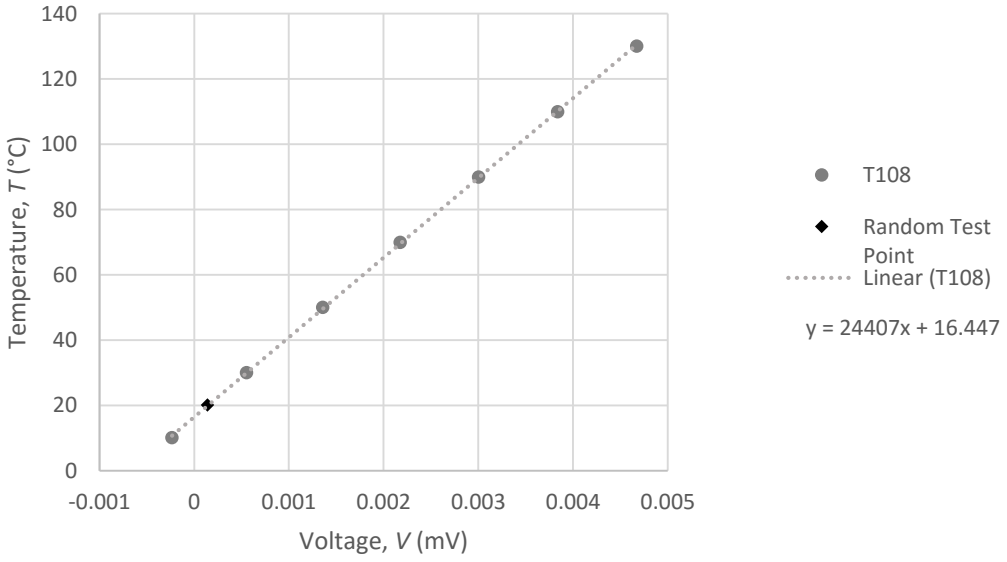

Figure 37: Thermocouple calibration data

From Figure 37 it is clear that the linear approximation holds for the give temperature range. Table 9 shows the experimental test data for the first test and Table 10 for the second test.

Table 9: Thermocouple calibration test 1 data

Thermocouple		Test01	Test02	Test03	Test04	Test05	Test06	Test07	Test08
Ref	(ohm)	103,93	111,69	119,42	127,08	134,72	142,32	149,89	107,82
	(T)	10,08	30,01	49,97	69,91	89,92	109,95	130,03	20,07
T102	(mV)	-0,00033	0,00043	0,00121	0,00201	0,00282	0,00364	0,00446	-0,00006
	(T)	10,95	29,88	49,40	69,37	89,62	110,04	130,63	17,76
T108	(mV)	-0,00023	0,00055	0,00135	0,00217	0,00300	0,00384	0,00467	0,00014
	(T)	10,74	29,89	49,52	69,52	89,73	110,06	130,43	19,83
T109	(mV)	-0,00023	0,00055	0,00135	0,00217	0,00300	0,00382	0,00465	0,00014
	(T)	10,68	29,89	49,55	69,56	89,78	110,07	130,36	19,79
T110	(mV)	-0,00023	0,00055	0,00135	0,00217	0,00300	0,00382	0,00465	0,00014
	(T)	10,68	29,90	49,54	69,56	89,78	110,08	130,36	19,79
T111	(mV)	-0,00023	0,00055	0,00136	0,00218	0,00301	0,00384	0,00468	0,00014
	(T)	10,74	29,90	49,51	69,51	89,73	110,06	130,43	19,84
T112	(mV)	-0,00023	0,00055	0,00136	0,00218	0,00301	0,00384	0,00468	0,00014
	(T)	10,74	29,89	49,52	69,51	89,74	110,07	130,43	19,83

Table 10: Thermocouple calibration test 2 data

Thermocouple		Test09	Test10	Test11	Test12	Test13	Test14	Test15	Test16
Ref	(ohm)	103,936	111,693	119,417	127,08	134,72	142,32	149,89	123,26
	(T)	10,10	30,02	49,98	69,91	89,92	109,95	130,03	59,96
T103	(mV)	-0,00027	0,00052	0,00132	0,00214	0,00297	0,00380	0,00462	0,00172
	(T)	10,72	30,04	49,64	69,59	89,93	110,19	130,29	59,46
T104	(mV)	-0,00027	0,00052	0,00132	0,00214	0,00297	0,00380	0,00462	0,00173
	(T)	10,71	30,04	49,64	69,59	89,95	110,20	130,27	59,48
T105	(mV)	-0,00027	0,00053	0,00133	0,00215	0,00299	0,00383	0,00465	0,00174
	(T)	10,73	30,04	49,63	69,58	89,94	110,20	130,29	59,46
T106	(mV)	-0,00027	0,00053	0,00133	0,00215	0,00299	0,00383	0,00465	0,00174
	(T)	10,73	30,04	49,64	69,60	89,93	110,20	130,29	59,44
T107	(mV)	-0,00027	0,00052	0,00133	0,00215	0,00298	0,00381	0,00464	0,00173
	(T)	10,74	30,05	49,65	69,61	89,95	110,20	130,30	59,38
T113	(mV)	-0,00029	0,00052	0,00133	0,00215	0,00298	0,00381	0,00464	0,00173
	(T)	10,39	30,20	49,81	69,77	89,97	110,18	130,13	59,43
T114	(mV)	-0,00030	0,00052	0,00133	0,00215	0,00298	0,00381	0,00462	0,00172
	(T)	10,30	30,23	49,83	69,81	89,99	110,18	130,06	59,49
T115	(mV)	-0,00030	0,00052	0,00133	0,00215	0,00298	0,00381	0,00463	0,00173
	(T)	10,34	30,25	49,80	69,74	89,97	110,14	130,14	59,50
T116	(mV)	-0,00029	0,00053	0,00133	0,00215	0,00299	0,00382	0,00464	0,00173
	(T)	10,36	30,23	49,81	69,76	89,95	110,14	130,15	59,47

Table 11 gives the constants for each thermocouple as calculated from the data in Table 9 and Table 10, Also listed in Table 11 are the R^2 values for each thermocouple indicating how accurate the linear approximation is,

Appendix G – Thermocouple Calibration

Table 11: Thermocouple calibration constants

Thermocouple	Slope	Intercept	R^2
T102	24966,334	19,168	0,99992
T103	24452,462	17,310	0,99996
T104	24452,064	17,294	0,99996
T105	24291,994	17,281	0,99996
T106	24294,083	17,252	0,99996
T107	24380,265	17,260	0,99995
T108	24407,368	16,447	0,99995
T109	24491,656	16,409	0,99996
T110	24490,348	16,416	0,99996
T111	24373,854	16,441	0,99995
T112	24374,521	16,443	0,99995
T113	24309,125	17,448	0,99998
T114	24337,749	17,511	0,99998
T115	24298,100	17,542	0,99998
T116	24276,242	17,478	0,99998

Appendix H – Safety

Due to the nature of this experimental system and the experience of the operator the following guidelines have been set out.

H.1 Pre-Operation Checks

Before the system is switched on the operator must ensure that:

1. There is a fire extinguisher present in case the heaters malfunction and ignites the oil.
2. Check the valves located in the refrigerant path to ensure that the fluid can be pumped through the entire system.
3. Check the oil level, the outlet of the oil tank should be completely submersed. If the oil level is too low circulation of the oil would stop and the thermostat located at the pump inlet would fail to detect the increase in oil temperature. This failure would then result in the heating elements being switched on permanently, causing the oil to smoke and/or catch fire.
4. Check all electrical connections and ensure that they are safe.

H.2 General Operation Checks

During the operation of the experimental system the following checks should be performed continuously to ensure the operator safety:

1. The system should never be left unattended.
2. Exposed surfaces may be hot so they should not be touched.
3. The inlet pressure to the scroll expander should not exceed 7 bar.
4. Monitor the oil temperature.
5. Check if the oil pump is still running. The oil pump is equipped with thermal protection that disables the pump if the inlet temperature exceeds 120°C. If the oil pump is switched off the heating elements should be switched off immediately.
6. Check for oil and refrigerant leaks so that they can be repaired at a later stage.

H.3 Post Operation Checks

After the conclusion of testing on the experimental system the system should not be left unattended until the shut off phase has been completed. All equipment should be stored neatly and spills should be cleaned.

Appendix I – Sample Calculations

Sample calculations for each component is presented in tabular form in this section. The calculations are presented in the same order as they appear in section 7.

Table 12: Boiler feed pump sample calculations

E_{in} (kW)	W_{out} (kw)	m_{R123} (kg/s)	T_{in} (K)	T_{out} (K)	h_{in} (kJ/kg)	h_{out} (kJ/kg)	dh (kJ/kg)	eta_{pump}	s_{in} (kJ/kgK)	$h_{isentropic}$ (kJ/kg)	$eta_{isentropic}$
0.2391	0.2106	0.066841345	297.2131	299.4677	222.99	226.14	3.15	88%	1.0804	223.08	3%
0.2391	0.2106	0.066841345	297.2131	299.4677	222.99	226.14	3.15	88%	1.0804	223.08	3%
0.2391	0.2106	0.066841345	297.2078	299.4598	222.99	226.14	3.15	88%	1.0804	223.08	3%
0.2391	0.2106	0.066841345	297.221	299.4862	222.99	226.14	3.15	88%	1.0804	223.08	3%
0.2391	0.2106	0.066841345	297.2315	299.4914	222.99	226.14	3.15	88%	1.0804	223.08	3%
0.2391	0.2119	0.067283884	297.221	299.4651	222.99	226.14	3.15	89%	1.0804	223.08	3%
0.2391	0.2119	0.067283884	297.2105	299.4756	222.99	226.14	3.15	89%	1.0804	223.08	3%
0.2391	0.2119	0.067283884	297.2342	299.4704	222.99	226.14	3.15	89%	1.0804	223.08	3%
0.2391	0.2119	0.067283884	297.2105	299.473	222.99	226.14	3.15	89%	1.0804	223.08	3%
0.2391	0.2119	0.067283884	297.1999	299.4809	222.99	226.14	3.15	89%	1.0804	223.08	3%

Table 13: Sample experimental data for the boiler

m_{oil} (kg/s)	$Q_{in,oil}$ (kW)	$Temperature_{R123,sensor}$ (K)	$Density_{R123,sensor}$ (kg/m³)	$m_{R123,Liquid}$ (kg/s)	Inlet $Temperature_{R123}$ (K)	Outlet $Temperature_{R123}$ (K)	X	$h_{out,R123}$ (kJ/kg)	$h_{in,R123}$ (kJ/kg)	$h_{fg,R123}$ (kJ/kg)	Q_{R123} (kW)
1.073	8.181	299.468	1459.364	0.067	339.971	384.396	0.735	390.910	268.510	122.400	8.181
1.073	8.181	299.468	1459.364	0.067	339.971	384.396	0.735	390.910	268.510	122.400	8.181
1.073	8.274	299.460	1459.384	0.067	339.697	384.315	0.758	394.253	268.510	125.743	8.405
1.070	8.244	299.486	1459.316	0.067	339.782	384.262	0.731	390.350	268.510	121.840	8.144
1.071	8.252	299.491	1459.303	0.067	339.616	384.194	0.730	390.200	268.510	121.690	8.134
1.086	8.431	299.465	1459.370	0.067	339.808	384.131	0.757	394.083	268.510	125.573	8.449
1.092	8.484	299.476	1459.343	0.067	339.687	384.089	0.754	393.744	268.510	125.234	8.426
1.100	8.543	299.470	1459.357	0.067	339.674	384.032	0.762	394.805	268.510	126.295	8.498
1.101	8.567	299.473	1459.350	0.067	339.560	383.969	0.766	395.432	268.510	126.922	8.540
1.093	8.504	299.481	1459.330	0.067	339.668	383.935	0.766	395.516	268.510	127.006	8.545

Table 14: Theoretical boiler performance sample calculation part 1

T_{hi} (°C)	T_{ho} (°C)	$T_{h,avg}$ (°C)	T_{ci} (°C)	T_{co} (°C)	$T_{c,avg}$ (°C)	P_{ci} (Bar)	P_{co} (Bar)	$\rho_{h,avg}$ (kg/m^3)	$nu_{h,avg}$ (m^2/s)	$cp_{h,avg}$ (J/kgK)	$k_{h,avg}$ (W/mK)	$Pr_{h,avg}$	dP (Bar)	$V_{h,avg}$ (m/s)	$m_{h,avg}$ (kg/s)	Q_{oil} (W)
112.29	108.82	110.56	66.82	84.00	75.41	5.39	5.29	834.03	1.49E-05	2267.53	0.14	206.86	0.33	1.29E-03	1.07	8432.22
112.29	108.82	110.56	66.82	84.00	75.41	5.39	5.29	834.03	1.49E-05	2267.53	0.14	206.86	0.33	1.29E-03	1.07	8432.22
112.26	108.75	110.50	66.55	84.00	75.27	5.39	5.29	834.06	1.49E-05	2267.30	0.14	207.00	0.33	1.29E-03	1.07	8527.18
112.18	108.68	110.43	66.63	84.00	75.32	5.39	5.29	834.11	1.49E-05	2266.98	0.14	207.19	0.33	1.28E-03	1.07	8494.77
112.11	108.60	110.36	66.47	84.00	75.23	5.37	5.27	834.15	1.49E-05	2266.67	0.14	207.38	0.33	1.28E-03	1.07	8502.35
112.05	108.52	110.29	66.66	84.00	75.33	5.39	5.29	834.19	1.49E-05	2266.38	0.14	207.55	0.33	1.30E-03	1.09	8685.33
111.99	108.46	110.22	66.54	84.00	75.27	5.38	5.28	834.23	1.49E-05	2266.10	0.14	207.72	0.33	1.31E-03	1.09	8739.19
111.92	108.39	110.15	66.52	84.00	75.26	5.38	5.28	834.27	1.50E-05	2265.80	0.14	207.90	0.33	1.32E-03	1.10	8798.41
111.86	108.32	110.09	66.41	84.00	75.21	5.38	5.28	834.31	1.50E-05	2265.53	0.14	208.07	0.33	1.32E-03	1.10	8821.76
111.80	108.26	110.03	66.52	84.00	75.26	5.38	5.28	834.34	1.50E-05	2265.26	0.14	208.24	0.33	1.31E-03	1.09	8756.67

Table 15: Theoretical boiler performance sample calculation part 2

Flow area (m^2)	V_{avg} (m/s)	$Re_{h,avg}$	$mu_{,avg}$ (Pa s)	mu_{avg} (Pa s)	$Nu_{h,avg}$	$h_{h,avg}$ (W/m^2K)	P*	R_p (µm)	q (w/m^2)	M (kg/mol)	h_c (W/m^2K)	H (W/m^2K)	HT Area (m^2)	dT1 (K)	dT2 (K)	LMTD (K)	Q_{R123} (W)
0.0057	0.23	60.17	1.24E-02	2.03E-02	21.27	735.74	0.15	800.00	24800.64	0.15	93413.45	729.99	0.34	28.29	42.00	34.70	8611.38
0.0057	0.23	60.17	1.24E-02	2.03E-02	21.27	735.74	0.15	800.00	24800.64	0.15	93413.45	729.99	0.34	28.29	42.00	34.70	8611.38
0.0057	0.23	60.12	1.24E-02	2.04E-02	21.25	735.19	0.15	800.00	25079.93	0.15	94116.62	729.49	0.34	28.26	42.20	34.76	8622.49
0.0057	0.23	59.88	1.24E-02	2.04E-02	21.19	733.17	0.15	800.00	24984.62	0.15	93879.67	727.49	0.34	28.18	42.05	34.65	8570.98
0.0057	0.23	59.87	1.24E-02	2.04E-02	21.19	733.19	0.15	800.00	25006.90	0.15	93984.91	727.51	0.34	28.11	42.14	34.65	8570.87
0.0057	0.23	60.65	1.25E-02	2.04E-02	21.42	741.04	0.15	800.00	25545.09	0.15	95287.32	735.32	0.34	28.05	41.86	34.50	8624.87
0.0057	0.23	60.93	1.25E-02	2.05E-02	21.50	743.77	0.15	800.00	25703.50	0.15	95723.64	738.04	0.34	27.99	41.92	34.49	8653.88
0.0057	0.23	61.33	1.25E-02	2.05E-02	21.61	747.80	0.15	800.00	25877.67	0.15	96132.79	742.03	0.34	27.92	41.86	34.42	8684.30
0.0057	0.23	61.30	1.25E-02	2.05E-02	21.61	747.63	0.15	800.00	25946.34	0.15	96304.44	741.88	0.34	27.86	41.91	34.41	8678.78
0.0057	0.23	60.84	1.25E-02	2.05E-02	21.49	743.57	0.15	800.00	25754.90	0.15	95830.95	737.84	0.34	27.80	41.74	34.30	8604.02

Table 16: Sample calculation of the super heater performance using experimental values

m_{oil} (kg/s)	$Q_{in,oil}$ (kW)	m_{R123} (kg/s)	Inlet Temperature$_{R123}$ (K)	Outlet Temperature$_{R123}$ (K)	$h_{in,R123}$ (kJ/kg)	$h_{out,R123}$ (kJ/kg)	dh_{R123} (kJ/kg)	Q_{R123} (kW)
1.072849	4.318917	0.066841	384.395771	386.1582378	390.9102	455.52	64.60982	4.318608
1.072849	4.318917	0.066841	384.395771	386.1582378	390.9101	455.52	64.6099	4.318613
1.072845	4.225945	0.066841	384.314567	386.0133225	394.2534	455.52	61.26655	4.095139
1.069668	4.256225	0.066841	384.2621608	386.0185908	390.3501	455.52	65.16991	4.356044
1.070725	4.247727	0.066841	384.1940644	386.0343957	390.2003	455.52	65.31972	4.366058
1.08575	4.069039	0.067284	384.1311818	385.9685296	394.0834	454.29	60.20662	4.050935
1.09177	4.015725	0.067284	384.0892764	385.9448099	393.7435	454.29	60.54646	4.073801
1.10008	3.957113	0.067284	384.031632	385.8420657	394.8049	454.29	59.48512	4.00239
1.100647	3.933402	0.067284	383.9687494	385.7524799	395.4315	454.29	58.85848	3.960227
1.093421	3.995618	0.067284	383.9347134	385.5811985	395.516	454.29	58.77402	3.954545

Table 17: Theoretical super heater performance sample calculation part 1

T_{hi} (°C)	T_{ho} (°C)	$T_{h,avg}$ (°C)	T_{ci} (°C)	T_{co} (°C)	$T_{c,avg}$ (°C)	P_{in} (Bar)	P_{out} (Bar)	$\rho_{h,avg}$ (kg/m³)	$nu_{h,avg}$ (m²/s)	$cp_{h,avg}$ (kJ/kgK)	$k_{h,avg}$ (W/mK)	$Pr_{h,avg}$	dP (Bar)	$V_{h,avg}$ (m³/s)	$m_{h,avg}$ (kg/s)	$Q_{h,avg}$ (W)
114.12	112.29	113.20	84	113.01	98.50	5.29	5.19	832.46	1.44E-05	2278.89	0.14	201.16	0.326	1.29E-03	1.073	4473.79
114.12	112.29	113.20	84	113.01	98.50	5.29	5.19	832.46	1.44E-05	2278.89	0.14	201.16	0.326	1.29E-03	1.073	4473.79
114.05	112.26	113.15	84	112.86	98.43	5.29	5.19	832.50	1.44E-05	2278.66	0.14	201.26	0.326	1.29E-03	1.073	4377.05
113.99	112.18	113.08	84	112.87	98.43	5.29	5.19	832.54	1.44E-05	2278.38	0.14	201.38	0.326	1.28E-03	1.070	4407.85
113.91	112.11	113.01	84	112.88	98.44	5.27	5.17	832.58	1.44E-05	2278.05	0.14	201.52	0.326	1.29E-03	1.071	4398.42
113.76	112.05	112.90	84	112.82	98.41	5.29	5.19	832.64	1.44E-05	2277.60	0.14	201.72	0.327	1.30E-03	1.086	4212.56
113.66	111.99	112.82	84	112.79	98.40	5.28	5.18	832.69	1.44E-05	2277.26	0.14	201.87	0.327	1.31E-03	1.092	4156.75
113.55	111.92	112.74	84	112.69	98.35	5.28	5.18	832.74	1.45E-05	2276.88	0.14	202.04	0.327	1.32E-03	1.100	4095.40
113.48	111.86	112.67	84	112.60	98.30	5.28	5.18	832.78	1.45E-05	2276.60	0.14	202.17	0.327	1.32E-03	1.101	4070.35
113.46	111.80	112.63	84	112.43	98.22	5.28	5.18	832.81	1.45E-05	2276.41	0.14	202.26	0.327	1.31E-03	1.093	4134.39

Table 18: Theoretical super heater performance sample calculation part 2

Flow area (m^2)	V_{avg} (m/s)	$Re_{h,avg}$	$mu_{h,avg}$ (Pa s)	$mu_{h,wall}$ (Pa s)	$Nu_{h,avg}$	$h_{h,avg}$ (W/m^2K)	P*	R_p (µm)	q (W/m^2)	M (kg/mol)	h_c (W/m^2K)	h (W/m^2K)	HT Area (m^2)	dT1 (K)	dT2 (K)	LMTD (K)	Q_{calc} (W)
0.00224	0.5753	157.16	1.20E-02	1.35E-02	46.95	1621.05	0.14	800	13556.95	0.15	62534.12	1580.09	0.33	1.11	28.29	8.40	4378.33
0.00224	0.5753	157.16	1.20E-02	1.35E-02	46.95	1621.05	0.14	800	13556.95	0.15	62534.12	1580.09	0.33	1.11	28.29	8.40	4378.33
0.00224	0.5753	157.06	1.20E-02	1.35E-02	46.93	1620.42	0.14	800	13263.77	0.15	61624.56	1578.90	0.33	1.18	28.26	8.53	4445.31
0.00224	0.5736	156.48	1.20E-02	1.35E-02	46.81	1616.12	0.14	800	13357.13	0.15	61916.77	1575.01	0.33	1.12	28.18	8.39	4360.76
0.00224	0.5741	156.49	1.20E-02	1.36E-02	46.82	1616.74	0.14	800	13328.56	0.15	61861.48	1575.57	0.33	1.03	28.11	8.18	4252.96
0.00224	0.5821	158.49	1.20E-02	1.36E-02	47.30	1633.45	0.14	800	12765.35	0.15	60066.32	1590.21	0.33	0.94	28.05	7.98	4185.76
0.00224	0.5853	159.21	1.20E-02	1.36E-02	47.48	1639.81	0.14	800	12596.23	0.15	59558.25	1595.87	0.33	0.87	27.99	7.80	4109.74
0.00224	0.5897	160.25	1.20E-02	1.36E-02	47.74	1648.64	0.14	800	12410.29	0.15	58951.95	1603.79	0.33	0.86	27.92	7.78	4116.56
0.00224	0.5900	160.21	1.21E-02	1.36E-02	47.73	1648.61	0.14	800	12334.41	0.15	58710.69	1603.58	0.33	0.88	27.86	7.81	4132.18
0.00224	0.5861	159.07	1.21E-02	1.37E-02	47.47	1639.53	0.14	800	12528.45	0.15	59329.97	1595.44	0.33	1.03	27.80	8.11	4270.95

Table 19: Sample calculation of the scroll expander performance using experimental values

m_{R123} (kg/s)	Inlet Temperature$_{R123}$ (K)	Outlet Temperature$_{R123}$ (K)	$h_{in,R123}$ (kJ/kg)	$s_{in,R123}$ (kJ/kgK)	$h_{out,R123}$ (kJ/kg)	$s_{out,R123}$ (kJ/kgK)	dh_{R123} (kJ/kg)	$h_{isentropic}$ (kJ/kg)	$\eta_{isentropic}$	W_{out} (kW)	$E_{electrical}$ (kW)	η_{ORC}
0.0668	386.16	369.50	455.52	1.7492	446.91	1.7729	-8.6065	437.63	48%	0.5753	0.0395	7%
0.0668	386.16	369.50	455.52	1.7492	446.91	1.7729	-8.6066	437.63	48%	0.5753	0.0395	7%
0.0668	386.01	371.00	455.52	1.7492	448.19	1.776	-7.3301	437.63	41%	0.4900	0.0395	8%
0.0668	386.02	369.50	455.52	1.7492	447.37	1.7729	-8.1473	437.63	46%	0.5446	0.0395	7%
0.0668	386.03	365.00	455.52	1.7492	444.29	1.7634	-11.2270	437.63	63%	0.7504	0.0395	5%
0.0673	385.97	366.50	454.29	1.746	445.66	1.7666	-8.6348	436.48	48%	0.5810	0.0395	7%
0.0673	385.94	366.50	454.29	1.746	445.07	1.7666	-9.2153	436.48	52%	0.6200	0.0395	6%
0.0673	385.84	369.50	454.29	1.746	447.55	1.7729	-6.7395	436.48	38%	0.4535	0.0395	9%
0.0673	385.75	368.00	454.29	1.746	446.27	1.7697	-8.0175	436.48	45%	0.5395	0.0395	7%
0.0673	385.58	368.00	454.29	1.746	446.45	1.7697	-7.8409	436.48	44%	0.5276	0.0395	7%

Table 20: Theoretical scroll expander performance sample calculation part 1

m_{R123} (kg/s)	T_{in} (°C)	T_{out} (°C)	P_{in} (Bar)	P_{out} (Bar)	ρ_{in} (kg/m³)	ρ_{out} (kg/m³)	Delta E (W)	v_{in} (m/s)	v_{out} (m/s)	W_{out} (W)	Heat Loss (W)
0.0668413	113.00824	75.86	5.19	2.20	26.225	11.119	-1632.848	26.820	63.256	-930.393	-702.455
0.0668413	113.00824	75.86	5.19	2.20	26.225	11.119	-1632.848	26.820	63.256	-919.487	-713.361
0.0668413	112.86332	75.83	5.19	2.21	26.368	11.119	-1793.691	26.674	63.256	-1081.689	-712.002
0.0668413	112.86859	75.82	5.19	2.20	26.368	11.119	-1759.556	26.674	63.256	-1048.120	-711.436
0.0668413	112.8844	75.79	5.17	2.20	26.368	11.119	-1832.578	26.674	63.256	-1121.378	-711.200
0.0672839	112.81853	75.79	5.19	2.20	26.368	11.119	-1789.280	26.851	63.675	-1077.441	-711.838
0.0672839	112.79481	75.76	5.18	2.20	26.368	11.119	-1840.837	26.851	63.675	-1129.365	-711.473
0.0672839	112.69207	75.74	5.18	2.20	26.368	11.119	-1827.034	26.851	63.675	-1116.509	-710.524
0.0672839	112.60248	75.73	5.18	2.20	26.368	11.119	-1822.844	26.851	63.675	-1112.913	-709.931
0.0672839	112.4312	75.71	5.18	2.20	26.368	11.119	-1803.301	26.851	63.675	-1094.067	-709.234

Table 21: Theoretical scroll expander performance sample calculation part 2

Heat Loss (W)	h (W/m²K)	Area (m²)	dT (K)	T_{film} (°C)	Ra	nu (m²/s)	mu (Pa s)	ρ (kg/m³)	Nu	k (W/mK)	q_rad (W)	sigma (W/m²K⁴)	Emissivity
702.455	4.4559111	0.2351985	61.213729	45.256956	224291673.1	1.75052E-05	1.93958E-05	1.1080032	60.758128	0.0269886	429.69232	5.67E-08	0.95
713.361	4.6340748	0.2351985	61.213729	45.256956	252285742.8	1.75052E-05	1.93958E-05	1.1080032	63.187461	0.0269886	429.69232	5.67E-08	0.95
712.002	4.6309489	0.2351985	61.107132	45.278871	251730497.7	1.75073E-05	1.93968E-05	1.1079258	63.141071	0.0269902	429.01843	5.67E-08	0.95
711.436	4.629462	0.2351985	61.061679	45.293739	251457584.6	1.75088E-05	1.93975E-05	1.1078733	63.118245	0.0269913	428.75319	5.67E-08	0.95
711.200	4.6293989	0.2351985	61.051848	45.264668	251506988.6	1.7506E-05	1.93962E-05	1.107976	63.122378	0.0269891	428.56622	5.67E-08	0.95
711.838	4.6311638	0.2351985	61.108368	45.231153	251863666.9	1.75027E-05	1.93947E-05	1.1080943	63.152203	0.0269867	428.83559	5.67E-08	0.95
711.473	4.6306461	0.2351985	61.084913	45.216728	251808868.7	1.75013E-05	1.9394E-05	1.1081453	63.147623	0.0269856	428.61008	5.67E-08	0.95
710.524	4.628269	0.2351985	61.010214	45.235783	251382153.2	1.75032E-05	1.93949E-05	1.108078	63.111933	0.026987	428.1528	5.67E-08	0.95
709.931	4.6267637	0.2351985	60.962064	45.252	251103712	1.75047E-05	1.93956E-05	1.1080207	63.088622	0.0269882	427.87374	5.67E-08	0.95
709.234	4.6252231	0.2351985	60.908917	45.25765	250841382.4	1.75053E-05	1.93959E-05	1.1080007	63.066645	0.0269886	427.51658	5.67E-08	0.95

Table 22: Sample calculation of the feed heater performance using experimental values for the hot side

	HP - Hot Side									
m_{R123} (kg/s)	Inlet $Temperature_{R123}$ (K)	Outlet $Temperature_{R123}$ (K)	$h_{in,R123}$ (kJ/kg)	$h_{f,R123}$ (kJ/kg)	$h_{g,R123}$ (kJ/kg)	x	$h_{out,R123}$ (kJ/kg)	dh_{R123} (kJ/kg)	Q_{R123} (kW)	$s_{out,R123}$ (kJ/kg K)
0.0668	349.01	315.19	430.78	249	410.34	0.864	388.41	-42.37	-2.832	1.599
0.0668	349.01	315.19	430.78	249	410.34	0.864	388.41	-42.37	-2.832	1.599
0.0668	348.98	315.20	430.78	249	410.34	0.864	388.41	-42.37	-2.832	1.599
0.0668	348.97	315.20	430.78	249	410.34	0.864	388.41	-42.37	-2.832	1.599
0.0668	348.94	315.21	430.78	249	410.34	0.864	388.41	-42.37	-2.832	1.599
0.0673	348.94	315.23	430.78	249	410.34	0.864	388.41	-42.37	-2.851	1.599
0.0673	348.91	315.23	430.78	249	410.34	0.864	388.41	-42.37	-2.851	1.599
0.0673	348.89	315.26	430.78	249	410.34	0.864	388.41	-42.37	-2.851	1.599
0.0673	348.88	315.25	430.78	249	410.34	0.864	388.41	-42.37	-2.851	1.599
0.0673	348.86	315.23	430.78	249	410.34	0.864	388.41	-42.37	-2.851	1.599

Table 23: Sample calculation of the feed heater performance using experimental values for the cold side

LP - Cold Side					
Inlet Temperature$_{R123}$ (K)	Outlet Temperature$_{R123}$ (K)	$h_{in,R123}$ (kJ/kg)	$h_{out,R123}$ (kJ/kg)	dh_{R123} (kJ/kg)	Q_{R123} (kW)
299.47	339.97	226.14	268.51	42.37	2.832
299.47	339.97	226.14	268.51	42.37	2.832
299.46	339.70	226.14	268.51	42.37	2.832
299.49	339.78	226.14	268.51	42.37	2.832
299.49	339.62	226.14	268.51	42.37	2.832
299.47	339.81	226.14	268.51	42.37	2.851
299.48	339.69	226.14	268.51	42.37	2.851
299.47	339.67	226.14	268.51	42.37	2.851
299.47	339.56	226.14	268.51	42.37	2.851
299.48	339.67	226.14	268.51	42.37	2.851

Table 24: Theoretical feed heater performance sample calculation part 1

T_{hi} (°C)	T_{ho} (°C)	$T_{h,avg}$ (°C)	T_{ci} (°C)	T_{co} (°C)	$T_{c,avg}$ (°C)	P_h (Bar)	P_c (Bar)	$c_{p,c}$ (kJ/kg K)	m_c (kg/s)	Q_c (W)	ρ (kg/m^3)	mu_c (Pa s)	k (W/mK)	Flow Area (m^2)	Volume Flow Rate (m^3/s)	Flow Velocity (m/s)	Reynold Number	Prandt Number	Nusselt Number	h_c (W/m^{2}K)
75.86	42.04	58.95	26.32	66.82	46.57	2.20	5.19	1044.6	0.0668	2828.1	1411.6	3.34E-04	0.0711	0.00224	4.74E-05	0.0211	178.75	4.90	14.39	511.78
75.86	42.04	58.95	26.32	66.82	46.57	2.20	5.19	1044.6	0.0668	2828.1	1411.6	3.34E-04	0.0711	0.00224	4.74E-05	0.0211	178.75	4.90	14.39	511.78
75.83	42.05	58.94	26.31	66.55	46.43	2.21	5.19	1044.6	0.0668	2809.5	1411.6	3.34E-04	0.0711	0.00224	4.74E-05	0.0211	178.75	4.90	14.39	511.78
75.82	42.05	58.94	26.34	66.63	46.48	2.20	5.19	1044.6	0.0668	2813.5	1411.6	3.34E-04	0.0711	0.00224	4.74E-05	0.0211	178.75	4.90	14.39	511.78
75.79	42.06	58.92	26.34	66.47	46.40	2.20	5.17	1044.6	0.0668	2801.6	1411.6	3.34E-04	0.0711	0.00224	4.74E-05	0.0211	178.75	4.90	14.39	511.78
75.79	42.08	58.93	26.32	66.66	46.49	2.20	5.19	1044.6	0.0673	2835.5	1411.6	3.34E-04	0.0711	0.00224	4.77E-05	0.0213	179.93	4.90	14.47	514.43
75.76	42.08	58.92	26.33	66.54	46.43	2.20	5.18	1044.6	0.0673	2826.2	1411.6	3.34E-04	0.0711	0.00224	4.77E-05	0.0213	179.93	4.90	14.47	514.43
75.74	42.11	58.92	26.32	66.52	46.42	2.20	5.18	1044.6	0.0673	2825.7	1411.6	3.34E-04	0.0711	0.00224	4.77E-05	0.0213	179.93	4.90	14.47	514.43
75.73	42.10	58.92	26.32	66.41	46.37	2.20	5.18	1044.6	0.0673	2817.5	1411.6	3.34E-04	0.0711	0.00224	4.77E-05	0.0213	179.93	4.90	14.47	514.43
75.71	42.08	58.90	26.33	66.52	46.42	2.20	5.18	1044.6	0.0673	2824.6	1411.6	3.34E-04	0.0711	0.00224	4.77E-05	0.0213	179.93	4.90	14.47	514.43

Table 25: Theoretical feed heater performance sample calculation part 2

g (m/s^2)	h_{fg} (kJ/kg)	ρ_l (kg/m^3)	ρ_v (kg/m^3)	k_l (W/mK)	mu_l (Pa s)	$c_{p,l}$ (kJ/kg K)	T_{sat} (K)	T_s (K)	h_h (W/m^2K)	h (W/m^2K)	HT Area (m^2)	dT1 (K)	dT2 (K)	LMTD	Q (W)
9.81	160.39	1397.4	13.08	0.0694	3.11E-04	1053.8	324.56	307.64	371.90	215.39	1.05	9.04	15.73	12.08	2731.32
9.81	160.39	1397.4	13.08	0.0694	3.11E-04	1053.8	324.56	307.64	371.90	215.39	1.05	9.04	15.73	12.08	2731.32
9.81	160.39	1397.4	13.08	0.0694	3.11E-04	1053.8	324.56	307.35	370.36	214.87	1.05	9.29	15.74	12.23	2759.55
9.81	160.39	1397.4	13.08	0.0694	3.11E-04	1053.8	324.56	307.47	371.00	215.08	1.05	9.19	15.71	12.16	2746.79
9.81	160.39	1397.4	13.08	0.0694	3.11E-04	1053.8	324.56	307.31	370.17	214.80	1.05	9.32	15.72	12.24	2761.58
9.81	160.39	1397.4	13.08	0.0694	3.11E-04	1053.8	324.56	307.49	371.12	215.59	1.05	9.13	15.76	12.14	2749.00
9.81	160.39	1397.4	13.08	0.0694	3.11E-04	1053.8	324.56	307.38	370.54	215.39	1.05	9.22	15.76	12.20	2759.00
9.81	160.39	1397.4	13.08	0.0694	3.11E-04	1053.8	324.56	307.36	370.45	215.36	1.05	9.22	15.79	12.21	2760.63
9.81	160.39	1397.4	13.08	0.0694	3.11E-04	1053.8	324.56	307.25	369.85	215.16	1.05	9.32	15.78	12.27	2771.65
9.81	160.39	1397.4	13.08	0.0694	3.11E-04	1053.8	324.56	307.39	370.60	215.41	1.05	9.19	15.75	12.18	2755.11

Table 26: Sample calculation of the condenser performance using experimental values

$T_{in,air}$ (K)	$T_{out,air}$ (K)	Volume $Flow_{air}$ (m^3/s)	Specific $Volume_{out}$ (m^3/kg)	Mass Flow (kg/s)	$RH\%_{in}$	Vapour $Pressure_{in}$ (kPa)	Humidity $Ratio_{in}$ (kg/kg dry air)	$Enthalpy_{in,air}$ (kJ/kg)	Vapour $Pressure_{out}$ (kPa)	Humidity $Ratio_{out}$ (kg/kg dry air)	$Enthalpy_{out,air}$ (kJ/kg)	$RH\%_{out}$	$Q_{out,air}$ (kW)	$T_{in,R123}$ (K)	$T_{out,R123}$ (K)	Mass Flow (kg/s)	h_{in} (kJ/kg)	h_{out} (kJ/kg)	$Q_{in,R123}$ (kW)
290.48	310.09	0.50	0.883	0.566	26.8%	0.5182	0.00320	25.52	0.5182	0.00320	45.405	8.3%	11.26	315.19	297.21	0.0668	388.41	222.99	11.06
290.48	310.09	0.50	0.883	0.566	26.8%	0.5182	0.00320	25.52	0.5182	0.00320	45.405	8.3%	11.26	315.19	297.21	0.0668	388.41	222.99	11.06
290.49	310.04	0.50	0.883	0.566	26.4%	0.5097	0.00314	25.40	0.5097	0.00314	45.219	8.2%	11.22	315.20	297.21	0.0668	388.41	222.99	11.06
290.30	310.13	0.50	0.883	0.566	25.9%	0.4956	0.00306	24.99	0.4956	0.00306	45.085	7.9%	11.38	315.20	297.22	0.0668	388.41	222.99	11.06
290.43	309.92	0.50	0.882	0.567	26.5%	0.5112	0.00315	25.36	0.5112	0.00315	45.120	8.2%	11.20	315.21	297.23	0.0668	388.41	222.99	11.06
290.48	310.05	0.50	0.883	0.566	27.1%	0.5227	0.00323	25.59	0.5227	0.00323	45.435	8.4%	11.24	315.23	297.22	0.0673	388.41	222.99	11.13
290.46	310.09	0.50	0.883	0.566	27.5%	0.5306	0.00327	25.70	0.5306	0.00327	45.602	8.5%	11.27	315.23	297.21	0.0673	388.41	222.99	11.13
290.22	310.12	0.50	0.883	0.566	27.6%	0.5236	0.00323	25.34	0.5236	0.00323	45.520	8.4%	11.43	315.26	297.23	0.0673	388.41	222.99	11.13
290.27	309.99	0.50	0.883	0.566	27.6%	0.5273	0.00325	25.46	0.5273	0.00325	45.444	8.5%	11.32	315.25	297.21	0.0673	388.41	222.99	11.13
290.20	309.82	0.50	0.882	0.567	27.6%	0.5249	0.00324	25.35	0.5249	0.00324	45.236	8.5%	11.27	315.23	297.20	0.0673	388.41	222.99	11.13

Table 27: Theoretical condenser performance sample calculation part 1

T_{ci} (°C)	T_{co} (°C)	$T_{c,avg}$ (°C)	T_{hi} (°C)	T_{ho} (°C)	$T_{h,avg}$ (°C)	P_{in} (Bar)	P_{out} (Bar)	RH %	$\rho_{c,avg}$ (kg/m^3)	$mu_{c,avg}$ (Pa s)	$c_{p,c,avg}$ (kJ/kg K)	$k_{c,avg}$ (W/mK)	$Pr_{c,avg}$	Q (kW)	t (mm)	s (m)	Beta (K^{-1})	Ra_s	Nu	h (W/m^{2}K)	HT Area (m^2)
14.65	24.06	19.36	112.29	26.32	69.30	1.85	1.65	26.82%	1.21	1.82E-05	1007	0.0251	0.731	11.26	0.2	0.00403	0.00173	1039.81	0.928	5.773	142.13
14.65	24.06	19.36	112.29	26.32	69.30	1.85	1.65	26.82%	1.21	2.05E-05	1007	0.0251	0.823	11.26	0.2	0.00403	0.00173	924.43	0.997	6.204	142.13
14.73	24.06	19.39	112.26	26.31	69.28	1.85	1.65	26.35%	1.21	2.05E-05	1007	0.0251	0.822	11.22	0.2	0.00403	0.00173	923.91	0.998	6.206	142.13
14.76	24.07	19.42	112.18	26.34	69.26	1.85	1.65	25.95%	1.21	2.05E-05	1007	0.0251	0.822	11.38	0.2	0.00403	0.00173	923.96	0.998	6.207	142.13
14.74	24.08	19.41	112.11	26.34	69.22	1.85	1.65	26.54%	1.21	2.05E-05	1007	0.0251	0.822	11.20	0.2	0.00403	0.00173	923.80	0.998	6.207	142.13
14.68	24.07	19.37	112.05	26.32	69.18	1.85	1.65	27.06%	1.21	2.05E-05	1007	0.0251	0.822	11.24	0.2	0.00403	0.00173	924.45	0.997	6.204	142.13
14.67	24.06	19.37	111.99	26.33	69.16	1.84	1.64	27.49%	1.21	2.05E-05	1007	0.0251	0.822	11.27	0.2	0.00403	0.00173	924.63	0.997	6.203	142.13
14.73	24.08	19.41	111.92	26.32	69.12	1.84	1.64	27.55%	1.21	2.05E-05	1007	0.0251	0.822	11.43	0.2	0.00403	0.00173	924.54	0.997	6.204	142.13
14.77	24.06	19.42	111.86	26.32	69.09	1.85	1.65	27.65%	1.21	2.05E-05	1007	0.0251	0.822	11.32	0.2	0.00403	0.00173	924.21	0.998	6.206	142.13
14.80	24.05	19.43	111.80	26.33	69.06	1.84	1.64	27.64%	1.21	2.05E-05	1007	0.0251	0.822	11.27	0.2	0.00403	0.00173	923.99	0.998	6.207	142.13

Table 28: Theoretical condenser performance sample calculation part 2

g (m/s^2)	h_{fg} (kJ/kg)	ρ_l (kg/m^3)	ρ_v (kg/m^3)	k_l (W/mK)	mu_l (Pa s)	$c_{p,l}$ (kJ/kgK)	T_{sat} (K)	T_s (K)	h_h (W/m^2K)	HT area Hot (m^2)	UA (W/K)	dT1 (K)	Q (kW)
9.81	162.72	1411.4	11.23	0.0707	3.29E-04	1046.8	319.43	306.07	397.18	1.92	394.73	26.92	10.63
9.81	162.72	1411.4	11.23	0.0707	3.29E-04	1046.8	319.43	306.07	397.18	1.92	408.36	26.92	10.99
9.81	162.72	1411.4	11.23	0.0707	3.29E-04	1046.8	319.43	306.06	397.12	1.92	408.41	26.89	10.98
9.81	162.72	1411.4	11.23	0.0707	3.29E-04	1046.8	319.43	306.29	398.75	1.92	409.32	26.86	11.00
9.81	162.72	1411.4	11.23	0.0707	3.29E-04	1046.8	319.43	306.06	397.06	1.92	408.40	26.87	10.97
9.81	162.72	1411.4	11.23	0.0707	3.29E-04	1046.8	319.43	306.08	397.24	1.92	408.40	26.91	10.99
9.81	162.72	1411.4	11.23	0.0707	3.29E-04	1046.8	319.43	306.12	397.50	1.92	408.52	26.91	10.99
9.81	162.72	1411.4	11.23	0.0707	3.29E-04	1046.8	319.43	306.35	399.22	1.92	409.50	26.87	11.00
9.81	162.72	1411.4	11.23	0.0707	3.29E-04	1046.8	319.43	306.24	398.37	1.92	409.07	26.86	10.99
9.81	162.72	1411.4	11.23	0.0707	3.29E-04	1046.8	319.43	306.19	398.01	1.92	408.91	26.85	10.98